Hochschule für Angewandte Wissenschaften Hamburg
Hamburg University of Applied Sciences

Master's Thesis

Yi Wang

Development of a simulation framework for dynamically loaded multifunctional composite structures and evaluation of vibration control performance

Fakultät Technik und Informatik
Department Fahrzeugtechnik und Flugzeugbau

Faculty of Engineering and Computer Science
Department of Automotive and Aeronautical Engineering

Yi Wang

Development of a simulation framework for dynamically loaded multifunctional composite structures and evaluation of vibration control performance

Masterarbeit eingereicht im Rahmen der Masterprüfung

im Studiengang Flugzeugbau
am Department Fahrzeugtechnik und Flugzeugbau
der Fakultät Technik und Informatik
der Hochschule für Angewandte Wissenschaften Hamburg

Erstprüfer: Prof. Dr.-Ing. habil. Thomas Kletschkowski
Zweitprüfer: Prof. M.Sc. Alexander Piskun

Abgabedatum: 30.08.2021

Executive Summary

Name of student

Yi Wang

Title of the paper

Development of a simulation framework for dynamically loaded multifunctional composite structures and evaluation of vibration control performance

Keywords

Comsol & Matlab simulation, dynamically loaded, multifunctional composite structures, cantilever, wingbox, vibration control, fibre orientation

Abstract

Within the framework of this master's thesis, a dynamically loaded multifunctional polymer electrolyte coated carbon fibre (PeCCF) composites structure is investigated. The PeCCF composite structure is a multifunctional structure, which provide the load bearing function simultaneously can store and transport electric energy. Due to electric resistance in the composite structure, the structure interior temperature rises which reduces the stiffness of polymer electrolyte coating, so that the structural stiffness is significantly reduced. Moreover, the structural stiffness depends on fibre orientation and fibre volume fraction. With this multi-physical material behavior, this composite structures can be used for sound reduction and vibration control since the natural frequency of structure depends on its stiffnesses. In this thesis a simulation framework of PeCCF composite structure in COMSOL and Matlab is developed to analyse its vibration reduction potential. Furthermore, suitable design parameters are identified to optimize the vibration reduction for exemplary application scenarios. Furthermore the developed PeCCF composite structure is able to withstand the load during the flight.

Zusammenfassung

Name des Studierenden

Yi Wang

Thema der Studienarbeit

Entwicklung eines Simulationsmodells für dynamisch belastete multifunktionale Fasverbundstrukturen und Auswertung der Vibrationsschutzleistung

Stichworte

Comsol & Matlab Simulation, dynamische Belastung, multifunktionale Faserverbundstruktur, Ausleger, Flügelkasten, Vibrationsschutzleistung, Faserorientierung

Kurzzusammenfassung

Im Rahmen dieser Masterarbeit wird die dynamische belastete multifunktionale mit Polymerelektrolyt beschichtete Kohlefaser (PeCCF) in einer Faserverbundstruktur untersucht. Die PeCCF Faserverbundstruktur ist eine multifunktionale Struktur, die Belastung aufnehmen und gleichzeitig elektrische Energie speichern und transportieren kann. Wegen des elektrischen Widerstands der PeCCF Faserverbundstruktur steigt die Temperatur in der Schicht, wodurch sich die Steifigkeit der Polymerelektrolyt Beschichtung reduziert. Die Steifigkeit ist zusätzlich abhängig von der Faserorientierung und Faservolumenanteil. Mit dieser multiphysikalischen Eigenschaft wird eine potentielle Leistung der PeCCF Composite Struktur zur Schallreduktion und Vibrationskontrolle erwartet, weil die Eigenfrequenzen der Struktur von der Steifigkeit abhängig sind. In dieser Arbeit wird eine Simulation der linear elastischen Faserverbundstruktur in COMSOL und Matlab durchgeführt, um das Potential zur Vibrationskontrolle und Schallreduktion zu analysieren. Außerdem werden geeignete Parameter optimiert, damit der Kabinenlärm in bestimmten Flugphasen reduziert werden kann. Die entwickelte Struktur hat weiterhin eine ausreichende Steifigkeit, um die Anforderungen an eine Flugzeugstruktur zu erfüllen.

Acknowledgements

This master’s thesis was written from March to August 2021 at HAW Hamburg.

Firstly, I would like to express my gratitude to my first supervisor Prof. Dr.-Ing. habil Thomas Kletschkowski for his great scientific and personal support during our weekly meeting. Professor Kletschkowski has looked after my work in a optimal and always friendly way, so that my motivation could never be lost. Futher thanks go to my second supervisor Prof. Alexander Piskun. He has declared himself to be available as my second examiner for this work.

In the same manner I would like to thank M. Sc. Maximilian Schutzeichel who has provided me technical aid and valuable information regarding the subject.

Finally I would like to thank my family, my boyfriend Simon and my friends for their personal support but also necessory distraction and relaxation during my studies.

Danksagung

Die vorliegende Masterarbeit ist von März bis August 2021 an der HAW Hamburg angefertigt worden.

Zuerst möchte ich meinem Erstprüfer Prof. Dr.-Ing. habil. Thomas Kletschkowski für die wissenschaftliche Unterstützung und persönliche Betreuung während der wöchentlichen Treffen bedanken. Professor Kletschkowski hat mich sehr gut und freundlich betreut, sodass ich immer motiviert war. Weiterhin möchte ich mich bei Prof. Alexander Piskun bedanken, der sich bereit erklärt hat, als Zweitprüfer für diese Arbeit zur Verfügung zu stehen.

Außerdem bedanke ich mich bei Herrn M. Sc. Maximilian Schutzeichel, der mir stets mit technischer Hilfe und wertvollen Informationen weitergeholfen hat.

Zuletzt bedanke ich mich bei meiner Familie, meinem Freund Simon und meinen Freunden für ihre persöliche Unterstützung aber auch notwendige Ablenkung und Entspannung während meines gesamten Studiums.

Table of Contents

List of Acronyms

CLPT	Classical Laminated Plates Theory
DMF	Dimethylformamide
DOF	Degree of Freedom
ESL	Equivalent Single Layer
FSDT	First-order Shear Deformation Theory
GA	Genetic Algorithm
li-triflate	lithium trifluoromethanesulfonate
LW	Layerwise
PeCCF	Polymer electrolyte Coated Carbon Fibre
SPE	Solid Polymer Electrolyte
SPL	Sound Pressure Level
SR209	tetraethylene glycol dimethacrylate
SR550	methoxy polyethylene glycol monomethacrylate

List of Symbols

A	cross-sectional area
a	side length of unit cell cube
E	elastic modulus
E_{k-tot}	total kinetic energy
$\mathbf{f}$	loading vector
G	elastic shear modulus
H	total energy
I	second-order moment of inertia
k	Spring stiffness
K_E	beam kinetic energy
$\mathbf{K}$	stiffness matrix
$\mathbf{K}_E$	stiffness element matrix
M	system mass
$\mathbf{M}$	mass matrix
$\mathbf{M}_E$	mass element matrix
$\mathbf{M}_{\rho A}$	part 1 of mass element matrix which is associated with the translational inertia
$\mathbf{M}_{\rho I}$	part 2 of mass element matrix which is associated with the rotatory inertia
m	moment per unit length
q	transversal force per unit length
r	carbon fibre radius
S_E	beam strain energy

t	layer thickness
T	transimmisibility
v_f	fibre volume fraction
W_E	external work
u	spring displacement
x	mass displacement
ẍ	mass acceleration
Π	potential energy
∅	ratio of the beam bending to shear stiffness
ρ	density
θ	rotation of cross-section
ϰ	shear coefficient
v	transversal displacement
ω	frequency of sinusoidal displacement
ω_0	natural frequency

List of Figures

List of Tables

1 Introduction

1.1 Background

Structures under dynamic loads induce vibrations, so that the value of stress and strains are changed with time. Furthermore, structural vibration cause noise and instabilities and can also develop resonance, which leads to increased deflections and failure. Therefore, structural vibration control has always been an important field for development in commercial aircraft manufacturing. Good vibration control improves flight comfort and at the same time reduces damage to the aircraft's structure. However, it is often not possible to predict the behaviour of the system straightforwardly. Hence numerical simulation plays a crucial role in predicting the response of a structure. Moreover, it enables the optimization of parameters, since the experimental investigations are expensive and prone to errors.

Moreover, multifunctional materials have been widely investigated and used in the aerospace, medicine and several others industries over the last few years. Multifunctional materials perform multiple functions in a system due to their special properties. They can be both naturally existing and specially engineered. For example, some traditional materials that provide a high strength-to-weight ratios can be modified at the nanoscale to attain other properties, such as the generation and transmission (conduction) of electrical energy, etc [1]. Fibre reinforced plastics in the manufacturing industry are increasingly used. Compared to traditional metallic engineering materials, fibre reinforced plastics are lighter and more corrosion resistant, and properties like strength, stiffness and toughness can often be tailored to a specific application [2].

The design of multifunctional, fibre reinforced plastics which can act as load-bearing structural parts and simultaneously, as vibration control devices, are of special interest in lightweight design related research [3, 4, 5]. Experimental and theoretical investigations on PeCCF composites have identified a multi-physical material behaviour. For example, such materials have been found to show a significant decrease in storage modulus when subjected to higher temperatures. Due to this stiffness reduction, it is expected that PeCCF composites offer increased potential for the reduction of vibrations in a dynamically loaded structure.

Since the stiffness drop can be tailored by temperature and fibre volume fraction, the direction of stiffness drop can be tailored by fibre orientation, structures made from this material can be made

to act as a vibration control device. The stiffness can be tailored to specific vibrations aiming at a reduction of excitation.

1.2 Research objective

As explained in the background, the reduction of vibration is important to prevent structure failure and to reduce the noise in the airplane cabin. It is expected that the application of composite structures made from PeCCFs whose stiffness depends on the temperature, fibre volume fraction and fibre orientations can reduce structural vibration significantly. To prove this expectation, a simulation framework for linear elastic composite structures under dynamic loads is constructed. The framework shall be based on the finite element method and should be able to handle typical engineering geometries such as beams and plates, including their internal structure, e.g laminates with several plies of different longitudinal orientation. Existing tools like Matlab and COMSOL Multiphysics will be used for the simulation framework.

Based on the developed framework, the vibration control performance of PeCCF composite structures shall be evaluated concerning given material properties. The vibration reduction potential shall be discussed based on the results from significant case studies (beams or plates). Furthermore, possible optimization parameters can be discussed in order to improve vibration reduction.

1.3 Thesis Structure

This thesis is structured as follows:

- Chapter 2 shows the state of research and expresses the basic theories which are used later
- Chapter 3 explains the development of the simulation framework in detail and presents results from the simulation.
- Chapter 4 analyses the structural vibration reduction potential of PeCCF composite structures based on a beam model.

- Chapter 5 discusses the optimization parameters which can improve vibration reduction in beams with different cross-sections and in a wingbox.
- Chapter 6 summarizes the most important conclusions of the thesis and suggests paths that are worthwhile for future research & development activities.

2 State of research

2.1 Fundamentals of Vibration

2.1.1 Natural frequency and resonance

The natural frequency is the frequency at which a system freely vibrates. In a mass-spring system, the natural frequency can be calculated as follow [6],

$$\omega_0 = \sqrt{\frac{k}{M}} \qquad 1)$$

where k and M are the spring stiffness and mass, respectively. Similarly, it can be clearly expressed by a mass-beam system, as shown in Figure 2.1. It means that a system with a lower mass or stiffer structure has a higher natural frequency. A higher mass and/or a softer structure lower the natural frequency.

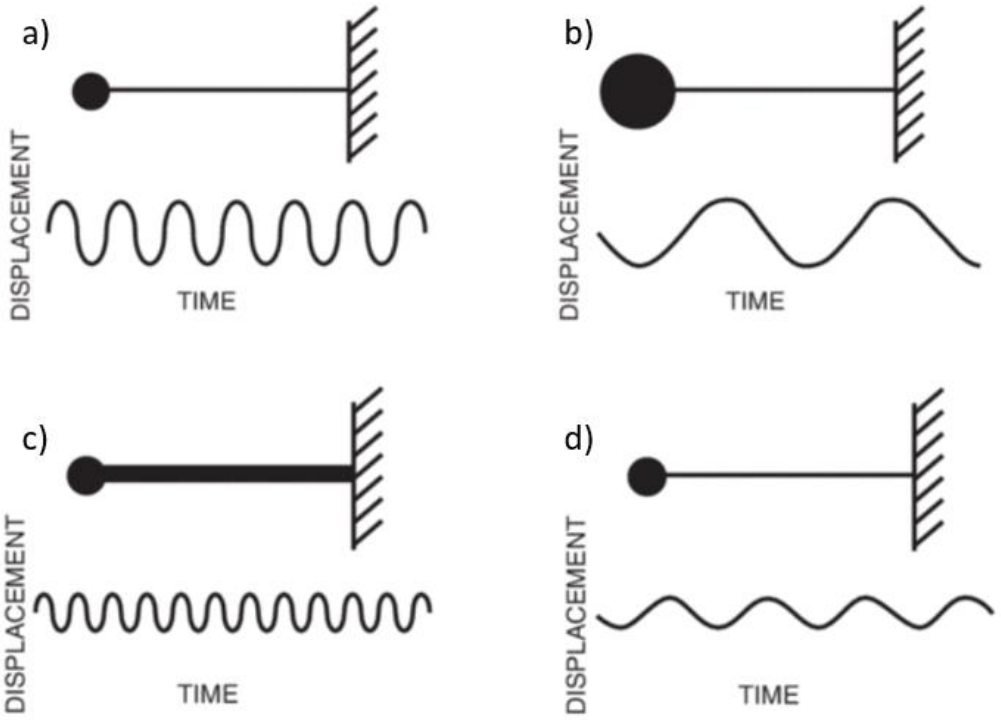

Figure 2.1: a) vs b) lower mass increases the natural frequency. c) vs d) stiffer beam increases the natural frequency [7].

If a periodically external force is applied to the system, the occurring oscillation is known as forced vibration. When the frequency of the applied force is equal or close to the natural frequency of the system, the amplitude of vibration increases manyfold. This is known as resonance [6].

2.1.2 Simple harmonic oscillator

In the cantilevered beam or tuning fork models, the systems are considered to be undamped, as there is no mechanism present which can dissipate the mechanical energy. A system without damping will vibrate for a long period of time before coming to rest. With damping, the mechanical energy in the system is dissipated and the vibrations are attenuated more quickly [7].

A simple harmonic oscillator consisting of a rigid mass *M* and an ideal linear spring is shown in Figure 2.2.

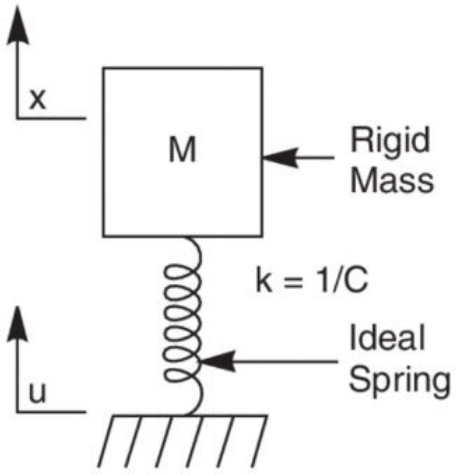

Figure 2.2: A simple harmonic oscillator [7]

The equilibrium equation of the system is given by [7],

$$M\ddot{\mathrm{x}} + k(\mathrm{x} - \mathrm{u}) = 0 \qquad 2)$$

If the spring-mass system is driven by a sinusoidal displacement with frequency ω and peak amplitude $|\mathrm{u}|$, a sinusoidal displacement of the mass M with peak amplitude $|\mathrm{x}|$ at the same frequency ω will be produced. The steady-state ratio of the amplitude of mass motion $|\mathrm{x}|$ to the spring end motion $|\mathrm{u}|$ which is also called transmissibility is given by [7],

$$\mathrm{T} = \frac{|\mathrm{x}|}{|\mathrm{u}|} = \frac{1}{1-\frac{\omega^2}{{\omega_0}^2}} \qquad 3)$$

Where ω_0 is the natural frequency of the system (see equation 1)). ω_0 is only determined by system mass and stiffness.

The transmissibility of the system is commonly plotted as a function of the ratio ω/ω_0 on a logarithmic-logarithmic plot like Figure 2.3. In this figure, three characteristic features are shown:

- a) If $\omega \ll \omega_0$, Transmissibility T=1 which means that the motion of the mass is the same as the motion at the other end of the spring.
- b) If $\omega \approx \omega_0$, Transmissibility T >1, the motion of the mass |x| is infinite which is much greater than that of |u|.
- c) If $\omega \gg \omega_0$, Transmissibility T <1, the resulting displacement decreases in proportion to $1/\omega^2$. The displacement |u| applied to the system is not transmitted to the mass which means that the spring acts as an isolator [7].

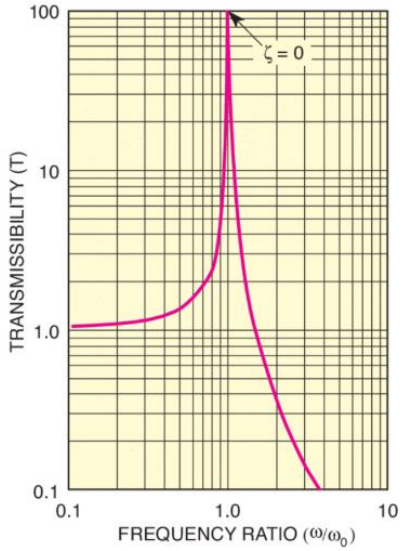

Figure 2.3: Transmissibility of a simple harmonic oscillator [7]

Hence the natural frequency of the system should be staggered from the frequency of applied force to avoid resonance if there is no damping to dissipate the mechanical energy.

2.2 Timoshenko beam theory with FEM method

A beam is a structural element that is used for support. Four theories are widely used to describe this structural element: Euler-Bernoulli [8], Rayleigh [9], Shear [10] and Timoshenko [11] [12]. In

the Euler-Bernoulli theory of flexural vibration of beams which is often called classic beam theory, the effects of rotatory inertia and shear are neglected. This theory is adequate for relatively slender beams. However, it tends to overestimate the natural frequencies of beams with larger cross-sections [13]. The Rayleigh beam theory includes the effects of the rotation of the cross-section which provides an improvement on the classic beam theory. As a result, the overestimation of natural frequencies which occurs with the Euler-Bernoulli model is partially corrected. Nevertheless, the natural frequencies are still overestimated [14]. When shear distortion is accounted for the Euler-Bernoulli model, this is known as the shear model, which improves the estimation of natural frequencies considerably. But it does not fit the purpose of obtaining an improved model to the Euler-Bernoulli model, because it excludes the most important factor, the bending effect [10]. In the Timoshenko beam theory, the effects of shear, as well as the effects of rotation, are added to the Euler-Bernoulli beam. It is a major improvement for non-slender beams and for high-frequency responses where shear and rotatory effects are no longer negligible [13]. Hence the Timoshenko beam theory is normally used for predicting the natural frequencies of transversely dynamically loaded beams. The equilibrium equations of a straight Timoshenko beam can be described by the following differential equations [15],

$$\delta v: -\kappa GA\left(\frac{d^2v}{dx^2}-\frac{d\theta}{dx}\right)+\rho A\frac{d^2v}{dt^2}-q=0 \tag{4}$$

$$\delta\theta: -EI\frac{d^2\theta}{dx^2}-\kappa GA\left(\frac{dv}{dx}-\theta\right)+\rho I\frac{d^2\theta}{dt^2}-m=0 \tag{5}$$

The transversal displacement of the beam and the rotation of the beam's cross-section are given by v and θ, respectively. The elastic modulus and elastic shear modulus of the beam are represented by E and G. ρ and A are the density and cross-sectional area of the beam. I is the second-order moment of inertia of the beam's cross-section. κ is the shear coefficient of the beam which depends on the cross-section and material of the beam. q and m are the applied transversal force per unit length and moment per unit length, respectively.

2.2.1 Derivation of shape functions

The shape functions of the Timoshenko beam can be obtained by solving the homogeneous differential equations of the static equilibrium in equations 4) and 5). Therefore, the dynamic and loading terms in the equilibrium equations are neglected as given below [15]. The displacement in x- and y-direction and the rotation are shown in Figure 2.4.

$$\frac{dv}{dx}\left(\kappa GA\left(\frac{dv}{dx}-\theta\right)\right)=0 \tag{6}$$

$$EI\frac{d^2\theta}{dx^2}+\kappa GA\left(\frac{dv}{dx}-\theta\right)=0 \tag{7}$$

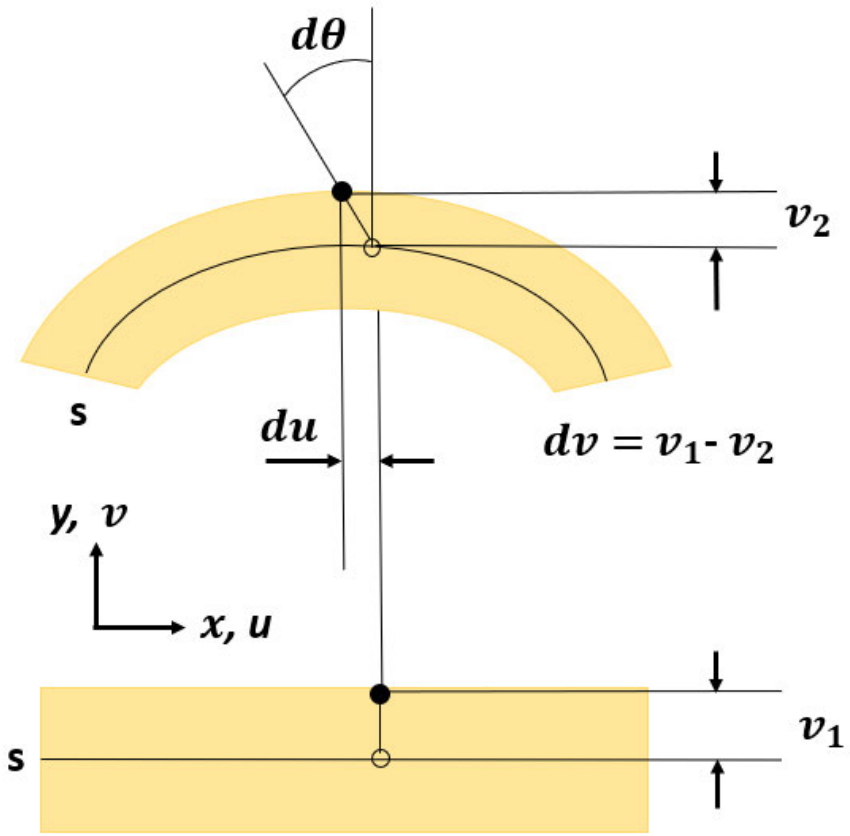

Figure 2.4: Conceptual kinematic of a straight Timoshenko beam

So that the shape functions for v and θ are as follows [15],

$$v = [N_{vv1} \quad N_{v\theta1} \quad N_{vv2} \quad N_{v\theta2}] \begin{Bmatrix} v_1 \\ \theta_1 \\ v_2 \\ \theta_2 \end{Bmatrix} \tag{8}$$

$$N_{vv1} = \frac{1}{4(1+\emptyset)}\{(\xi - 1)(\xi^2 + \xi - 2(1+\emptyset))\} \tag{9}$$

$$N_{v\theta1} = \frac{L}{8(1+\emptyset)}\{(\xi^2 - 1)(\xi - (1+\emptyset))\} \tag{10}$$

$$N_{vv2} = \frac{1}{4(1+\emptyset)}\{(\xi + 1)(-\xi^2 + \xi + 2(1+\emptyset))\} \tag{11}$$

$$N_{v\theta2} = \frac{L}{8(1+\emptyset)}\{(\xi^2 - 1)(\xi + (1+\emptyset))\} \tag{12}$$

$$\theta = [N_{\theta v1} \quad N_{\theta\theta1} \quad N_{\theta v2} \quad N_{\theta\theta2}] \begin{Bmatrix} v_1 \\ \theta_1 \\ v_2 \\ \theta_2 \end{Bmatrix} \tag{13}$$

$$N_{\theta v1} = \frac{3}{2L(1+\emptyset)}(\xi^2 - 1) \quad 14)$$

$$N_{\theta\theta1} = \frac{1}{4(1+\emptyset)}\{(\xi - 1)(3\xi + 1 - 2\emptyset)\} \quad 15)$$

$$N_{\theta v2} = \frac{3}{2L(1+\emptyset)}(-\xi^2 + 1) \quad 16)$$

$$N_{\theta\theta2} = \frac{1}{4(1+\emptyset)}\{(\xi + 1)(3\xi - 1 + 2\emptyset)\} \quad 17)$$

The shape functions (equation 8)-12) and 14)-17)) are function of the ratio of beam bending to shear stiffness $\emptyset$ and ξ. Where,

$$\emptyset = \frac{12EI}{\kappa GAL^2} \quad 18)$$

$$\xi = \frac{2x-L}{L} \quad 19)$$

These shape functions interpolate the vertical displacement or rotation of an arbitrary point along the beam from the nodal displacement and rotation of DOFs (Degree of Freedom) at both ends of the beam as follows,

$$\begin{Bmatrix} v \\ \theta \end{Bmatrix} = \begin{bmatrix} N_{vv1} & N_{v\theta1} & N_{vv2} & N_{v\theta2} \\ N_{\theta v1} & N_{\theta\theta1} & N_{\theta v2} & N_{\theta\theta2} \end{bmatrix} \begin{Bmatrix} v_1 \\ \theta_1 \\ v_2 \\ \theta_2 \end{Bmatrix} \quad 20)$$

2.2.2 Governing equation in matrix form

Via Hamilton's principle the equation of motion is derived as follows:

$$\delta H = \int_{t_1}^{t_2}(\delta S_E - \delta K_E - \delta W_E)dt = 0 \quad 21)$$

δH is the variation of total energy, δS_E, δK_E and δW_E are the variation of beam strain energy, beam kinetic energy and external work, respectively.

The internal strain energy and kinetic energy of the beam at an instant time of $t_1 = t_2$ are given as,

$$S_E = \frac{1}{2}\int_0^L \left\{EI\left(\frac{d^2\theta}{dx^2}\right)^2 - \kappa GA\left(\frac{dv}{dx} - \theta\right)^2\right\}dx \quad 22)$$

$$K_E = \frac{1}{2}\int_0^L \left\{\rho A(\frac{dv}{dt})^2 + \rho I(\frac{d\theta}{dt})^2\right\}dx \quad 23)$$

The external work is defined as,

$$W_E = \int_0^L \{qv + m\theta\}\, dx \tag{24}$$

Where q and m are the applied distributed transversal forces per unit length and moments per unit length, respectively.

The derivatives by x of vertical displacement and roration can be represented by the nodal general displacement vector $\mathbf{d}$,

$$\frac{dv}{dx} = [N'_{vv1} \quad N'_{v\theta 1} \quad N'_{vv2} \quad N'_{\theta\theta 2}] \begin{Bmatrix} v_1 \\ \theta_1 \\ v_2 \\ \theta_2 \end{Bmatrix} = N'_v \mathbf{d} \tag{25}$$

$$\frac{d\theta}{dx} = [N'_{\theta v1} \quad N'_{\theta\theta 1} \quad N'_{\theta v2} \quad N'_{\theta\theta 2}] \begin{Bmatrix} v_1 \\ \theta_1 \\ v_2 \\ \theta_2 \end{Bmatrix} = N'_\theta \mathbf{d} \tag{26}$$

By substituting equations 25) and 26), the internal strain energy equation, the kinetic energy equation and the external work together with boundary conditions equation can be expressed in matrix form as,

$$\boldsymbol{S_E} = \frac{1}{2} \begin{Bmatrix} v_1 \\ \theta_1 \\ v_2 \\ \theta_2 \end{Bmatrix}^T \int_0^L \left\{ \begin{Bmatrix} N'_v - N_\theta \\ N'_\theta \end{Bmatrix}^T \begin{bmatrix} \kappa GA & 0 \\ 0 & EI \end{bmatrix} \begin{Bmatrix} N'_v - N_\theta \\ N'_\theta \end{Bmatrix} \right\} dx \begin{Bmatrix} v_1 \\ \theta_1 \\ v_2 \\ \theta_2 \end{Bmatrix} \tag{27}$$

$$\boldsymbol{K_E} = \frac{1}{2} \begin{Bmatrix} \ddot{v}_1 \\ \ddot{\theta}_1 \\ \ddot{v}_2 \\ \ddot{\theta}_2 \end{Bmatrix}^T \int_0^L \left\{ \begin{Bmatrix} N_v \\ N_\theta \end{Bmatrix}^T \begin{bmatrix} \rho A & 0 \\ 0 & \rho I \end{bmatrix} \begin{Bmatrix} N_v \\ N_\theta \end{Bmatrix} \right\} dx \begin{Bmatrix} \ddot{v}_1 \\ \ddot{\theta}_1 \\ \ddot{v}_2 \\ \ddot{\theta}_2 \end{Bmatrix} \tag{28}$$

$$\boldsymbol{W_E} = \begin{Bmatrix} v_1 \\ \theta_1 \\ v_2 \\ \theta_2 \end{Bmatrix}^T \begin{Bmatrix} N_{v1} Q_1 \\ N_{\theta 1} M_1 \\ N_{v2} Q_2 \\ N_{\theta 2} M_2 \end{Bmatrix} - \begin{Bmatrix} v_1 \\ \theta_1 \\ v_2 \\ \theta_2 \end{Bmatrix}^T \int_0^L \begin{Bmatrix} N_{v1} q \\ N_{\theta 1} m \\ N_{v2} q \\ N_{\theta 2} m \end{Bmatrix} dx \tag{29}$$

Where,

$$N'_v = [N'_{vv1} \quad N'_{v\theta 1} \quad N'_{vv2} \quad N'_{\theta\theta 2}] \tag{30}$$

$$N'_\theta = [N'_{\theta v1} \quad N'_{\theta\theta 1} \quad N'_{\theta v2} \quad N'_{\theta\theta 2}] \tag{31}$$

The finite element formulation for a straight Timoshenko beam can be developed by using the theory of minimum potential energy to obtain the equilibrium equation in matrix form,

$$\Pi = \frac{1}{2}\mathbf{d}^T\mathbf{K}\mathbf{d} - \frac{1}{2}\ddot{\mathbf{d}}^T\mathbf{M}\ddot{\mathbf{d}} - \mathbf{d}^T\mathbf{f} \quad 32)$$

$$\frac{\partial \Pi}{\partial \mathbf{d}^T} = \mathbf{K}\mathbf{d} - \mathbf{M}\ddot{\mathbf{d}} - \mathbf{f} = \mathbf{0} \quad 33)$$

The two points on $\mathbf{d}$ means the second derivative with respect to time. $\mathbf{K}$, $\mathbf{M}$ and $\mathbf{f}$ are the stiffness matrix, the mass matrix and the loading vector as follows,

$$\mathbf{K} = \int_0^L \left\{ \begin{Bmatrix} N'_v - N_\theta \\ N'_\theta \end{Bmatrix}^T \begin{bmatrix} \kappa GA & 0 \\ 0 & EI \end{bmatrix} \begin{Bmatrix} N'_v - N_\theta \\ N'_\theta \end{Bmatrix} \right\} dx \quad 34)$$

$$\mathbf{M} = \int_0^L \left\{ \begin{Bmatrix} N_v \\ N_\theta \end{Bmatrix}^T \begin{bmatrix} \rho A & 0 \\ 0 & \rho I \end{bmatrix} \begin{Bmatrix} N_v \\ N_\theta \end{Bmatrix} \right\} dx \quad 35)$$

$$\mathbf{f} = \begin{Bmatrix} N_{v1}Q_1 \\ N_{\theta 1}M_1 \\ N_{v2}Q_2 \\ N_{\theta 2}M_2 \end{Bmatrix} + \int_0^L \begin{Bmatrix} N_{v1}q \\ N_{\theta 1}m \\ N_{v2}q \\ N_{\theta 2}m \end{Bmatrix} dx \quad 36)$$

So that the stiffness element matrix of the Timoshenko beam can be given as,

$$\mathbf{K}_E = \frac{EI}{(1+\emptyset)L^3} \begin{bmatrix} 12 & 6L & -12 & 6L \\ 6L & (4+\emptyset)L^2 & -6L & (2-\emptyset)L^2 \\ -12 & -6L & 12 & -6L \\ 6L & (2-\emptyset)L^2 & -6L & (4+\emptyset)L^2 \end{bmatrix} \quad 37)$$

The mass element matrix of a Timoshenko beam consists of $\mathbf{M}_{\rho A}$ which is associated with the translational inertia and $\mathbf{M}_{\rho I}$ which is associated with the rotatory inertia,

$$\mathbf{M}_E = \mathbf{M}_{\rho A} + \mathbf{M}_{\rho I} \quad 38)$$

Where,

$$\mathbf{M}_{\rho A} = \frac{\rho AL}{210(1+\emptyset)^2}$$

$$\times \begin{bmatrix} (70\emptyset^2 + 147\emptyset + 78) & (35\emptyset^2 + 77\emptyset + 44)\frac{L}{4} & (35\emptyset^2 + 63\emptyset + 27) & -(35\emptyset^2 + 63\emptyset + 26)\frac{L}{4} \\ (35\emptyset^2 + 77\emptyset + 44)\frac{L}{4} & (7\emptyset^2 + 14\emptyset + 8)\frac{L^2}{4} & (35\emptyset^2 + 63\emptyset + 26)\frac{L}{4} & -(7\emptyset^2 + 14\emptyset + 6)\frac{L^2}{4} \\ (35\emptyset^2 + 63\emptyset + 27) & (35\emptyset^2 + 63\emptyset + 26)\frac{L}{4} & (70\emptyset^2 + 147\emptyset + 78) & -(35\emptyset^2 + 77\emptyset + 44)\frac{L}{4} \\ -(35\emptyset^2 + 63\emptyset + 26)\frac{L}{4} & -(7\emptyset^2 + 14\emptyset + 6)\frac{L^2}{4} & -(35\emptyset^2 + 77\emptyset + 44)\frac{L}{4} & (7\emptyset^2 + 14\emptyset + 8)\frac{L^2}{4} \end{bmatrix}$$

$$\mathbf{M}_{\rho I} = \frac{\rho I}{30(1+\emptyset)^2 L}$$

$$\times \begin{bmatrix} 36 & -(15\emptyset-3)L & -36 & -(15\emptyset-3)L \\ -(15\emptyset-3)L & (10\emptyset^2+5\emptyset+4)L^2 & (15\emptyset-3)L & (5\emptyset^2-5\emptyset-1)L^2 \\ -36 & (15\emptyset-3)L & 36 & (15\emptyset-3)L \\ -(15\emptyset-3)L & (5\emptyset^2-5\emptyset-1)L^2 & (15\emptyset-3)L & (10\emptyset^2+5\emptyset+4)L^2 \end{bmatrix}$$

2.3 Polymer electrolyte coated carbon fibre (PeCCF) composite structure

A composite material made from polymer electrolyte coated carbon fibres (PeCCF) and a polymeric matrix material can provide several functions. Apart from load bearing, research identified other potential functions like energy storage, energy transmission and thermal heating. Structures made from this material are usually architectured in several plies with similar thickness but different fibre orientations. This can be compared with classic fibre reinforced plastics. [4].

LI batteries consist of four main components: anode, cathode, electrolyte and separator. They are shown in Figure 2.5. The anode and cathode store the lithium. When the battery is charging, lithium ions are released by the cathode and resolved in electrolyte then through the separator until they are received by the anode. While the battery is discharging and providing an electric current, the anode releases positively charged lithium ions to the cathode through the separator. The movement of the lithium ions creates free electrons in the anode which creates a charge at the positive current collector. The electrical current flows from the positive current collector through a device being powered to the negative current collector. The separator blocks the flow of electrons inside the battery [16].

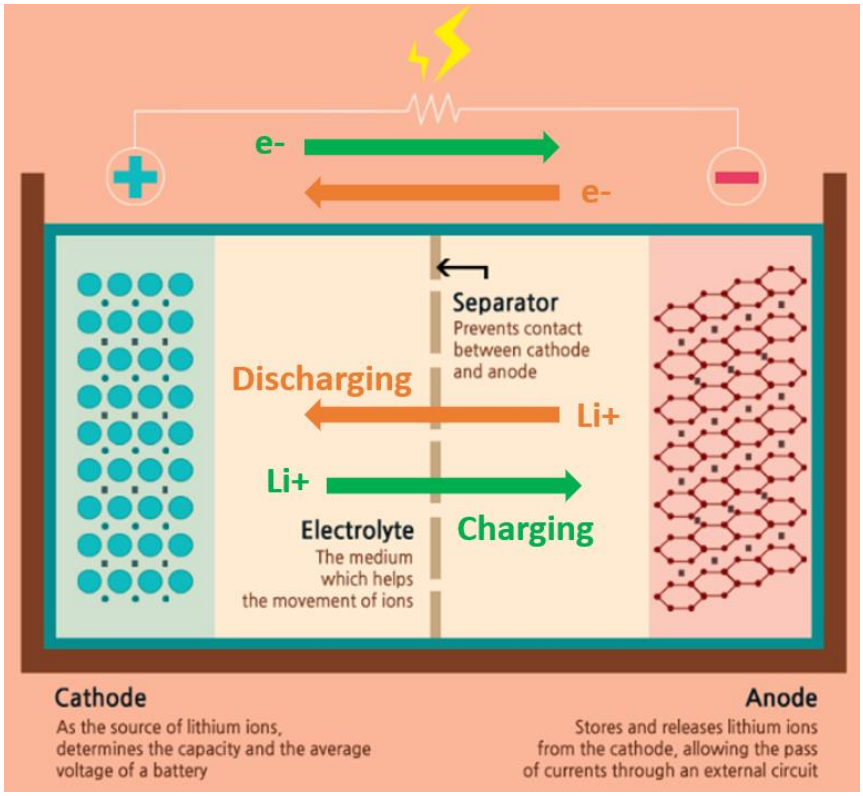

Figure 2.5: Structure of LI battery [17]

Compared with a normal carbon fibre composite material the carbon fibres in the battery are coated with a thin layer of solid polymer electrolyte (SPE) which functions both as a separator and an electrolyte. The carbon fibre is used as an anode and the matrix material represents the cathode and current collector [4]. The detailed structure of the battery is shown in Figure 2.6.

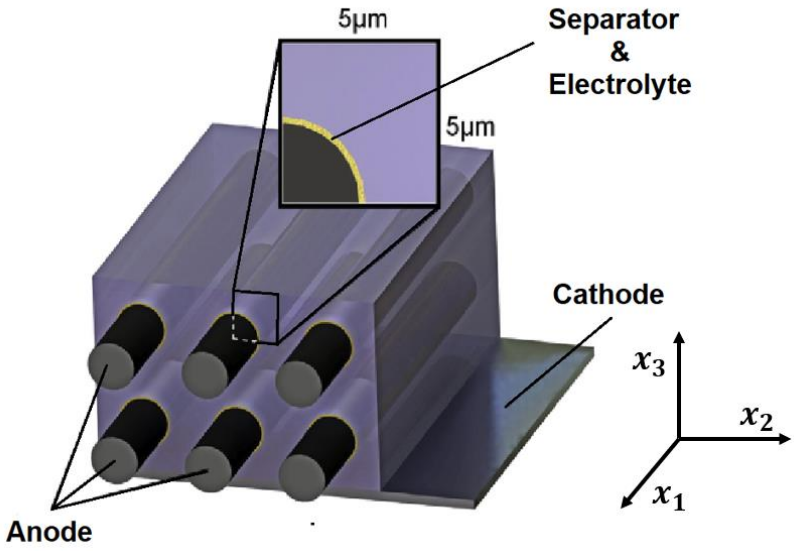

Figure 2.6: Cross-section of structural battery [4]

However, there are two limiting parameters for such a structural battery with SPE. The first limitation is the ion conductivity. The second is the ion transport distance between two electrodes. These two parameters influence the loss of potential during cycling due to the ion transport resistance, which is also called “ohmic drop”. To reduce ohmic drop, the ion conductivity should be increased or the ion transport distance should be decreased [4].

2.3.1 Carbon fibres

In the last few years, many advanced and specialised carbon fibre types are developed and are applied widely in the aerospace and automobile industry. The fibre types with different multifunctional properties have different potential for application in energy storage devices. Major factors are the lithium ions intercalate ability within the carbon microstructure, the usability for electropolymerization and classical mechanical properties [4]. Collected different sources the parameters of different carbon fibre types are shown in Table 2.1.

Fibre type	Diameter [µm]	Tensile modules [GPa]	Tensile strength [MPa]	Specific resistance [Ωmm]	Reversible capacity [mAh/g]
IMS65	5	290	6000	$1.45 \cdot 10^{-2}$	N.s.
IMS65 (unsized)	5	290	6000	N.s.	360
HTS40	7	240	4400	$1.60 \cdot 10^{-2}$	N.s.
T800 (unsized)	5	294	5490	$1.40 \cdot 10^{-2}$	130
UMS45	4.7	430	4500	$9.70 \cdot 10^{-3}$	30
Cytec P-120 2K	N.s.	828	2240	$2.20 \cdot 10^{-3}$	N.s.

Table 2.1: Multifunctional properties of commercially available carbon fibres. (specific resistance at 293.15 K. reversible capacity after 10 cycles charge-discharge) [18] [19] [20]

For the application in structure batteries, a high reversible capacity is important. The carbon fibre type IMS65 has the biggest reversible capacity. Therefore, IMS65 has been chosen for this work due to its desired characteristics.

2.3.2 Polymer electrolyte coating

Compared with liquid polymer electrolytes the SPE has a substantially lower ion conductivity, whilst this property is not desirable, it is feasible since the liquid polymer electrolytes can not bear any mechanical loads. The ion transport distance is equal to the thickness of the SPE since the SPE is used as an electrolyte and a separator.

As in Table 2.2 shown with the same thickness the effective conductivity of SPE is three magnitudes lower compared to a liquid electrolyte, therefore, its ohmic drop increases three magnitudes. When the electrolyte thickness decreases to 500 nm the ohmic drop is cut down significantly, thus making the battery performance better. Since the recent studies found out that property gradient effects are only significant below the thickness of 200 nm, meaning the effects are less noticeable with the thickness of 500 nm. 500 nm is a very thin SPE layer and its ohmic drop is much better, this thickness is used for later studies [4] [21].

	Liquid electrolyte	Solid polymer electrolyte	
Electrolyte thickness	30 µm	30 µm	500 nm
Effective conductivity	0.7 mS/cm	1.5 µS/cm	1.5 µS/cm
Ohmic drop at $1\ \mathrm{mA/cm^2}$	4 mV	2 V	34 mV

Table 2.2: Dependency of ohmic drop on type of electrolyte and ion transport distance [22]

During research in the past years, the monomer-salt mixtures presented in Table 2.3 are well investigated. The monomers are available in liquid condition and are solved in Dimethylformamide (DMF) prior to electropolymerization. The resulting mechanical properties are presented below. Comply with the recommendations from Leijonmarck [23] systems with a salt content between 8 and 12 weight percentage are chosen. However, the elastic modulus varies between 1400 MPa and nearly no elastic modulus. The polymer made only from monomer A, methoxy polyethylene glycol monomethacrylate (SR550), has nearly no mechanical behaviour and behaves like a viscous gel. Different from monomer A the monomer B, tetraethylene glycol dimethacrylate (SR209), generates a very brittle surface that tends to peel off the carbon fibre. Moreover, monomer B has very low ionic conductivity. The mixture of both monomer A and B by a 1:1 ratio could have increased surface stability while its modulus is decreased by monomer A. Furthermore, because of monomer A, the ion conductivity of the mixture can be increased significantly. This indicates that ionic conductivity is inversely proportional to mechanical stiffness.

The higher the elastic modulus the polymer has, the lower its ionic conductivity becomes [4]. In this work, the coating which consists of a mixture of monomer A and monomer B by a 1:1 ratio and 8% lithium trifluoromethanesulfonate (li-triflate) is chosen.

Monomer	Chemical indication	Salt content [%]	Ionic conductivity [S/cm]	Modulus [MPa]	Comment
A	SR550	12	$1.50 \cdot 10^{-5}$	<1	Viscous
B	SR209	12	$2.08 \cdot 10^{-10}$	1417	Brittle
A+B	-	12	$5.50 \cdot 10^{-8}$	770	N.s.
A+B	-	8	$5.00 \cdot 10^{-8}$	820	N.s.

Table 2.3: Physical properties of polymers. Resulting from monomers after electropolymerization [22] [23]

The material properties of applied carbon fibre, resin and SPE are shown in Table 2.4. The layer of laminate is made of IMS65 carbon fibre, epoxy resin and the SPE coating which consists of monomer A and monomer B by 1:1 ratio. To enable ion conductivity this mixture contains 8% li-triflate and is dissolved in Dimethylformamide (DMF). The modulus of the SPE varies with temperature which changes due to altitude or heat generation while the battery is operating. In the table below the modulus and CTE of coating are expressed in a range which is calculated from the temperature range of [273.5K, 343.5K] and studied in former research [21].,

Phase	Symbol	Value	Unit	Explanation
Fibre	$E_{1,f}$	290	GPa	Longitudinal modulus, x_1
IMS65	$E_{2,f}$	8	GPa	Transverse modulus x_2x_3 plane
	$G_{12,f}$	15	GPa	Shear modulus x_1x_2 plane
	$G_{23,f}$	3	GPa	Shear modulus x_2x_3 plane
	$\nu_{12,f}$	0.2	1	Poisson's ratio x_1x_2 plane
	$\nu_{23,f}$	0.4	1	Poisson's ratio x_2x_3 plane
	$\alpha_{1,f}$	$-4.2 \cdot 10^{-7}$	1/K	Fibre CTE, x_1
	$\alpha_{2,f}$	$4.9 \cdot 10^{-6}$	1/K	Fibre CTE, x_2x_3 plane
SPE Coating	E_c	[0.5, 2]	GPa	Young's modulus range studied
	ν_c	0.3	1	Poisson's ratio
	α_c	$[4 \cdot 10^{-5}, 4 \cdot 10^{-4}]$	1/K	CTE range studied
Matrix Epoxy resin	E_m	2	GPa	Young's modulus Epoxy matrix
	ν_m	0.3	1	Poisson's ratio
	α_m	$2.44 \cdot 10^{-5}$,	1/K	Matrix CTE

Table 2.4: Material constants of PeCCF [21]. Directions correspond to the coordinate system in Figure 2.6

2.4 Micromechanics analysis of PeCCF composite in COMSOL

The micromechanics analysis of a single electrolyte coated carbon fibre in a resin can be performed using the *Cell Periodicity* node available in the *Solid Mechanics* interface. Using this functionality, the elastic matrix of the homogenized material can be computed for a given coated fibre and resin properties, and the fibre volume fraction [2].

With the help of the COMSOL tutorial [2] the unit cell is created and shown in Figure 2.7a). The blue cube represents the matrix, the yellow ring is the electrolyte coating whose thickness t is 500 nm and the black circle is the carbon fibre whose radius r is $2.5 \cdot 10^{-6}$ m. The fibre volume fraction v_f is 0.5, from that the side length of the cube a can be calculated by following:

$$a = \sqrt{\pi(t+r)^2/v_f} \tag{39}$$

After inputting the parameters of matrix, carbon fibre and coating according to Table 2.4 under the material section in COMSOL, the *Cell Periodicity Study* function is used to generate the PeCCF composite material. Then the cross-section of a unit cell is meshed with the *Free Triangular* element type. The meshed model is shown in Figure 2.7b). After computing this study the PeCCF composite material is successfully created and its material properties (stiffness, density. etc) can be used for the following beam simulation. Furthermore, this special arrangement related to PeCCF was studied by Schutzeichel et al [3] [21]

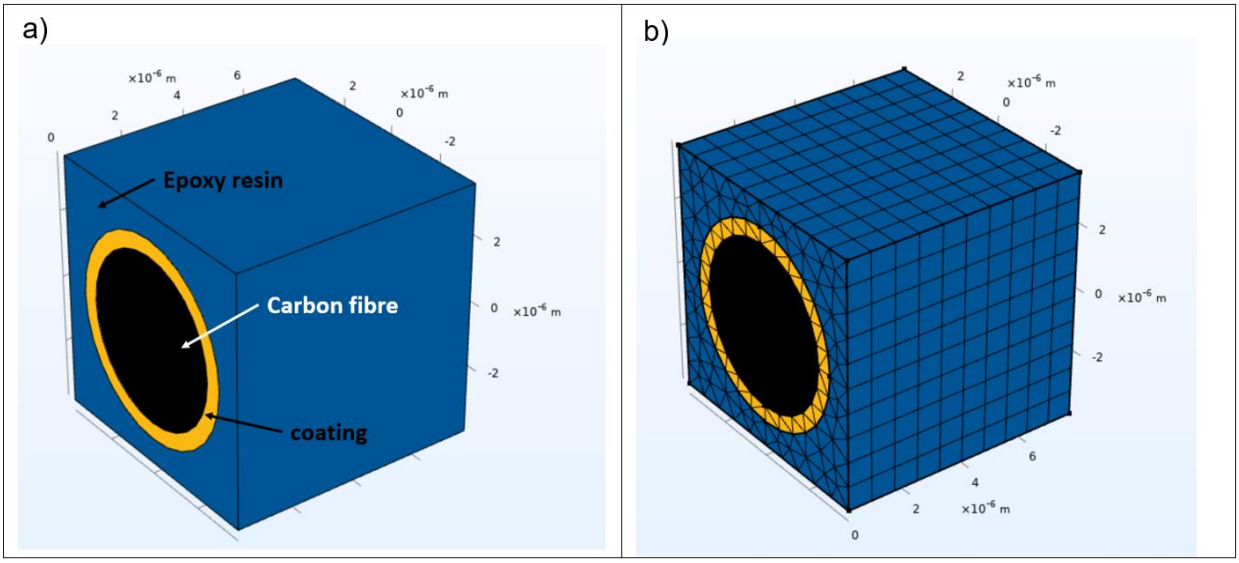

Figure 2.7: a) Components of unit cell model in COMSOL; b) Unit cell with mesh

2.5 Layerweise (LW) Theory

Modelling individual coated fibres in every layer in the laminate is unfeasible. A simplified micromechanics model of a single carbon fibre in epoxy is instead used to estimate the elastic properties of a single layer. These properties are then used in the homogenized model of the laminated composite cantilever beam. Two approaches are available in COMSOL to model the laminate, namely the Layerwise (LW) theory and the Equivalent Single Layer (ESL) theory [2].

The LW theory describes laminated composites as an assembly of individual layers, or uses a 1D interpolation function to simulate the displacement and/or stress fields along the thickness direction. The LW theory is useful for detailed modelling of thick composite laminates because it can capture interlaminar shear stresses [2]. Besides, with LW theory In-plane finite element meshing is independent of the out-of-plane (thickness direction) meshing and a separate shape function order can be chosen in the thickness direction in order to avoid shear locking [24].

The classical laminated plates theory (CLPT) and the first-order shear deformation theory (FSDT) are two most popular ESL theories, and widely used in design, analysis and optimize of the composite engineering structures. The ESL theory can provide good results for the global responses of very thin laminated composite plates and shells, for example, the gross deflection, the critical buckling loads, the fundamental vibration frequencies and the associated mode shapes, but poor results for the thick laminated composites, especially the local responses, such as the distribution of ply-level stresses [25].

In this thesis, the LW theory is used. Because the LW theory is more accurate than the ESL theory, although it is significantly more expensive in terms of computer resources. Furthermore, the LW theory is suitable for thick composite laminates while the ESL theory gives only good results for the very thin laminates [25]. Moreover, with LW theory the fibre orientation, layer thickness and stacking sequence can be defined, which is important for subsequent optimization.

The degrees of freedom in the LW theory are the displacements (u, v, w) available on the modelled surface as well as in the through-thickness direction. From a constitutive equation point of view, the LW theory is similar to 3D solid elasticity [2]. There are two approaches depending on the way degrees of freedom are defined: partial displacement field approach and full displacement field approach. In the partial displacement field approach, the laminate thickness remains constant, whereas the full displacement field approach allows a change in thickness of the laminate. In COMSOL Multiphysics, a full displacement field based LW theory is implemented [24].

Modelling a composite laminated structure based on LW theory requires a surface geometry (2D), typically referred to as a base surface, and a *Layered Material* node which adds an extra dimension (1D) to the base surface geometry in the surface normal direction. Using the *Layered Material* functionality in COMSOL, several layers of different thickness, material properties and fibre orientations can be modeled. Furthermore, symmetric, antisymmetric or repeated laminate can be constructed using a transform option [2].

2.6 Frequency of noise in an aircraft cabin

The noise produced by an aircraft engine is harmful to people working in close proximity due to its high sound pressure level (SPL) and it is a key factor in the realm of flight comfort. At the same time, the vibration due to engine operation influences the service life of the aircraft. Furthermore, airframe noise which is caused by unstable flow around the airframe is a major cause of cabin noise. Therefore, it is important to take care of the frequency of cabin noise to avoid resonance and reduce its SPL.

In this paper, a Cessna 172 was observed. In Figure 2.8 the noise in a Cessna Skyhawk 172 cabin during the cruise is shown. The bold curve is the modified reference signal [26]. In this figure, we can see the resonance frequencies. The first resonance frequency is approximately 90 Hz. The second one is 170 Hz and the third and fourth are 250 Hz and 295 Hz. These resonance frequencies are the mixed effect of the propeller and flow. In this work, these resonance frequencies will be used as references to optimize the structure so that their natural frequencies can be tuned to avoid the resonant frequencies of cabin noise or do not coincide with these resonant frequencies [26].

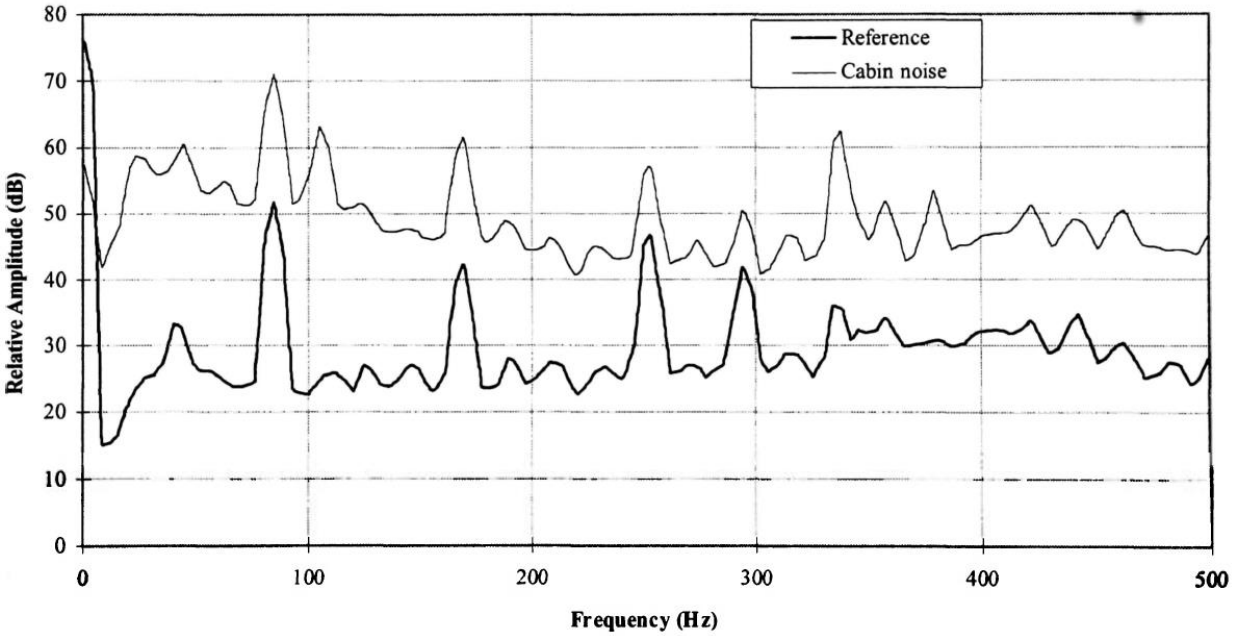

Figure 2.8: Cessna Skyhawk 172 cabin noise and reference signal spectra during cruise [26]

2.7 Genetic Algorithm (GA)

A Genetic Algorithm (GA) is an evolutionary stochastic optimisation procedure that is based on Darwin theory. In this context the stochastic means that the stochastic changes are applied in current solutions to find a better solution. Furthermore, the solution is changed slightly each time to find the best solution.

GA works on a population that consists of many solutions. Each solution is referred to as an individual. Each individual has a chromosome that includes a lot of parameters, these parameters define the particular individual. Every individual has a fitness value, this allows the best individual to be chosen using a fitness function. The result of the fitness function is the fitness value which represents the quality of the solution. The greater the fitness value, the higher the quality of the solution which in turn, allows the best individuals to be selected depending on the quality of the solution. These selected best individuals together create a mating pool, so that the higher quality individuals are more likely to be selected. The individuals in the mating pool are called parents and together the two parents generate two offspring. This process is called crossover which is shown in Figure 2.9. The offspring with higher quality is kept and the lower quality of offspring will

be sorted out. By the means of continuous selection and summarization, only the individuals with good quality are left. In the end, the procedure finds the best solution [27].

However, the offspring which are generated by the parents are not changed and have only the properties of their parents. So that these offsprings could have some of the same disadvantages as their parents. In order to solve this problem, a few changes in the offspring are made and then new offspring are generated. This process is called mutation which is shown in Figure 2.9. These newly generated individuals create a new population that replaces the old population. The new population is called generation. The whole process of GA is shown in Figure 2.10.

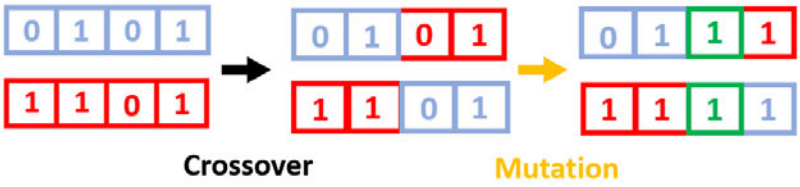

Figure 2.9: The mating steps

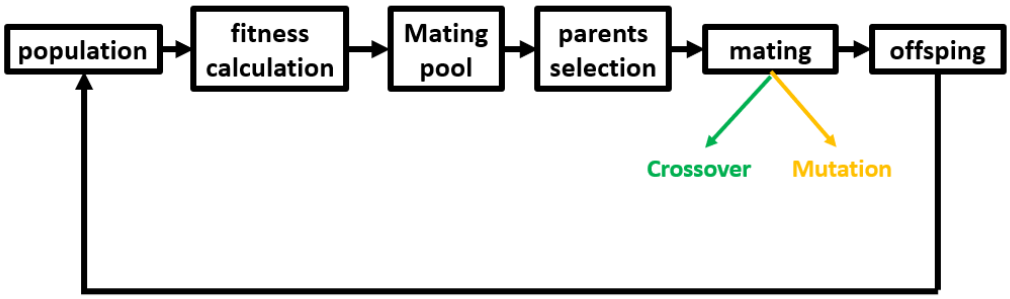

Figure 2.10: The flow chart of GA

Today GA is very often used for solving problems whose fitness functions are discontinuous, not differentiable, stochastic or highly non-linear. This optimization procedure is used in many software programs. For example, in Matlab, the GA is used to find the minimum value of the fitness function. In this thesis, the GA is used to find the best combination of fibre orientation which causes the least kinetic energy at the resonant frequency.

3 Simulation framework for dynamically loaded structures

Before the potential of vibration control with PeCCF is investigated, a simulation framework for dynamically loaded structures will be created and developed. In this chapter, it was chosen to simulate the span of an airplane wing. Due to their transverse loaded character and beam structure, it may show significant vibration reduction by reducing structural stiffness. At first, the span is simulated in Matlab using the FEM method. Simultaneously a simulation in COMSOL was carried out. In the end, both results were compared and verified, then the simulation framework in COMSOL is used for investigation on PeCCF composites afterwards. At the same time, the Matlab simulation is validated.

3.1 FEM Simulation with Matlab and COMSOL 5.5

In this chapter, a Timoshenko beam is created analytically via Matlab and with FEM software COMSOL. The Young's modulus of both beams is $7 \cdot 10^{10}$ Pa. After comparing their natural frequencies the accuracy of the Matlab model is verified.

3.1.1 Timoshenko beam simulation with Matlab

In this numerical simulation, the Timoshenko beam theory was used (see chapter 2.2). The beam consists of 15 elements and measures 1400 mm x 150 mm x 30 mm (length x height x width). From equations 33), 37) and 38) the equilibrium equation in matrix form for Timoshenko beam is:

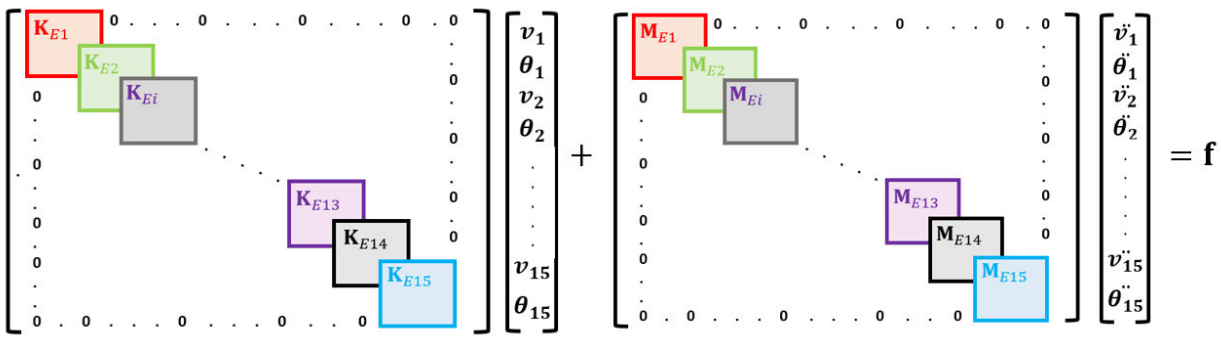

After resolving the equation above, the natural frequencies of the Timoshenko beam are generated. The Matlab codes are shown in Appendix A. The results of the simulation are shown

in Figure 3.1. In the figure, we can see the first 10 natural frequencies of the beam and their mode shapes. The Timoshenko beam consists of 15 elements and has a Boundary condition of clamped-free which means that at x=0 the displacement is zero and at x=1400 mm the displacement is maximum. Here $\mathbf{f}$ is a zero vector.

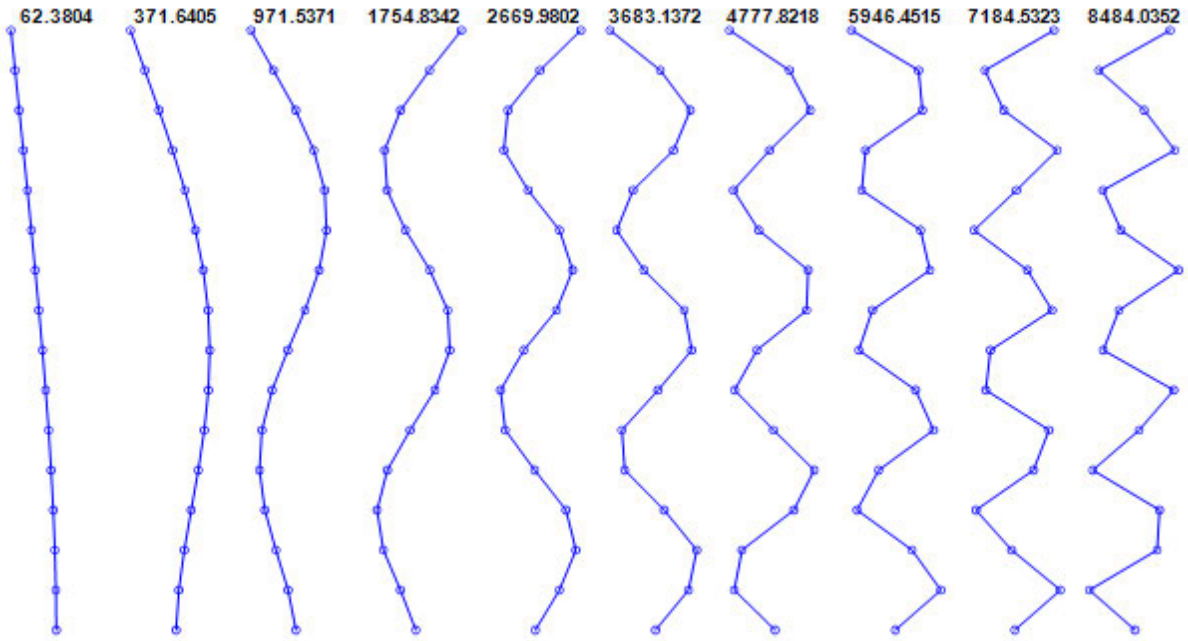

Figure 3.1 First 10 natural frequencies and their mode shapes of Timoshenko beam

3.1.2 Timoshenko beam simulation with COMSOL 5.5

Then a 2D Timoshenko beam was built in COMSOL. This COMSOL model has same dimension, element number and boundary condition as Matlab model in chapter 3.1.1. Therefore, the COMSOL model can be verified by the Matlab model and be used for later investigation. The *Eigenfrequency* functionality was used to calculate the natural frequencies. The tutorial for the COMSOL model is shown in Appendix B. The results of the COMSOL simulation are shown below. In Figure 3.2, Figure 3.3 and Figure 3.4 we can see the first 14 natural frequencies and their mode shapes. Comparing with Figure 3.1 we can see that most natural frequencies and their mode shapes are identical to the results of the Matlab simulation. But the third, the seventh, the ninth and the twelfth natural frequencies are not shown in Figure 3.1. This could be caused by the theory in chapter 3.1.1 which does not consider longitudinal deformation. At these inconsistent frequencies, the mode shapes show that the beam undergoes only axial deformation. In this case it is understandable that these natural frequencies do not match the results in chapter 3.1.1.

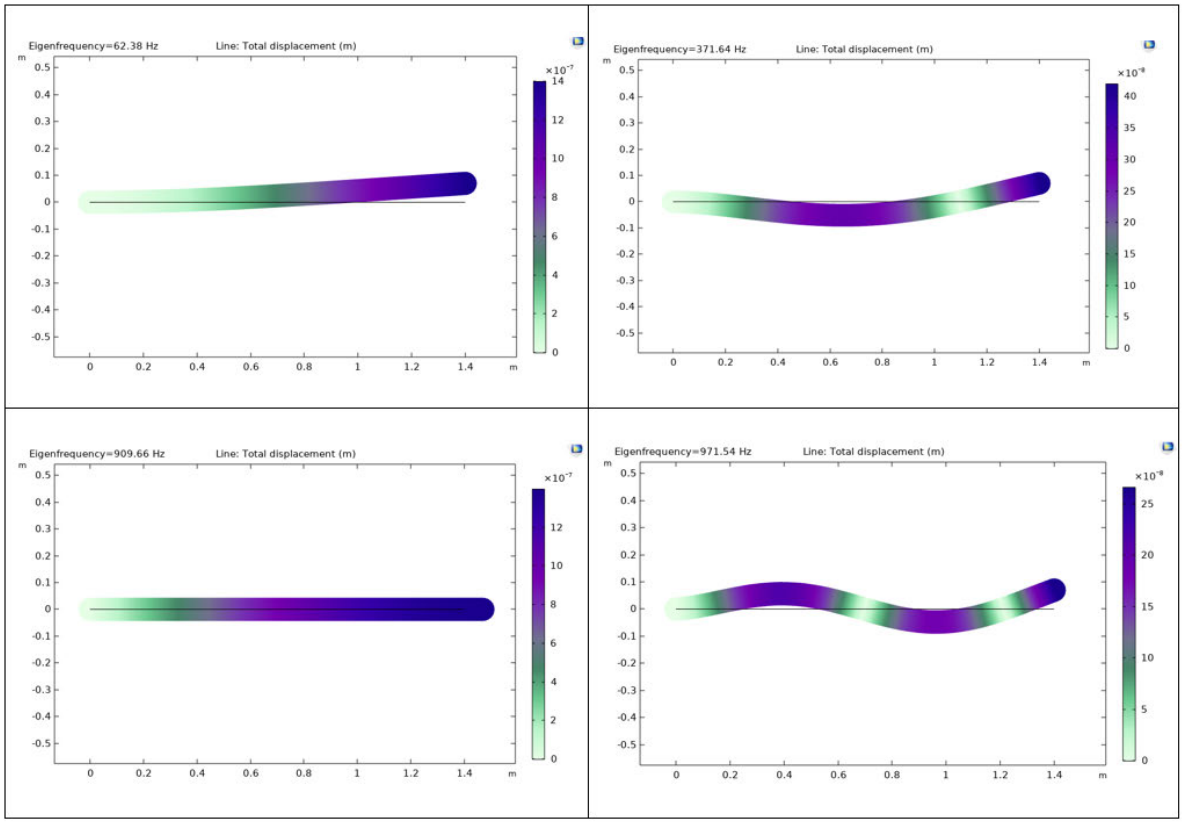

Figure 3.2: The first four natual frequencies and their mode shapes of the Timoshenko beam

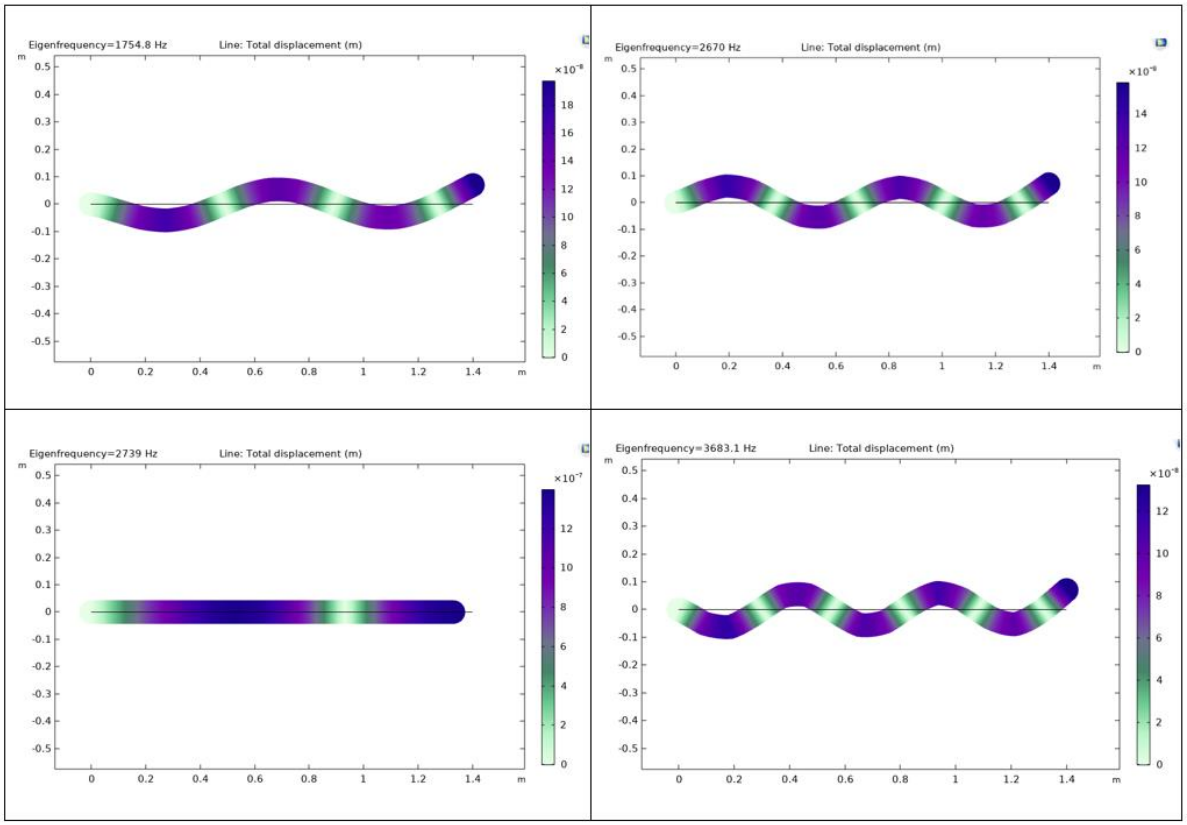

Figure 3.3: The fifth to eighth natual frequencies and their mode shapes of the Timoshenko beam

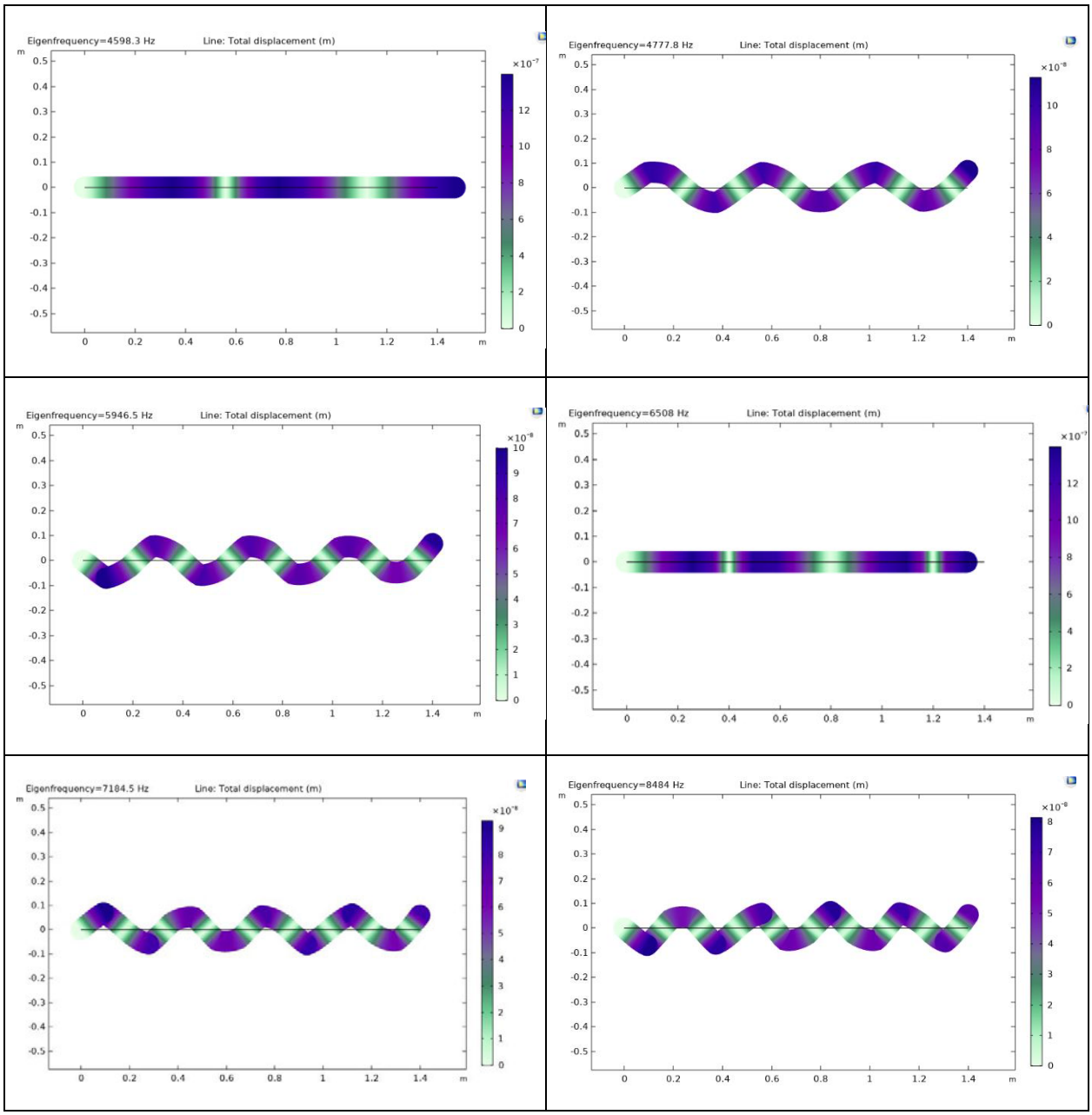

Figure 3.4: The ninth to fourteenth natural frequencies and their mode shapes of the Timoshenko beam

In order to compare the natural frequencies from these two methods conveniently and intuitively, the first 10 natural frequencies of the Matlab and COMSOL models are shown in Table 3.1. In the table, we can see that the natural frequencies of the two models are identical. However, in the COMSOL model the natural frequencies, which are shown in the left column, are not shown in the Matlab model. At these frequencies, the beam is elongated axially, this is because the Matlab simulation does not consider axial displacement. After verification, the COMSOL model was used for the subsequent investigations.

Number of natural frequency	Matlab [Hz]	COMSOL [Hz]	Only axial displacement [Hz]
1.	62.38	62.38	
2.	371.64	371.64	
			909.66
3.	971.54	971.54	
4.	1754.83	1754.83	
5.	2669.98	2669.98	
			2739.00
6.	3683.14	3683.14	
			4598.30
7.	4777.82	4777.82	
8.	5946.45	5946.45	
			6508.00
9.	7184.53	7184.53	
10.	8484.04	8484.04	

Table 3.1: The natural frequencies of Matlab and COMSOL models

3.2 Vibration control potential investigation of beam

In this chapter, the potential of vibration reduction will be investigated. The structural natural frequency is related to stiffness (Young's modulus) and mass (see chapter 2.1). In the PeCCF structure, Young's modulus of the fibre coating varies with temperature (see Table 2.4), which is caused by joule heat generated from energy production and transmission. The fibre orientation

changes the stiffness in specific direction as well. To simulate this effect Young's modulus of the COMSOL beam model is changed and their total kinetic energy phys.Wk_tot at specific frequencies are compared. In COMSOL the total kinetic energy phys.Wk_tot is a global variable containing integration and summation of all kinetic energy contributions in a physics interface [28] Wk is defined as,

$$\mathrm{Wk} = \frac{1}{4}\rho\omega^2|v^2| \qquad 40)$$

3.2.1 Results comparison

At first, the same 2D Timoshenko beam as in chapter 3.1.2 is created in COMSOL. To obtain the total kinetic energy of the beam, the study *Frequency Domain* is used. From chapter 3.1 we know that the first resonant frequency is 62.38 Hz so that the total kinetic energy of the beam with different Young's modulus were compared at 60 Hz to see if a change in Young's modulus can reduce the vibrations near the resonant frequency. The COMSOL beam is excited with a 60 Hz sinusoidal force. The results from the COMSOL model are exported in Matlab and shown in Figure 3.5. The Matlab code is shown in Appendix C. After considering the Young's modulus of applied structural materials, the Young's modulus from $7 \cdot 10^9$ Pa to 10^{11} Pa is chosen. As shown in Figure 3.5, when Young's modulus is equal to $6.48 \cdot 10^{10}$ Pa, the total kinetic energy reaches its maximum. Except for this value, the total kinetic energy is significantly lower. From this result, we can conclude that beam vibration can be controlled by adjusting the stiffness of the beam. By avoiding the stiffness of the beam at a specific value, the total kinetic energy of the beam is much smaller.

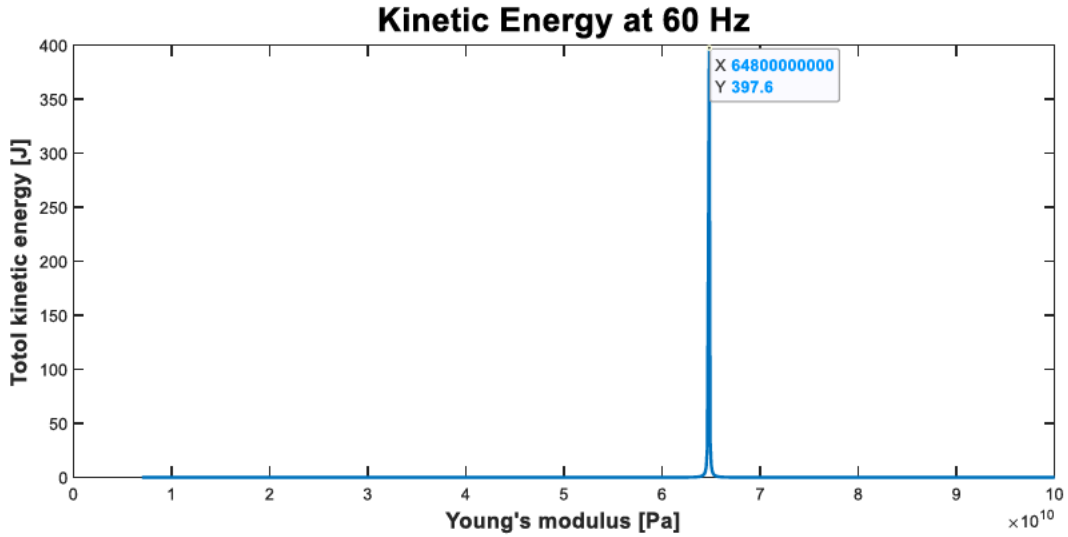

Figure 3.5: Total kinetic energy vs Young's modulus of Timoshenko beam at 60 Hz

To verify the result in Figure 3.5, the frequency spectrum of the COMSOL model with different Young's moduli are compared (see Figure 3.6). The blue curve represents the model with E=$6.48 \cdot 10^{10}$ Pa. Compared with Figure 3.5 and Figure 3.6 we can found that their results are correspond with each other. The peak of blue curve is at 60 Hz while the red and black curve has much smaller value at 60 Hz. Furthermore, the peak of red and black curve are lower than the peak of blue curve. This result shows that by varying the stiffness of the beam, the resonant frequency of the structure can be moved to a frequency range that is not in a similar range as the cabin noise frequency, so that the resonance can be avoided and cabin noise reduced.

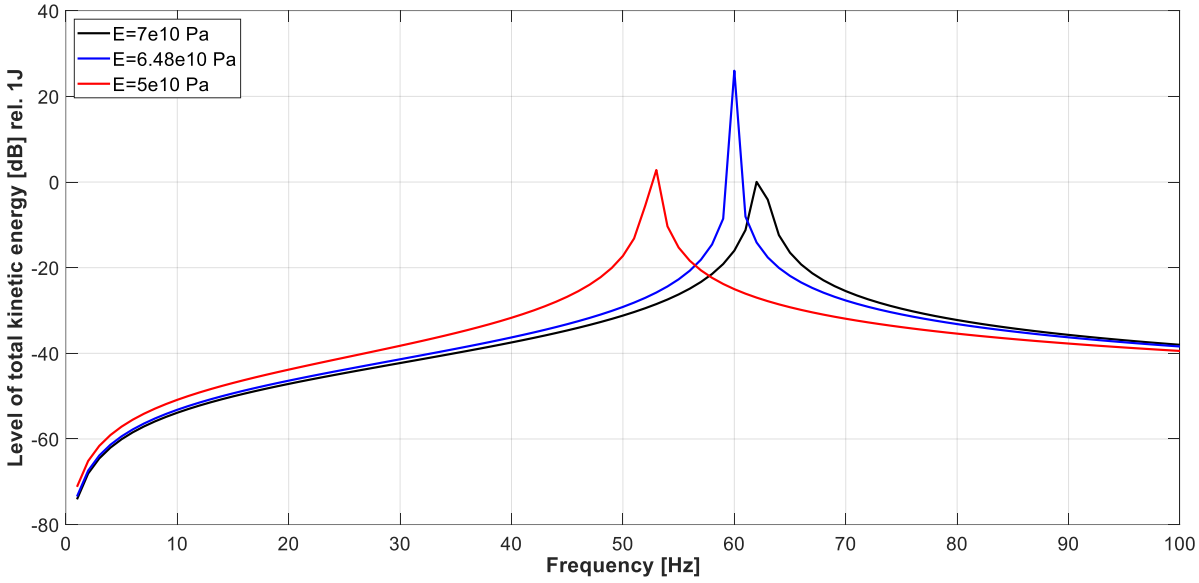

Figure 3.6: The frequency spectrum of the COMSOL beam with different Young's moduli.

4 Analysis of the structural vibration reduction potential of multifunctional PeCCF

In this chapter a PeCCF composite beam is constructed via COMSOL and the vibration reduction effect of different variables are analyzed. At first the properties for carbon fibre and resin are defined in micro level (see Figure 4.1). Based on the properties in micro level the layer material can be defined. From layer level the properties of laminate can be gotten which are used for beam model in macro level. In the end the COMSOL model is used for testing effect of different variables, for example, fiber volume fraction, stiffness of fibre coating and fibre orientation.

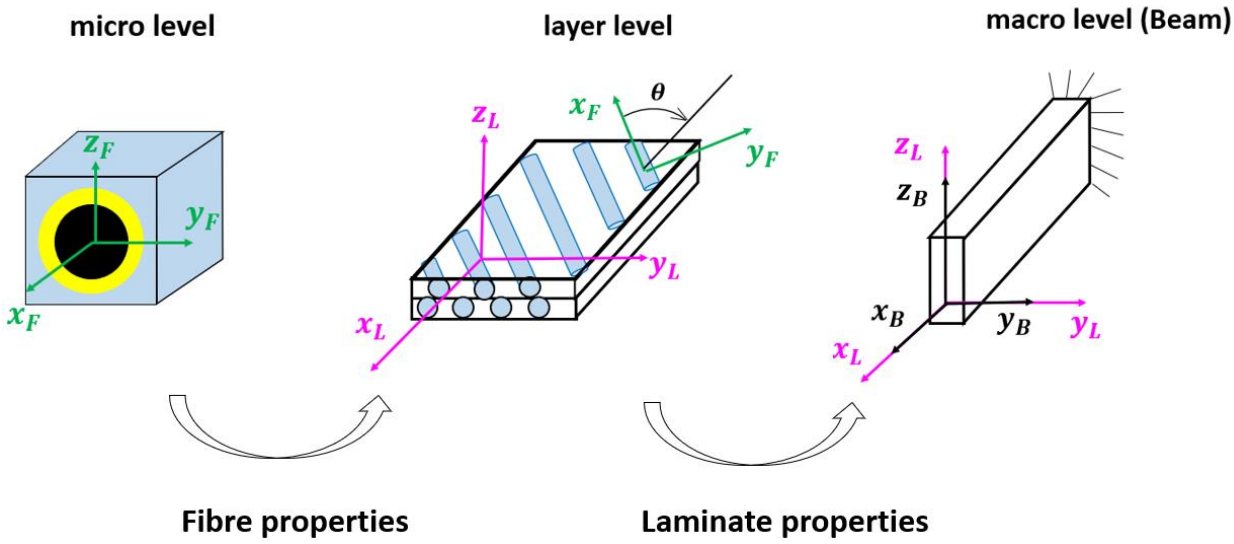

Figure 4.1: Coordinate systems for different levels.

4.1 COMSOL model - microstructure

After validating the results of the COMSOL model, a PeCCF composite structure is simulated via COMSOL to analyse its potential for vibration reduction. Since no available material in the COMSOL material library can represent PeCCF composite material, the microstructure, a unit cell must be created before creating the macrostructure. The unit cell defines the properties of the carbon fibre, epoxy resin and electrolyte coating which are shown in Table 2.4. The carbon fibres

is assumed to be transversely isotropic and the epoxy resin and polymer electrolyte coating are isotropic. The details of microstructure are shown in chapter 2.4.

4.2 Layered material

Based on the microstructure in chapter 4.1 the laminate layers can be constructed. From chapter 2.5 we know that the *Layered Material* functionality in COMSOL should be used. At first, a homogenous layered material was under the global definition constructed, where the effective material properties calculated from the unit cell model in chapter 4.1 are applied. Simultaneously, the layer thickness, fibre orientation and layer transform are set. In Figure 4.2 the layer position and fibre orientation are shown. The material consists of 6-layer symmetric laminate with the stack sequence $[0°/45°/90°]_s$. These orientations are randomly selected. The layer thickness is equal to 1 mm. The layers are in xy direction and the positive fibre orientation is in clockwise which starts from x axis. The further details for setting up can be found in COMSOL tutorial [2].

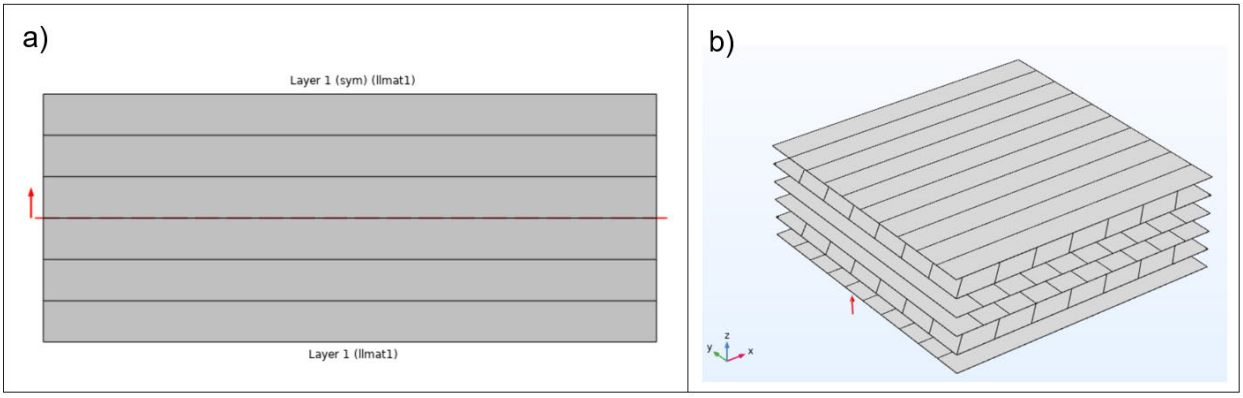

Figure 4.2: a) cross section view of 6-layer laminat; b) layer stack view with stack sequence $[0°/45°/90°]_s$

4.3 COMSOL model – macrostructure

Then a 3D beam with the size of 150 mm x 30 mm x 1400 mm is constructed based on the layered material in chapter 4.2. The beam is a cantilever which is only one side fixed supported (yellow surface in Figure 4.3). To get the velocity of the beam, a vertical force (0; 0; 50 kN) acts on the

left corner of the free side (blue arrow in Figure 4.3), so that there are bending moment and torsion on the model. Afterwards, the beam is meshed with *Mapped* type and has a fixed element distribution number of 20, so that the beam will not be too soft. The three views of the meshed beam are shown in Figure 4.4. The layer position is in the xy surface. In the end, the *Frequency Domain* functionality is used to get the velocity and total kinetic energy Wk_tot of the beam.

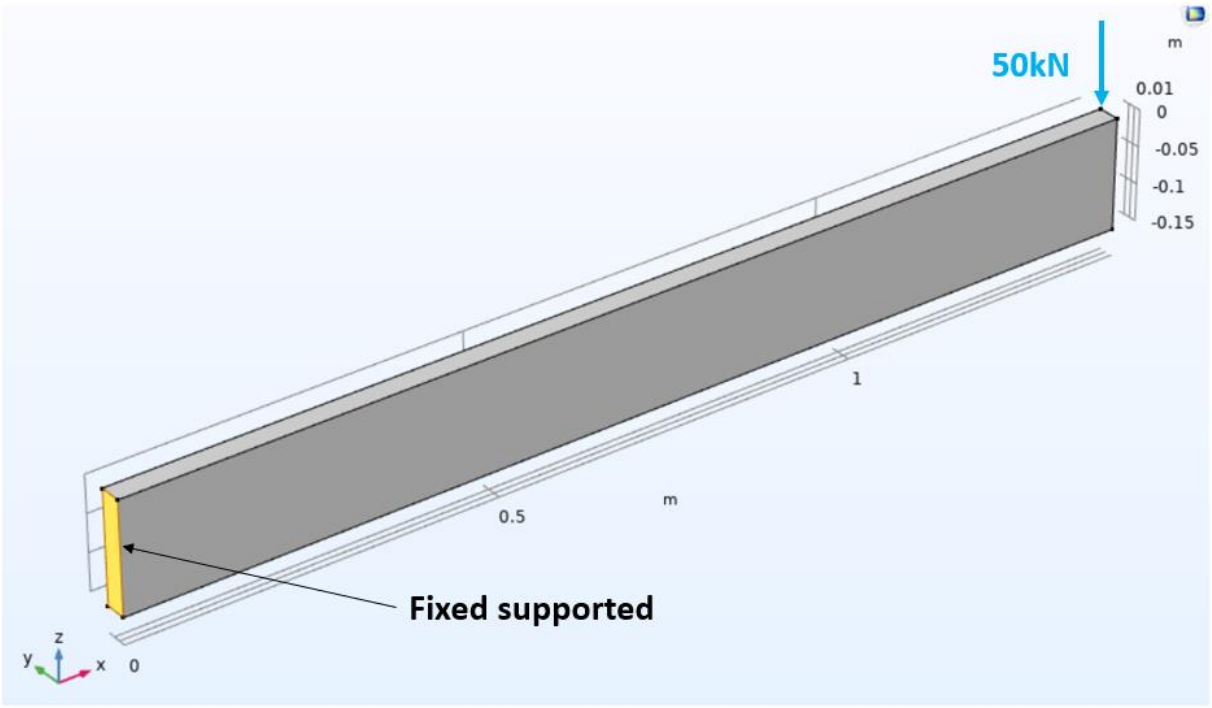

Figure 4.3: Cantilever beam in COMSOL with vertical force

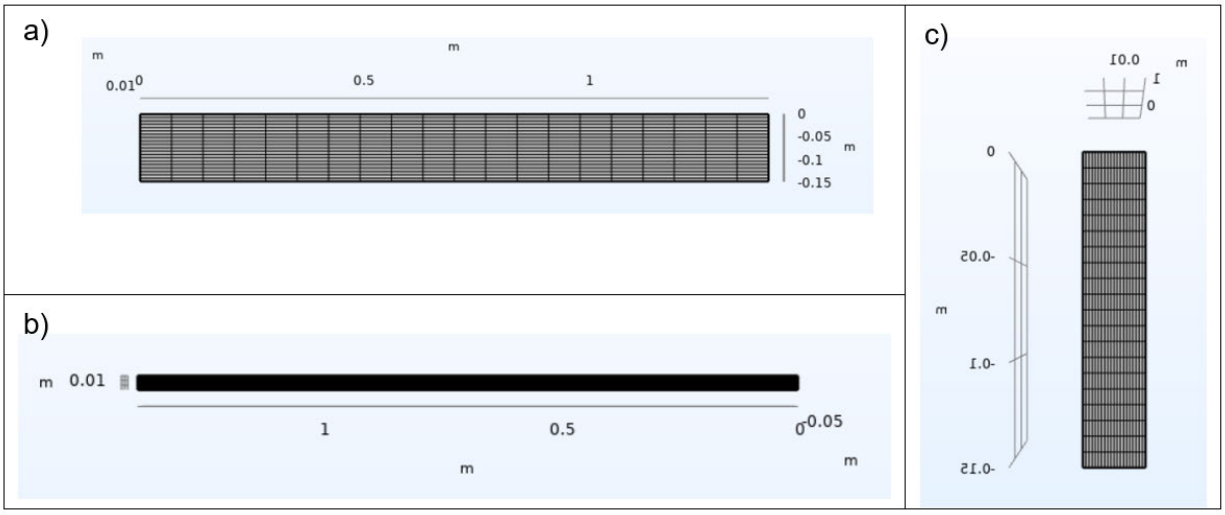

Figure 4.4: Three standard views of a meshed cantilever beam: a) xz view; b) xy view; c) yz view.

4.4 Comparison of model with different laminate parameters

To analyse the vibration reduction potential of the PeCCF composite beam, the parameters of the composite material are varied. In this chapter, the tested parameters are fibre volume fraction, the Young's modulus of the fibre coating and the fibre orientation. The fibre volume fraction v_f and Young's modulus modulus E_c can be changed in the parameter table under *Global Definitions*. The fibre orientation is set under *Layered Material*. In this chapter, the fibre volume fraction and Young's modulus of fibre coating of beam model in chapter 4.3 are changed to investigate their influences of vibration reduction. Then the model in chapter 4.3 is compared with the models with different layer stacks, these are shown in Figure 4.5. All three-layer stacks consist of 6 layers and are symmetric. They have the same fibre volume fraction and Young's modulus of fibre coating. The only difference is the fibre orientations which are $[0°/45°/90°]_s$, $[90°/45°/0°]_s$ and $[30°/10°/80°]_s$

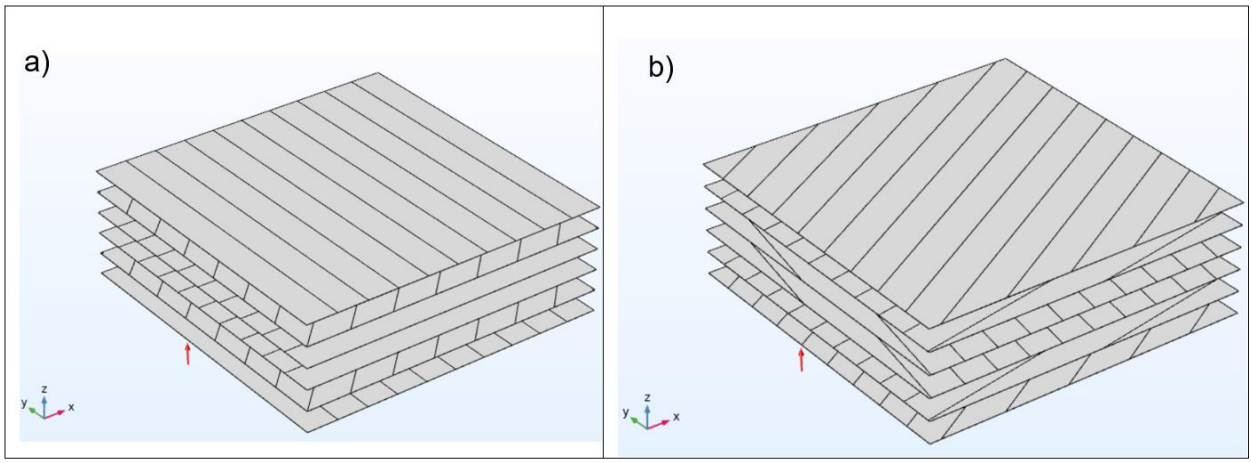

Figure 4.5: a) Layer stack sequence $[90°, 45°, 0°]_s$; b) Layer stack sequence $[30°, 10°, 80°]_s$

After computing the function *Frequency Domain* the velocity along the beam at 90Hz of the different models are exported into Matlab since 90 Hz is the first resonant frequency of the investigated airplane cabin noise in chapter 2.6. The Matlab code is shown in Appendix D and the results are shown in Figure 4.6. The x-axis represents the x coordinate along the beam. Because the beam is fixed at x = 0 the y-value, the velocity is always zero. Therefore in all situations the sampling starts from x = 0.1 m. The yellow, pink, blue and black solid curves represent the model with the same layer stack sequence of $[0°/45°/90°]_s$. The only difference is that the black solid curve shows the velocity of the beam with a smaller Young's modulus of the fibre coating of 0.5 GPa, the pink and blue curves are for the model with higher (0.8) and lower (0.2) fibre volume fractions. The green curve and black dotted curve represent the model with the same layer stack sequence of $[-45°/45°/-45°]_s$ but different Young's modulus of fibre coating E_c. Similarly, compared with the yellow curve the red, cyan and black dotted curves represent the

models with different fibre orientations. Their fibre volume fraction is all equal to 0.5 and Young's modulus of the fibre coatings are 2.0 GPa.

From the coincident yellow and black solid curves, green and black dotted curves, we can derive that the Young's modulus of the fibre coating has almost no influence on vibration reduction. It could be caused by two reasons. The first reason is that the layers are in the xy plane and the force is in the z-direction. The carbon fibres withstand most of the bending stress and strain. The second reason is that compared with the longitudinal modulus of carbon fibre (290 GPa) the Young's modulus of the coating is quite small, even though it changes from 2.0 GPa to 0.5 GPa. By comparing the yellow, pink and blue curves we can conclude that a higher fibre volume fraction can reduce the structural vibration. This can be seen by the fact that the pink curve, the one representing the lowest fibre volume fraction, is below the yellow and blue curves. Moreover, the yellow, red, green and cyan curves show that the sequence of layers and the fibre orientation have a greater impact on the vibration reduction ability of the structure since the distance between the yellow and red curves are much greater than it is between the yellow and blue curves. However, the exact effects of the layer sequence and fibre orientation on the vibration reduction ability are too complex to be understood by this diagram alone, as can be seen by the intersection of the red, green and cyan curves. A definitive rule can not be found in the results below as there are multiple possible combinations of layer sequence and fibre orientation. The fibre orientation is investigated in the next chapter.

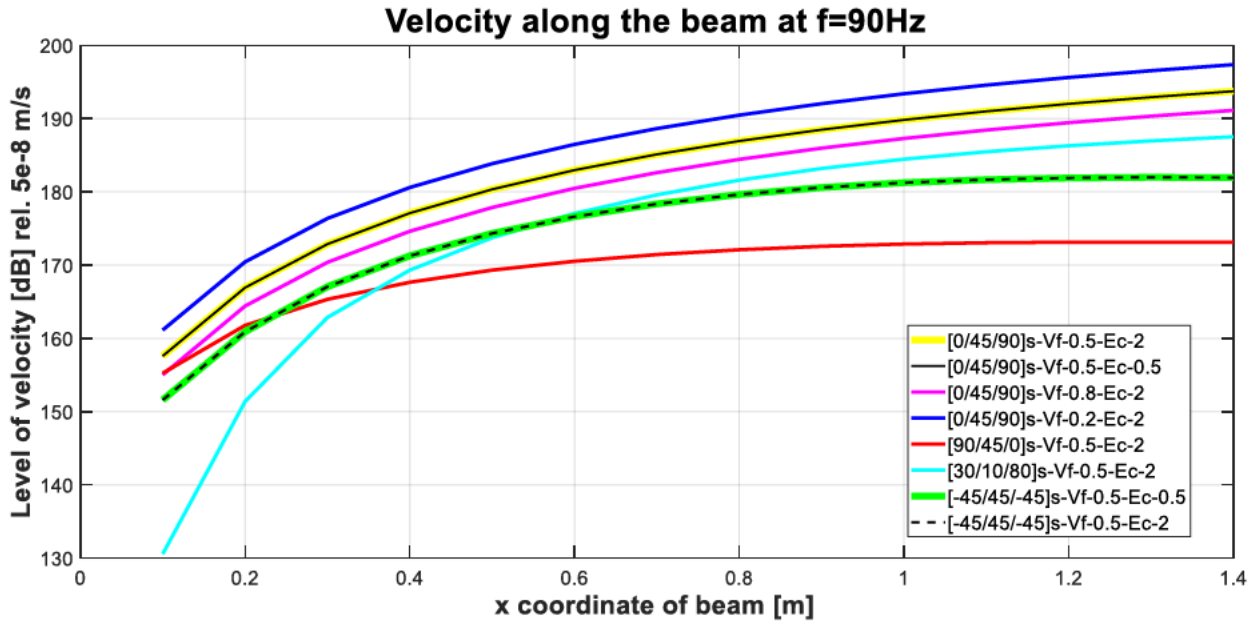

Figure 4.6: Velocity along the beam at 90 Hz with different parameters

5 Discussion of parameter optimisation

In chapter 4 the influence of fibre orientation on vibration reduction has been confirmed. However, it is too complex to find out how the fibre orientation influences the effect of vibration reduction. In this chapter the parameters, layer sequence and fibre orientation, will be studied. Because there are thousands of possible combinations of fibre orientation, it is unpractical to find the best combinations manually. Therefore, an optimization method, the Genetic Algorithm (GA), is used to find the best combination. The fitness function of GA is the result of COMSOL, the total kinetic energy of the beam at the resonant frequency. At first, the fibre orientation for the beam with rectangular cross-section, T cross-section and double T cross-section were optimized. At the same time, the wingbox is simulated in COMSOL and optimized using the GA. This procedure is achieved with COMSOL and Matlab. The software COMSOL Multiphysics with Matlab integrates COMSOL and Matlab. The results of the COMSOL model are exported into Matlab and are then used as the population for the optimization procedure of the GA in Matlab. In the end, the best parameters for the COMSOL model are determined from this procedure. After optimization procedure for the fibre orientation, the stiffness of the optimized beams and wingbox are tested, to see if they are within reasonable range.

5.1 Optimisation of beams with different cross-sections

5.1.1 Optimization procedure for fibre orientation

In reality, the cross section of spars in airplane wingboxs are not simple rectangular. In order to find the compellent results, two more different cross-sections, T cross-section and double T cross-section are investigated as well. The dimensions of these three cross-sections are shown in Figure 5.1. All three cantilevers are 1.4 m long and consists of 4-layer laminates with the layer stack sequence of $[\mathrm{wink1}/\mathrm{wink2}]_s$ to shorten optimisation time. As same as in chapter 4.2, the load (0; 0; 50 kN) acts on the left corner of the free side of the cantilever which is same with the force in Figure 4.3.

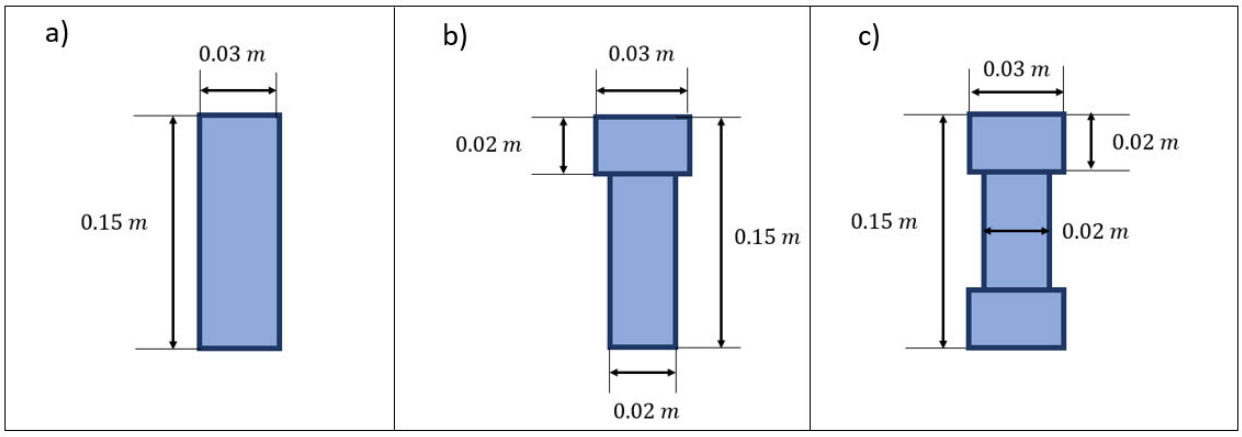

Figure 5.1: Three different beam cross-sections and their measurements: a) rectangular cross-section; b) T cross-section; c) double T cross-section.

Then the optimization procedure GA starts via COMSOL and Matlab. The procedure steps are shown in Figure 5.3. At first, the parameters, also called the solutions of the fitness function, are set up under layered material in the COMSOL model (see Figure 5.2). Here the best solutions are two angles of fibre orientation in the layer stack $[\mathrm{wink1}/\mathrm{wink2}]_s$. Then the fitness function is defined in Matlab, this fitness value is the total kinetic energy of the beam E_{k-tot}. This total kinetic energy is the result of COMSOL model. So in the fitness function, there is a command code to run COMSOL and export fitness value E_{k-tot} in Matlab. After the GA analysis the input fitness value and parameters are used to find a new group of solution which is then used as new parameters in the COMSOL model. The parameters and fitness value exchanging between the COMSOL and Matlab creates populations for GA. When the best solution for $\mathrm{wink1}$ and $\mathrm{wink2}$ is determined, the optimization procedure is completed. The Matlab code for the fitness function and GA is shown in Appendix E [29] [30] [31].

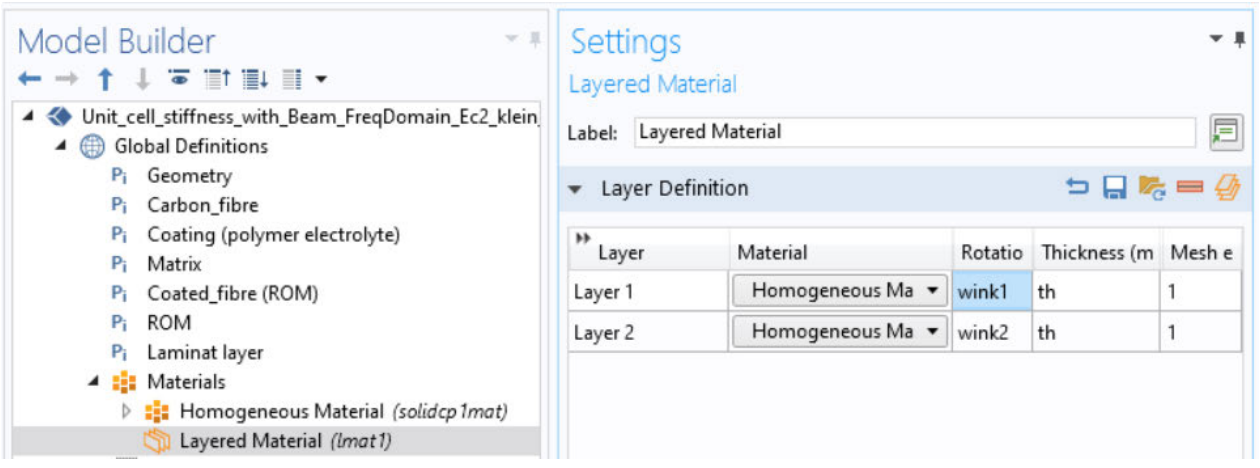

Figure 5.2: Parameters set up in COMSOL model

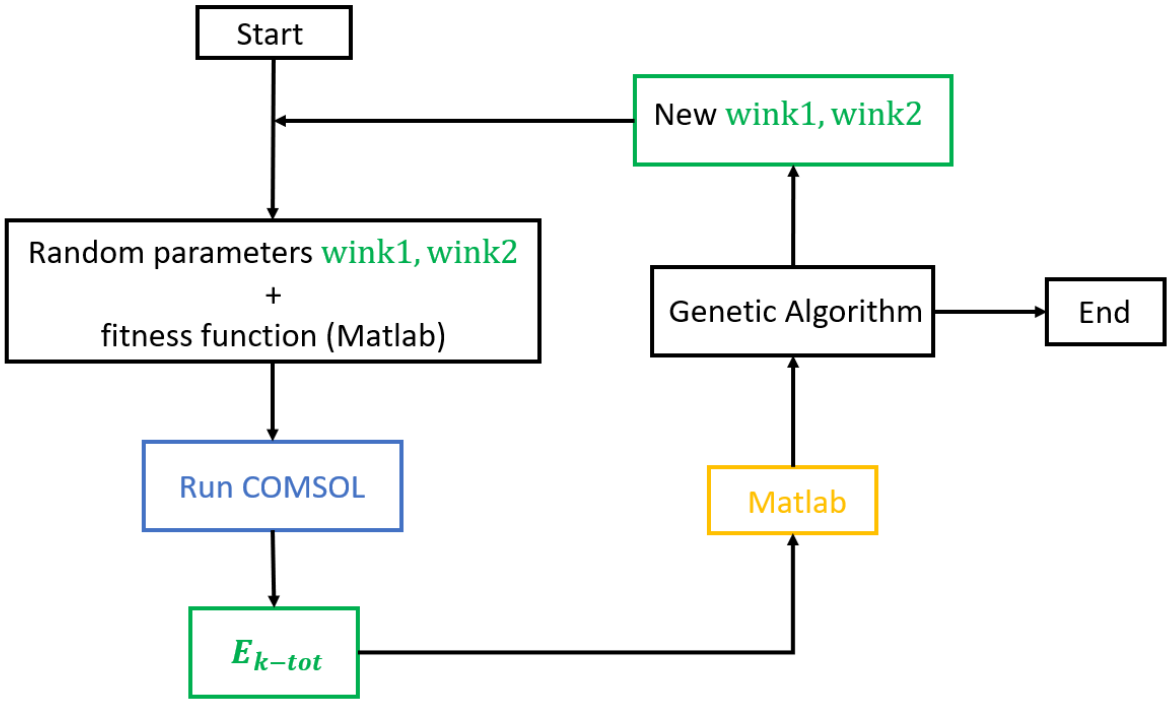

Figure 5.3: Flow chart of the optimization procedure via COMSOL and Matlab.

In Table 5.1 the best fibre orientation for beams excited at 20 Hz with different cross-sections are shown since the first natural frequencies of all beams are near 20 Hz. The results of the rectangular and double T cross-section are closer than 10° while the angular difference between the T and the double T is more than 50°. The reason may be that the rectangular and double T cross-sections both have two axes of symmetry, but the T cross-section has only one. All cross-section types have the same wink2 which is 0°.

Cross-section	Wink1	Wink2	E_{k-tot}
Rectangular	66.1°	0°	66.12 J
T	19.7°	0°	75.98 J
Double T	74.0°	0°	73.98 J

Table 5.1: The optimisation results at 20Hz of beams with different cross-section

Figure 5.4 to Figure 5.6 show the optimization procedure in effect. The y-axes represent the fitness value. The x-axes show the GA generations. From the figures, we can see that it takes 65 generations to find out the best fibre orientations for a rectangular cross-section whose minimum kinetic energy is 66.12 J. The T cross-section needed 85 generations to converge the best fitness

value of 75.98 J. The double T cross-section needed only 19 generations to find out the best solution which is 73.98 J.

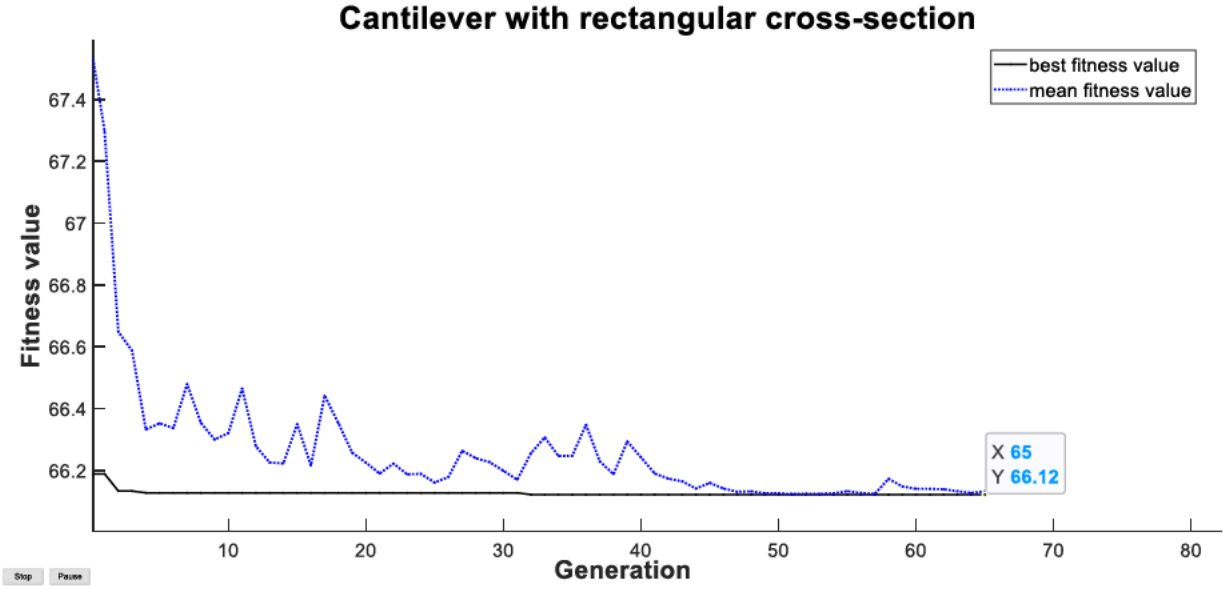

Figure 5.4: GA generations and their best fitness value for a cantilever with rectangular cross-section

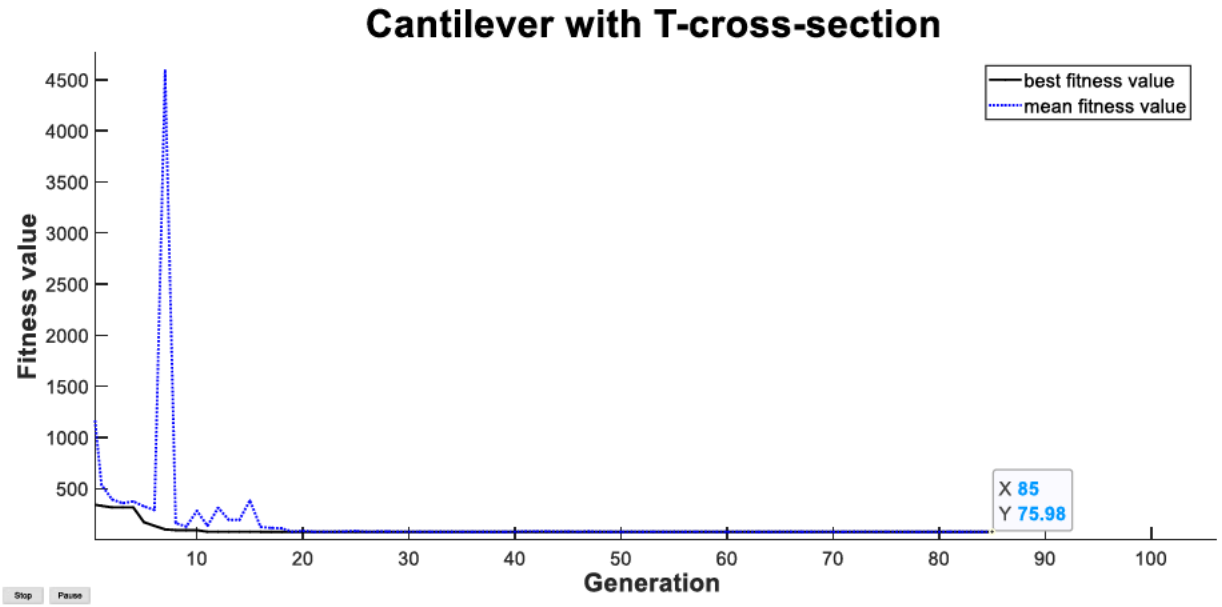

Figure 5.5: GA generations and their best fitness value for a cantilever with T cross-section

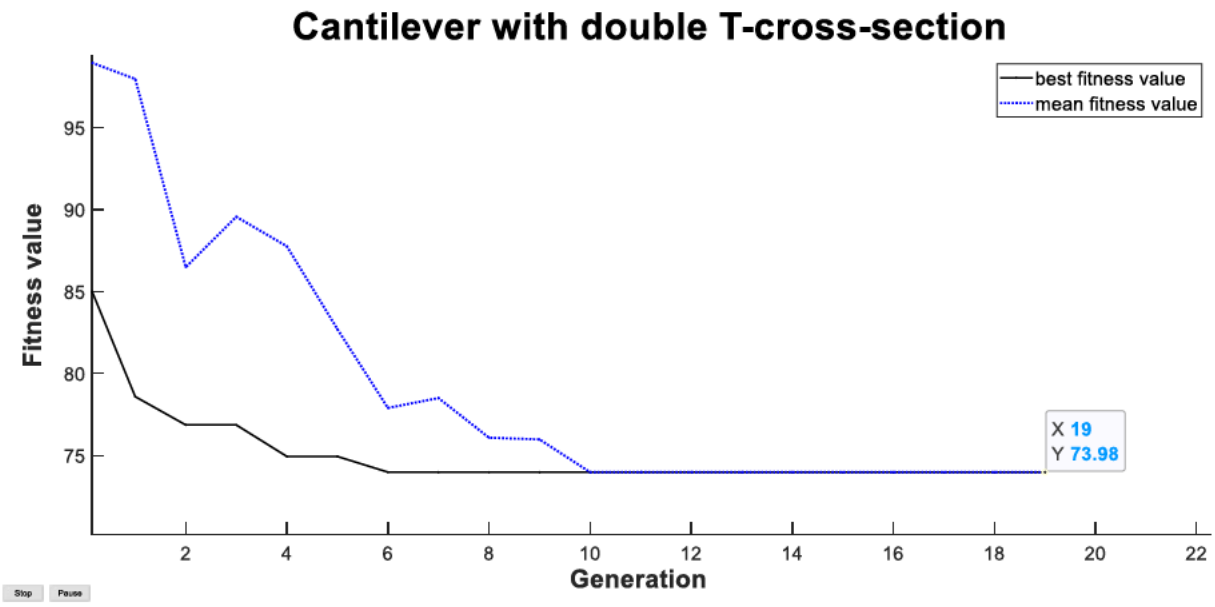

Figure 5.6: GA generations and their best fitness value for a cantilever with double T cross-section

In order to get more meaningful optimization results, the excited frequency of model is changed to 90 Hz (see chapter 2.6). The boundary conditions and loads remain the same as for the 20 Hz analysis. The optimized results are shown in Table 5.2. From the table, we can see that the fibre orientation for the T cross-section and double T cross-section are closer than in the previous case. Because the T and double T cross-sections both have horizontal sections which are perpendicular to the load, their second orientation is both 90.0° while the rectangular cross-section has an orientation near 45.0°. These results are more plausible than the results at 20 Hz. This is because the orientations are more relative to the cross-section.

Cross-section	Wink1	Wink2	E_{k-tot}
Rectangular	54.1°	44.8°	3663.00 J
T	43.4°	90.0°	4355.00 J
Double T	48.0°	90.0°	3411.30 J

Table 5.2: The optimisation results at 90 Hz of beams with different cross-section

Because the optimized results for 90 Hz are very different from the results for 20 Hz, the eigenmodes of the optimized beam for 90 Hz are observed. In Figure 5.7 to Figure 5.10 the first four eigenmodes for beam with rectangular cross-section are shown.

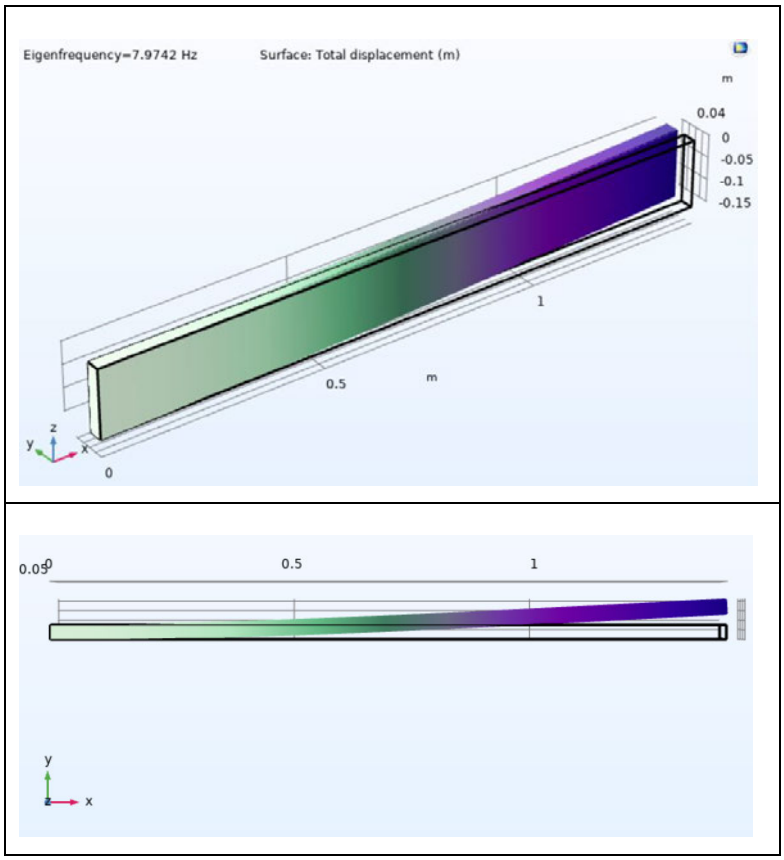

Figure 5.7: First eigenmode of beam with rectangular cross-section

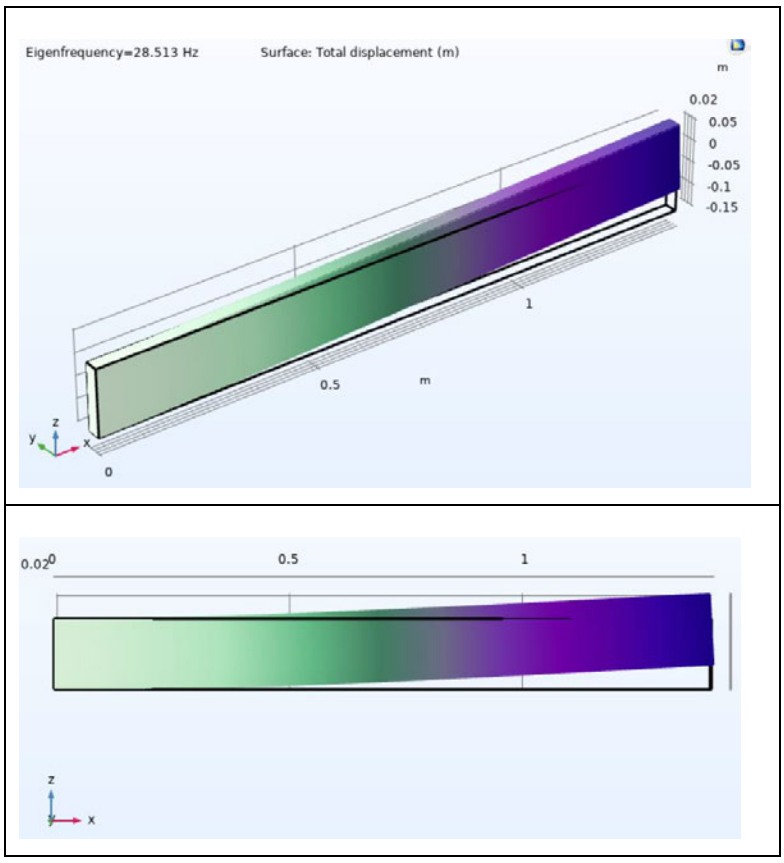

Figure 5.8: Second eigenmode of beam with rectangular cross-section

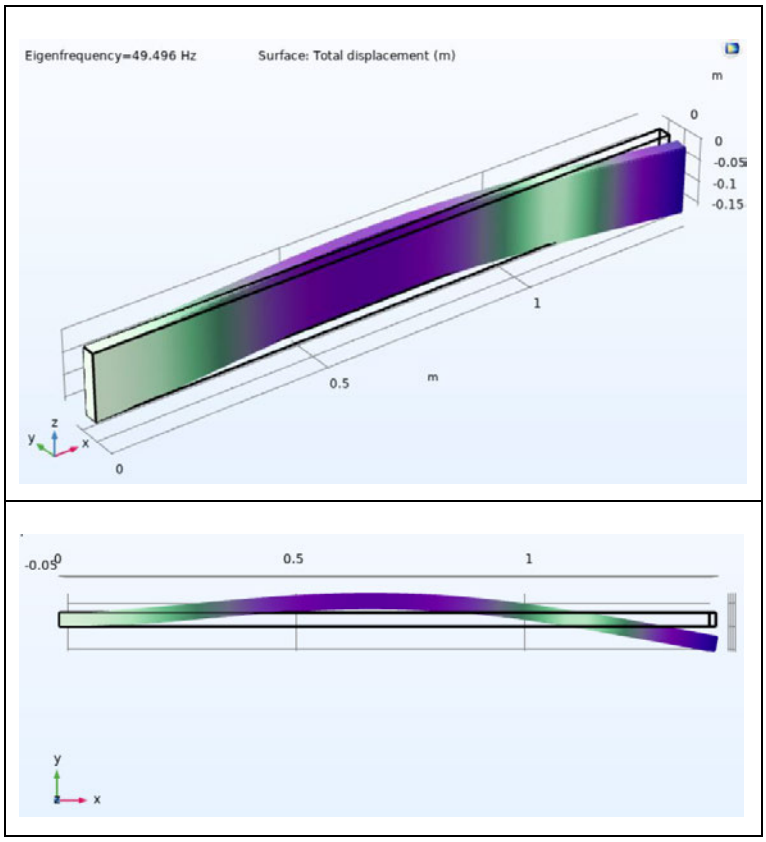

Figure 5.9: Third eigenmode of beam with rectangular cross-section

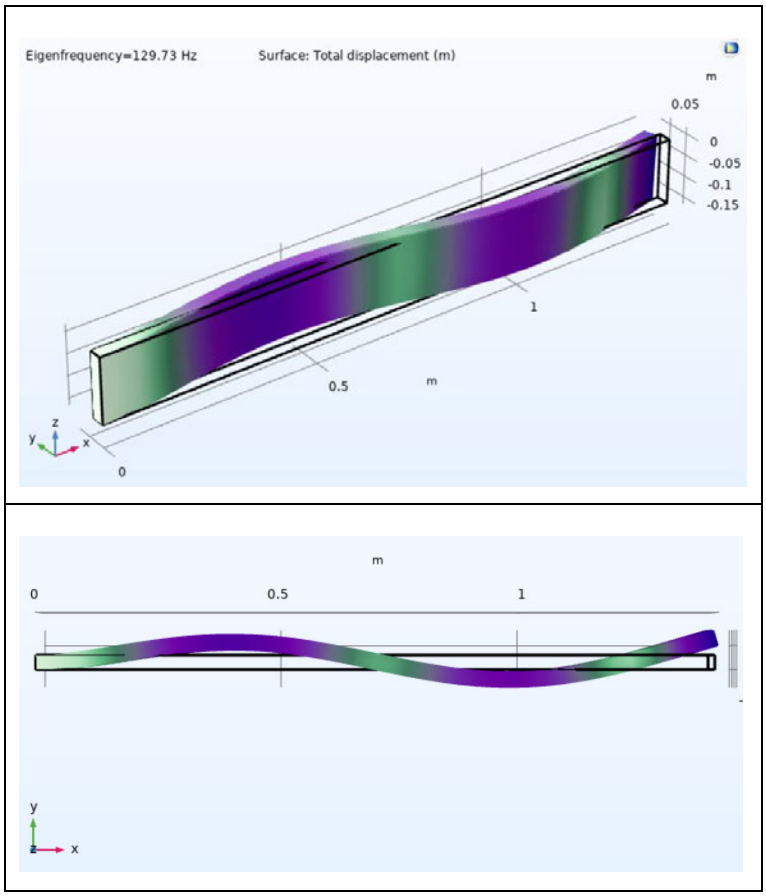

Figure 5.10: Forth eigenmode of beam with rectangular cross-section

The beam with T and double T cross-section have same eigenmodes as rectangular cross-section but different natural frequencies. Therefore, only the natural frequencies are compared. As in Table 5.3 shown, we can find that the natural frequencies for all beams are relative far away from the resonant frequency of cabin noise (90 Hz). This means that the optimized results are rational and meet the optimized condition.

Cross-section	1.NF [Hz]	2.NF [Hz]	3.NF [Hz]	4.NF [Hz]
Rectangular	7.97	28.51	49.50	129.73
T	5.94	29.93	37.79	102.48
Double T	5.59	32.06	35.45	99.09

Table 5.3: First four natural frequencies for beam with different cross-section

5.1.2 Comparing the optimized results with other fibre orientation

Furthermore, these optimized fibre orientations (see Table 5.2) are compared with other common fibre orientations. They are compared with fibre orientation $[0°/0°]_s$ and $[45°/-45°]_s$ for both layers. As in Figure 5.11, Figure 5.12 and Figure 5.13 show the total kinetic energy of the beams from 80 Hz to 100 Hz for different fibre orientations are compared. In Figure 5.11 we can see that the optimized fibre orientation for a rectangular cross-section is better than orientation $[0°/0°]_s$, as the red curve is much higher than the yellow curve. The maximum reduction of level of kinetic energy is up to 20 dB . However, the blue curve and yellow are almost coincident, this could be caused by their similar fibre orientations. $[45°/-45°]_s$ and the optimized orientation $[54.1°/44.8°]_s$ have similar first orientation. Their second orientation are symmetrical with x axis.

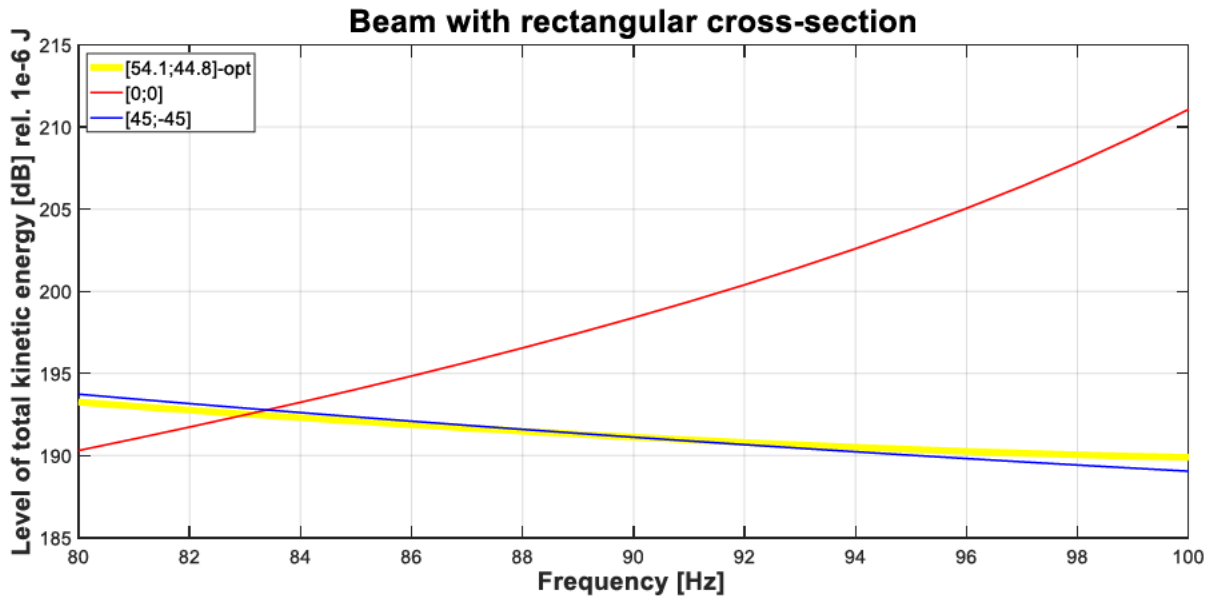

Figure 5.11: Level of total kinetic energy vs frequency for the beam with rectangular cross-section

From Figure 5.12 we can see that the orientation $[0°/0°]_s$ has the greatest total kinetic energy in the frequency range. At 80 Hz the level of kinetic energy for the orientation $[0°/0°]_s$ (red curve) is even 50 dB higher than other two orientations. The blue curve is lower than the yellow curve. This could caused by the angle range of GA procedure. In GA the angles are limited between 0° to 90°, so that no negative angles are considered.

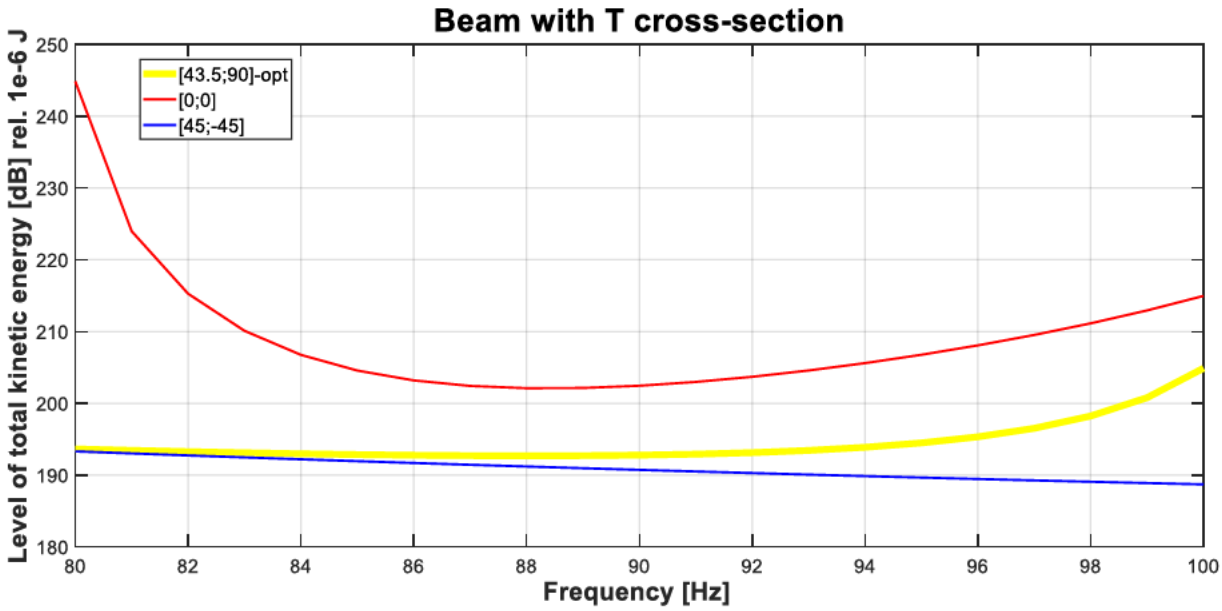

Figure 5.12: Level of total kinetic energy vs frequency for the beam with T cross-section

Figure 5.13 also shows that the optimized orientation is better than $[0°/0°]_s$ as the yellow curve is lower than the red curve. Even though after 98 Hz the yellow curve is higher than the red curve, the red curve has higher total kinetic energy near 90 Hz which should generally be avoided.

Moreover, the blue curve and yellow curve are coincident until 92 Hz. After that the optimized orietntation has greater kinetic energy. Because of time limit the angle range for GA process is under 90°, so that the higher kinetic energy at some frequency ranges should be accepted when at the resonant frequency the velocity is much smaller.

In summary, these three figures reveal that the optimized orientations meet the optimization condition since their level of kinetic energy at resonant frequency are 10 dB lower than $[0°/0°]_s$ and almost same as $[45°/-45°]_s$.

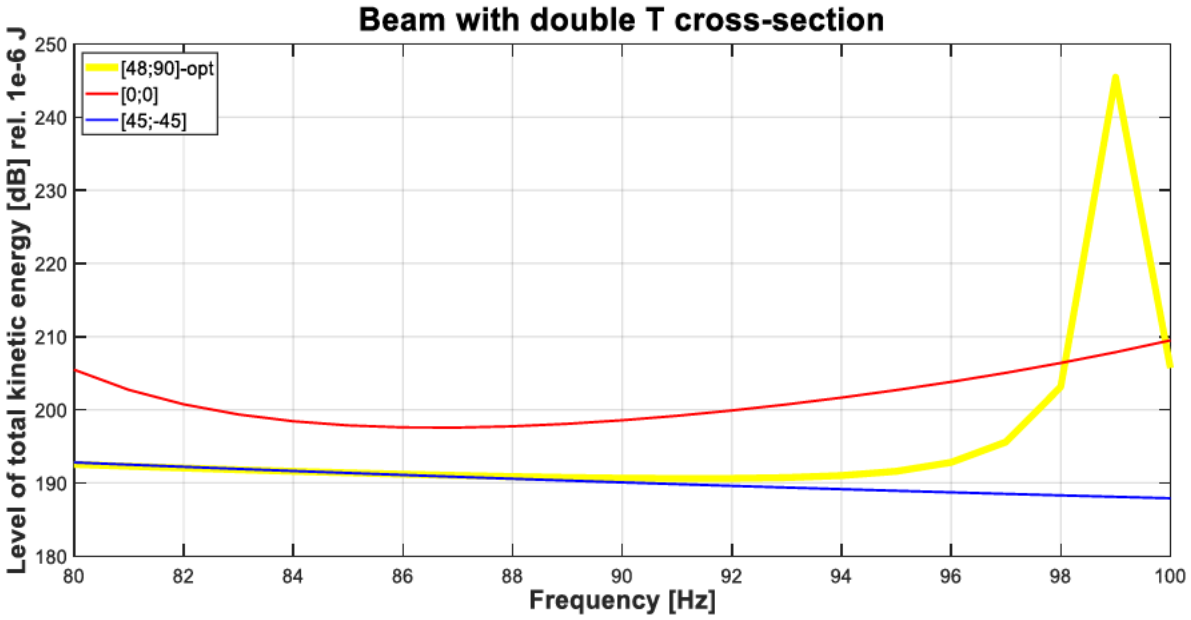

Figure 5.13: Level of total kinetic energy vs frequency for the beam with double T cross-section

5.1.3 Stiffness of the optimized beam

In the previous chapter, the fibre orientations were optimized. However, as a structure, the stiffness is still a major factor. In this chapter, the stiffness of the beam which are constructed in chapter 5.1.1 are tested, to see if they are within a reasonable range.

The form of elastic curves in z-direction for optimized PeCCF composite beam and aluminium beam are compared to verify the stiffness. To compare the static beam bending displacement the study *Stationary* is used. The beam has same boundary condition as in chapter 5.1.1 but different

loading position. The same force (0; 0; 50kN) acts at the free side of the beam but on the symmetry line of the cross-section. In Figure 5.14, Figure 5.15 and Figure 5.16 the sampling positions on the beams for displacement are shown. At x = 0 the beam is fixed which means that the displacement is always zero. Therefore the sampling points start at x = 0.1 m. The distance between the adjacent two points is 0.1 m. The displacement in z-direction along the beam with different cross-sections are shown in Figure 5.17, Figure 5.18 and Figure 5.19.

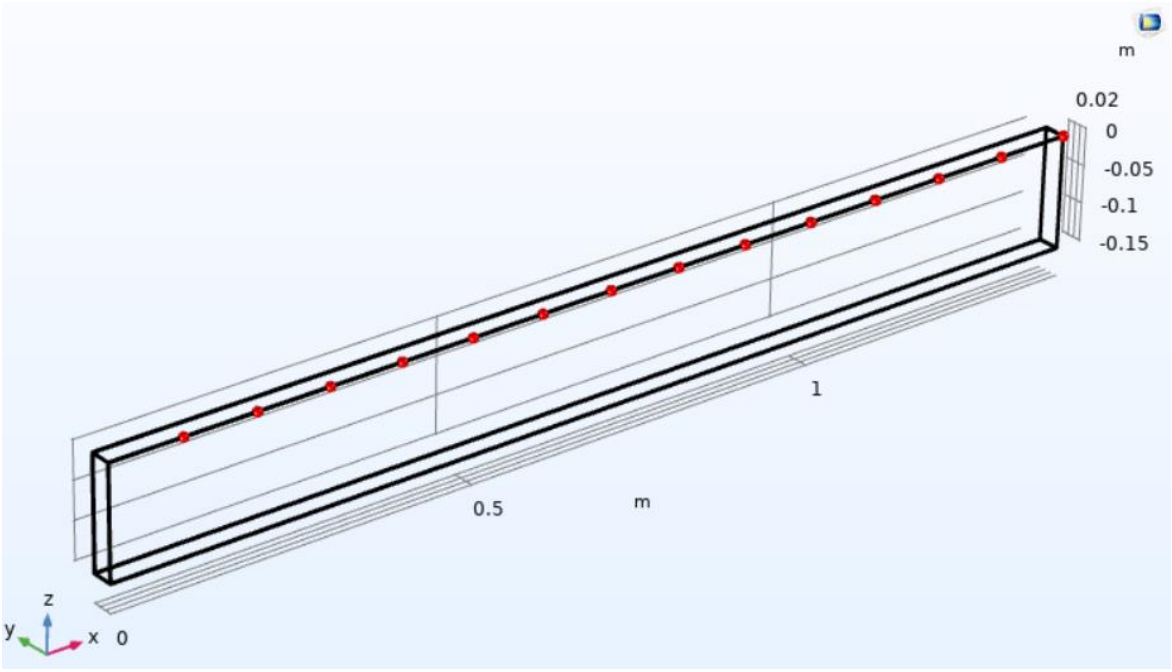

Figure 5.14: Sampling positions on the beam with rectangular cross-section

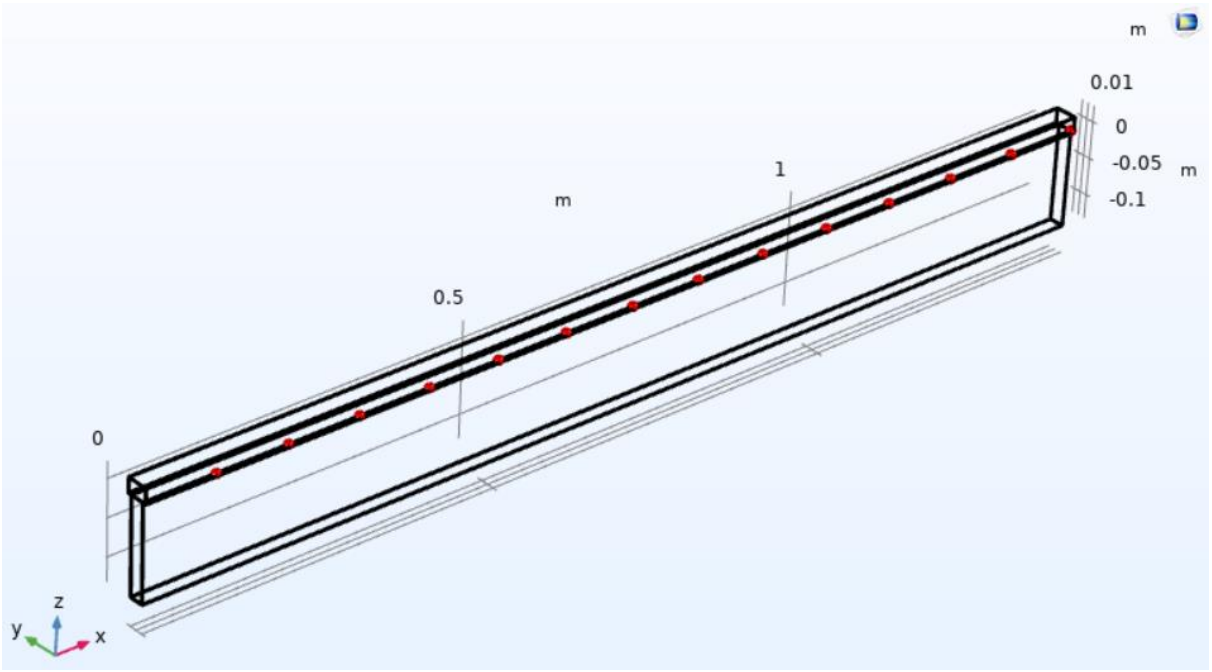

Figure 5.15: Sampling positions on the beam with T cross-section

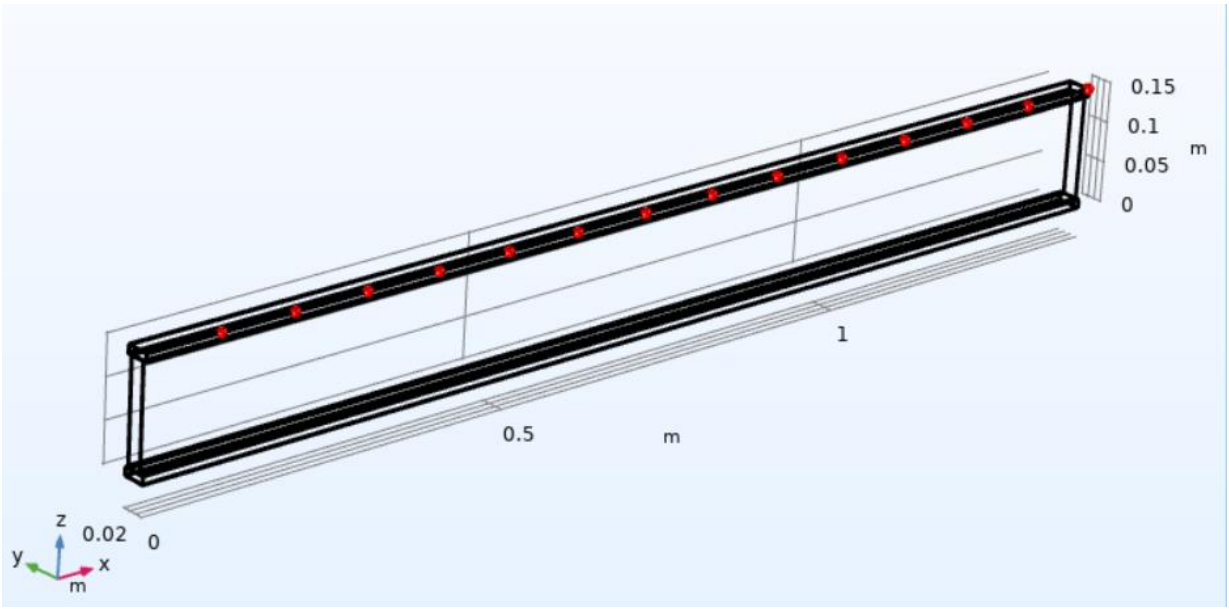

Figure 5.16: Sampling positions on the beam with double T cross-section

Figure 5.17, Figure 5.18 and Figure 5.19 show the displacement in the z-direction for beam with rectangular, T and double T cross-section. The black and blue curves represent the optimized PeCCF beam for 90 Hz and 20 Hz. The red curves are for the beam made of aluminium. In these figures we can find that the optimized PeCCF beam for 20 Hz for all cross-sections are stiffer than aluminium beams since the blue curves in three figures are lower than red curves. In contrast, the optimized PeCCF beams for 90 Hz are much softer, because their displacements are maximum. This could be caused by the target frequency for GA procedure. In the optimization

procedure the goal is to avoid resonant frequency. To avoid 90 Hz the fibre orientation changes to the position which can not bearing bending load as well as 0°.

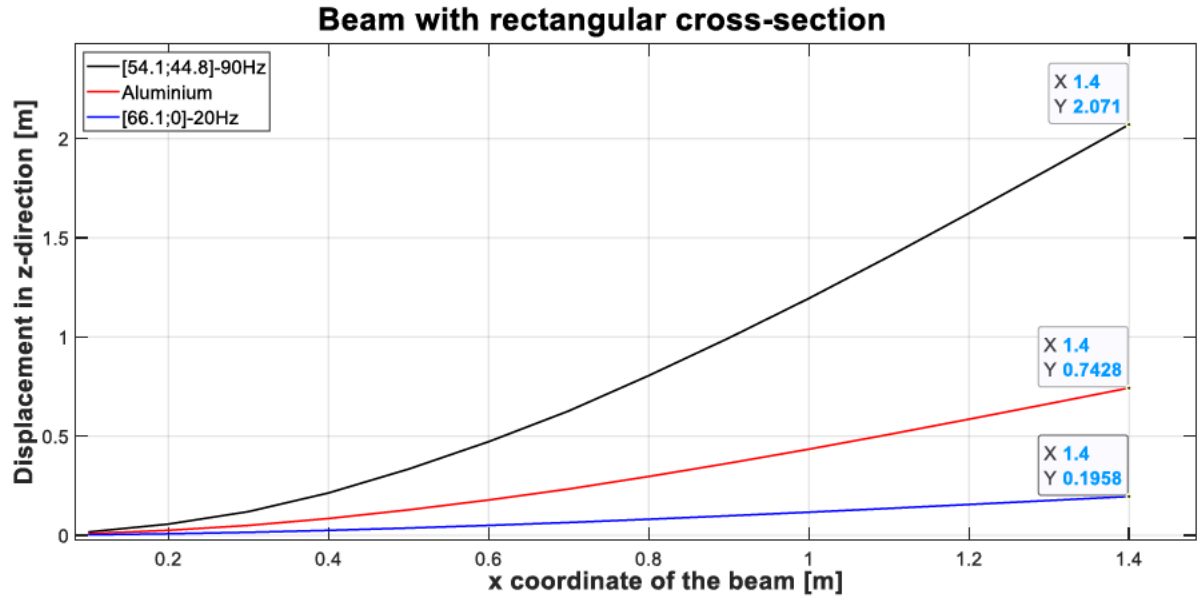

Figure 5.17: Displacement in z-direction along the beam with rectangular cross-section

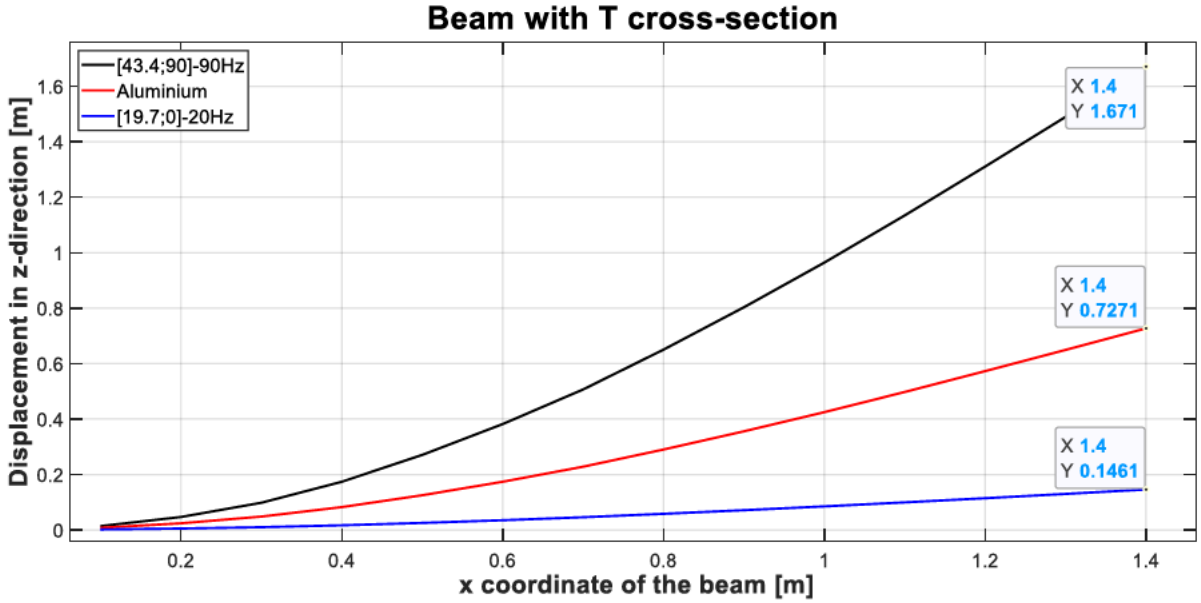

Figure 5.18: Displacement in z-direction along the beam with T cross-section

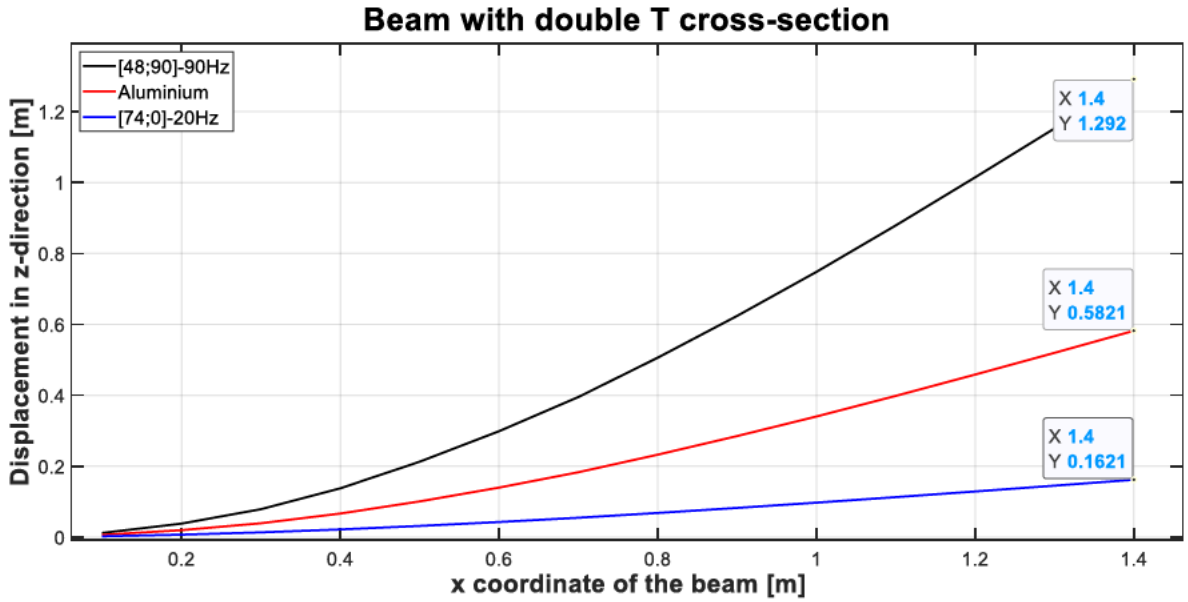

Figure 5.19: Displacement in z-direction along the beam with double T cross-section

5.2 Optimisation of wingbox

5.2.1 Optimization procedure for fibre orientation

To optimize the fibre orientations practically, the wingbox of the Cessna airplane is observed [32]. At first, the wingbox was constructed in COMSOL, the measurements and loads are shown in Figure 5.20. Similar to the cantilever beam in the previous chapter, the wingbox is 5.5 m long and has fixed support on the left side and the right side is free. The wingbox is subjected to a distributed load of q = 1000 N/m acting on the centre line of the upper surface as shown in Figure 5.20 a). Figure 5.20 b) shows the cross-section of the wingbox. The wingbox is 0.680 m wide and 0.165 m deep. The vertical wall is four-time thicker than the horizontal board. This is because the major load of an airplane wing is a vertical bending load. Also with this dimension relationship, the fibre orientation may be change significantly to minimize structural vibrations.

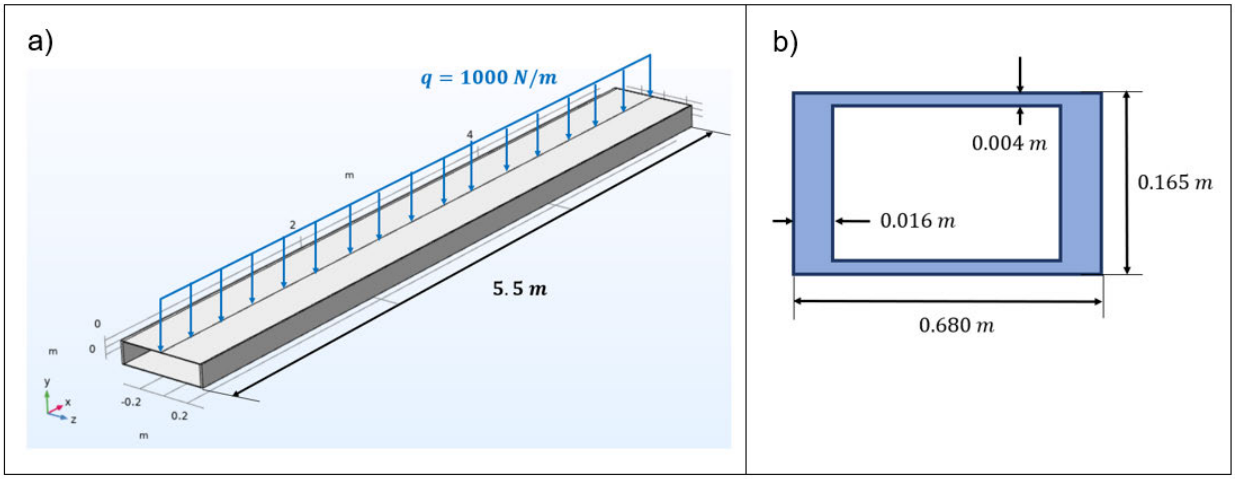

Figure 5.20: a) Oblique view of wingbox; b) yz view of wingbox

Similarly, the GA is used to find out the best $\mathrm{wink1}$ and $\mathrm{wink2}$. The result are shown in Table 5.4, Figure 5.21 and Figure 5.22. As introduced in chapter 2, the resonance frequency of the Cessna cabin noise is 90 Hz. Furthermore, according to the COMSOL model the natural frequency of wingbox near noise resonant frequency is 92 Hz. Hence, the best fibre orientations are found at 90 Hz and 92 Hz. For f = 90 Hz the best fibre orientation is $[42.0°/84.5°]_s$, with this orientation the min. kinetic energy is 3.98 J. The result for 92 Hz is $[36.2°/86.0°]_s$ and 3.44 J which are not significantly different from the results at 90 Hz.

Frequency	Wink1	Wink2	E_{k-tot}
90 Hz	42.0°	84.5°	3.98 J
92 Hz	36.2°	86.0°	3.44 J

Table 5.4: The optimization results for wingbox at different frequencies

In Figure 5.21 and Figure 5.22 the solution-finding process at 90 Hz and 92 Hz are shown. They needed a similar amount of generation (62 and 61 respectively) to find the best solution. However, the GA process at 90 Hz was more changeable than at 92 Hz. This is because the blue curve in Figure 5.21 has higher peaks than in Figure 5.22. From these two figures, we can affirm the reliability of the result since the results at two close frequencies are so close to each other. Furthermore, it shows that the fibre orientation combination is more flexible in a complex structure as 50% of the results in chapter 5.1 are the same.

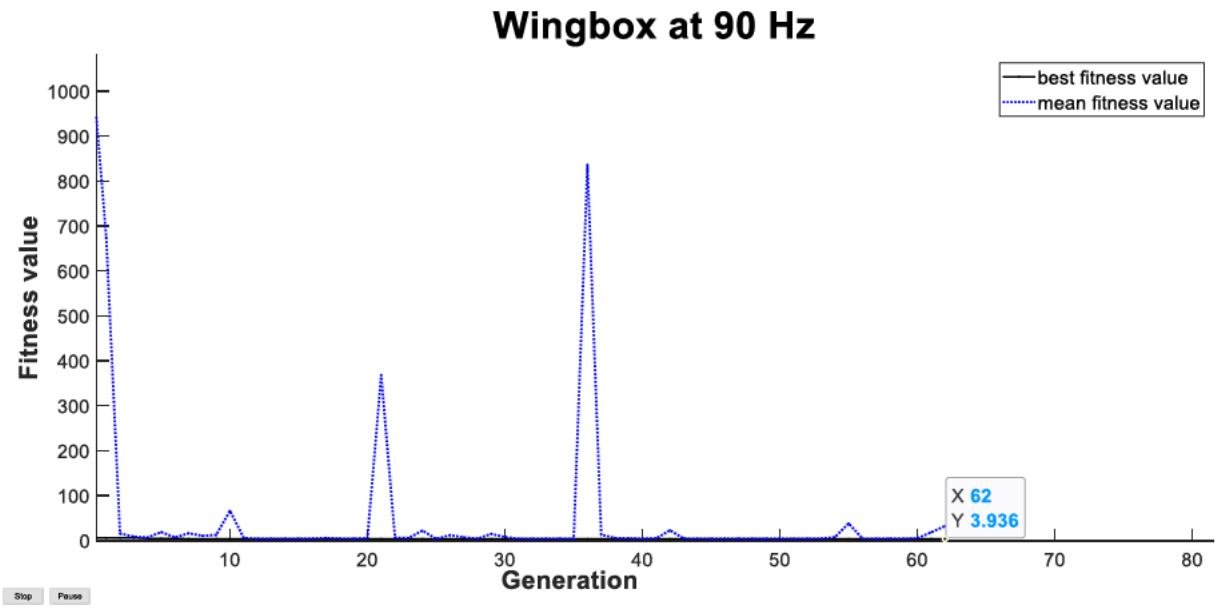

Figure 5.21: GA generations and their best fitness value for wingbox at 90 Hz

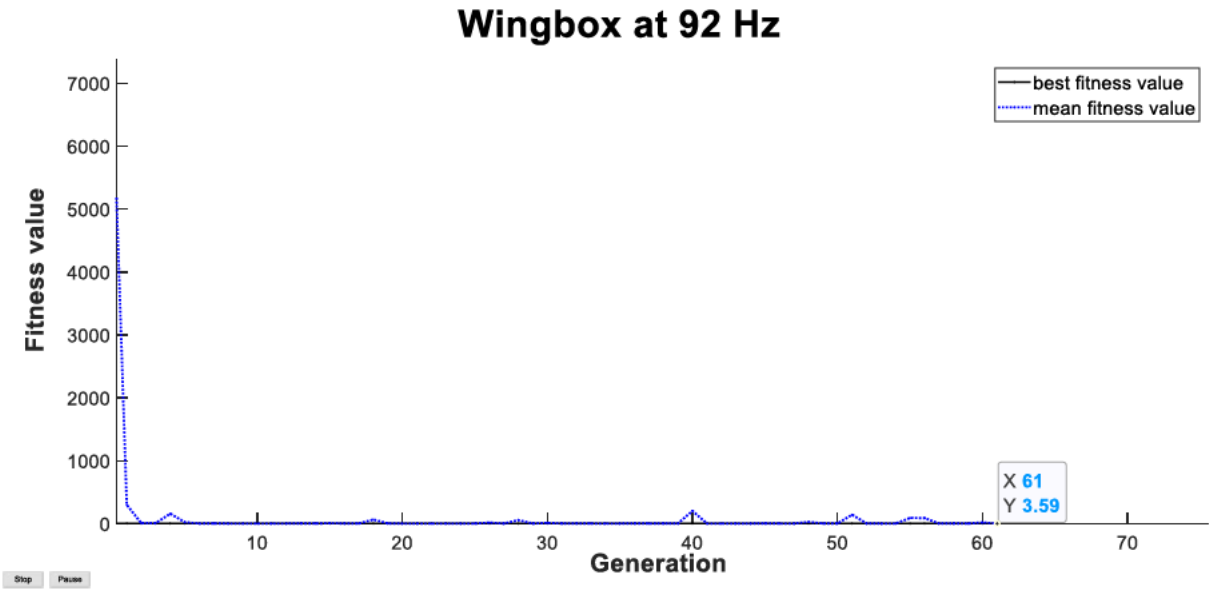

Figure 5.22: GA generations and their best fitness value for wingbox at 92 Hz

5.2.2 Comparing the optimized results with other fibre orientation

Additionally, the optimized orientation is compared with $[0°/0°]_s$ and $[45°/-45°]_s$. As shown in Figure 5.23 the optimized orientation is much better than other orientations since the yellow curve is much lower than the other two curves. At 90 Hz the level of kinetic energy of optimized orientation (yellow curve) is even 25 dB lower than the orientation $[0°/0°]_s$ (red curve) and up to 3 dB lower than the the orientation $[45°/-45°]_s$ (blue curve). Although the blue and red curves

have lower kinetic energy at some frequencies, their much higher kinetic energy near 90 Hz are unwanted. This comparison shows that this optimized solution is the most desirable and plausible.

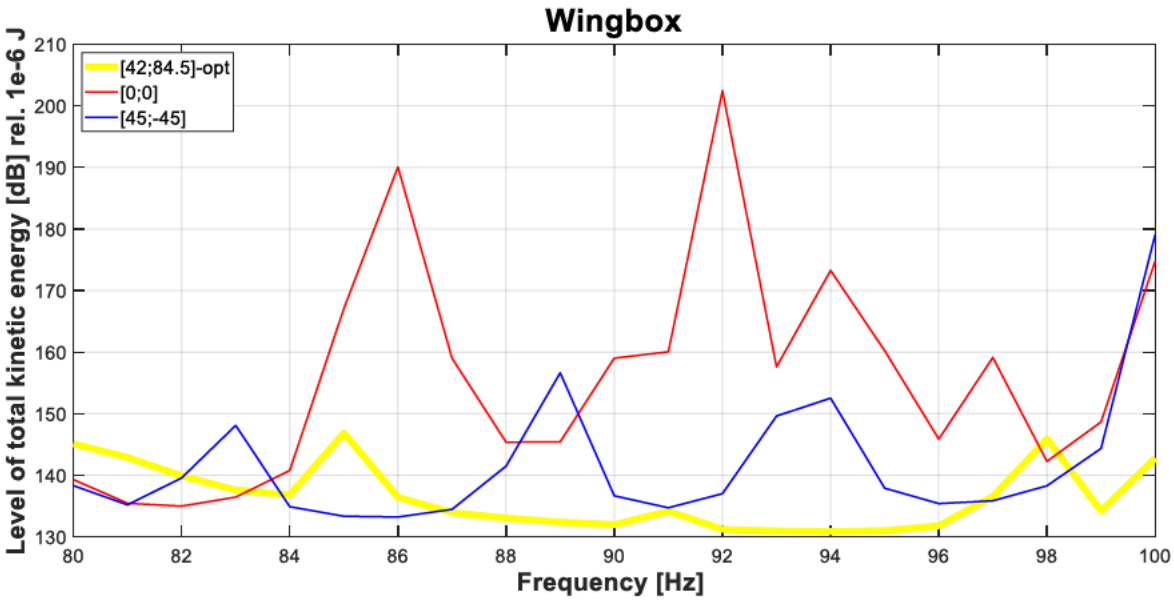

Figure 5.23: Level of total kinetic energy vs frequency for wingbox

5.2.3 Stiffness of the optimized wingbox

Similarly, stiffness of the optimized wingbox which is constructed in chapter 5.2.1 is also evaluated. At first, the sampling points are chosen after running the model with optimized fibre orientations. The position of sampling points is shown in Figure 5.24. Every two neighbouring points are 0.1 m apart. The left side of the wingbox is fixed so that the sampling starts at x=0.1 m. In Figure 5.25 we can see the elastic curves of the optimized wingboxs and aluminium wingbox. Figure 5.25 shows that both optimized PeCCF composite wingboxes are softer than aluminium wingbox since the blace and blue curves are above the red curve. This means that the stiffness limitation is not negligible for GA process. Otherwise, the optimized results will not fulfill the requirements as structure.

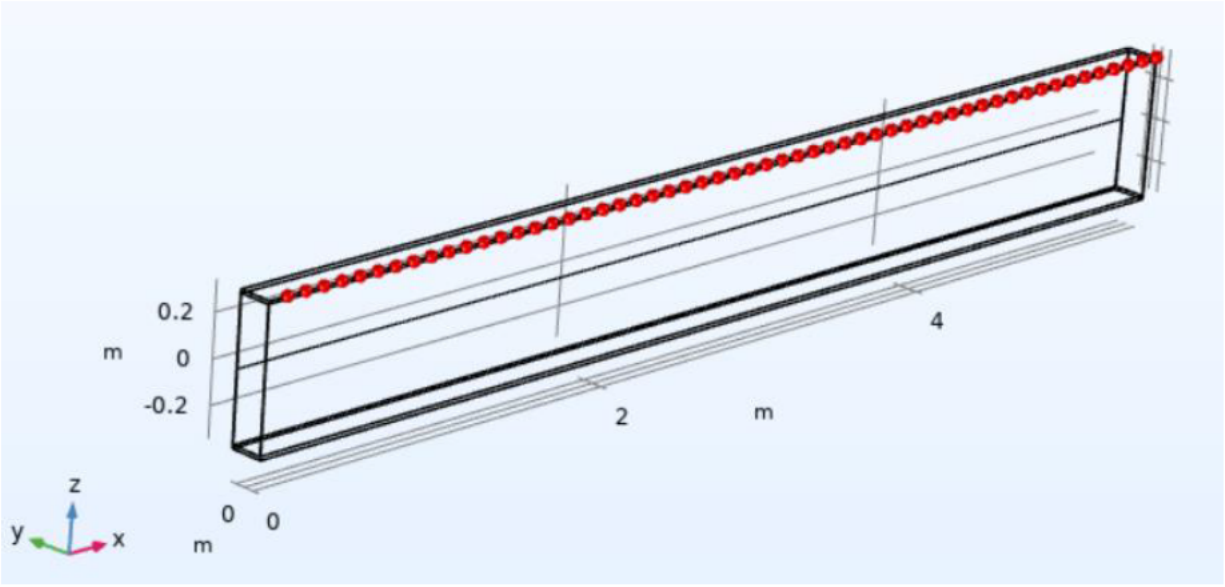

Figure 5.24: Sampling positions on the wingbox

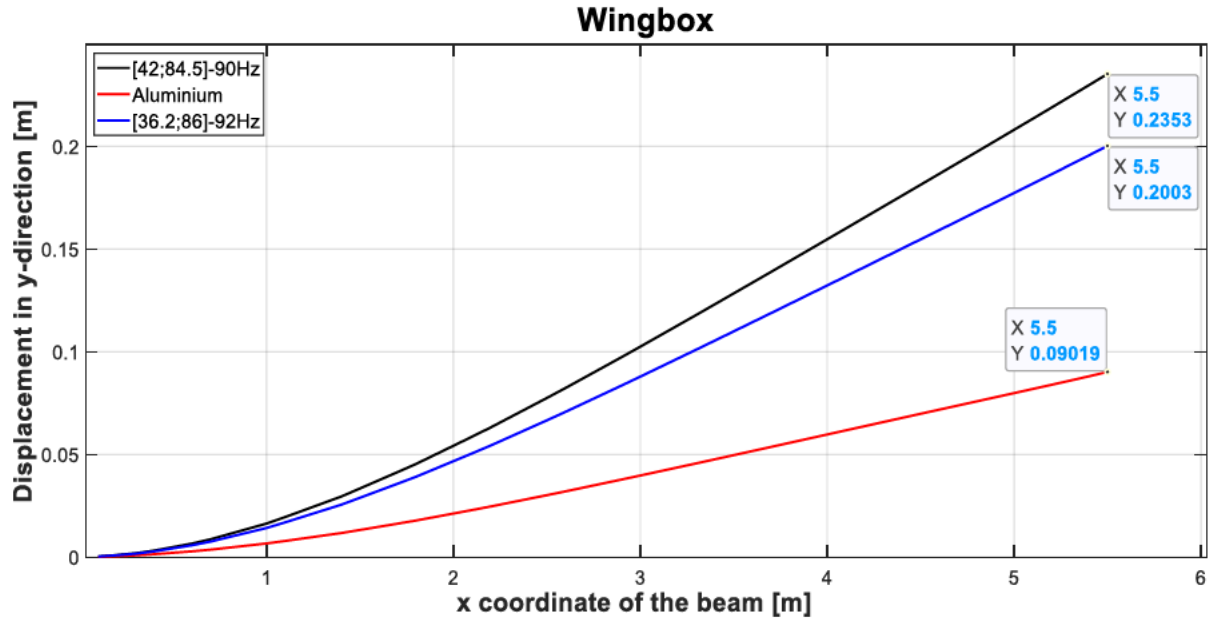

Figure 5.25: Displacement in y-direction along the wingbox for different material and fibre orientation

6 Conclusion and Future Work

This chapter consists of two parts. The first part summarizes the whole thesis and concludes. The second part makes observations on all results in previous chapters and raises questions. Based on that prediction about the future development of the PeCCF composite structure and possible difficulties and problems with this development.

6.1 Conclusion

In this thesis a simulation framework for dynamically loaded PeCCF composite structure was constructed by the means of Matlab and COMSOL Multiphysics 5.5. Afterwards, its potential for vibration reduction was investigated.

At first a dynamically loaded Timoshenko beam was simulated via COMSOL and Matlab. The results of both softwares are identical. Compared with the Matlab model the results of the COMSOL model also shows the natural frequencies and their shape modes when the beam undergose only axial deformation. Simultaneously, the influence of Yong's modulus on the vibration reduction effect is proven, since the total kinetic energy of the system is much smaller by avoiding a specific value of Young's modulus.

Then a COMSOL model for the PeCCF composite structure is construted. Based on the microstructure and LW theory, the beam with different variables is compared. The results reveal that the vibration can be reduced by greater fibre volume fraction. The velocity magnitude decreases by 6 dB when the fibre volume fraction increases from 0.2 to 0.8. Moreover, the fibre orientation can influence the vibration control effect significantly while Young's modulus of the polymer coating E_c makes almost no difference. This can depend on the relative direction between the layer and loading. In addition, big difference of Young's modulus between the carbon fibre and polymer coating may be another reason for the little impact of E_c. Even though we find that the fibre orientation can influence the damping effect of PeCCF structure, the exact effects of the fibre orientation on the vibration reduction ability are too complex to be understood as there are multiple possible combinations of fibre orientation.

Hence, the fibre orientation is optimized via GA in Matlab and COMSOL. The model and the variables of the fitness function are set up in COMSOL. The fitness function is defined in Matlab which can control the COMSOL model and export the results from COMSOL and then use them

for finding the best solution (fibre orientation) of the fitness function. The fibre orientation is then determined for the min.total kinetic energy of the beam (fitness value). For this optimization the beam with different cross-sections and a wingbox model are created.

In the end, the rationality of the optimization fibre orientations were tested. However, the beams with optimized fibre orientation for 90 Hz are much softer than aluminium beams while the optimized beams for 20 Hz are stiffer than aluminium beams. This could be caused by the target frequency for GA process. In the optimization procedure the goal is to avoid resonant frequency. To avoid 90 Hz the fibre orientation changes to the position which can not bearing bending load as well as 0°. Moreover, the optimized wingbox is softer than aluminium wingbox as well. This means that a siffness limitation must be set up for the GA optimization although the best fibre orientation can reduce the level of the total kinetic energy up to 20 dB. Otherwise, the optimized results will not fulfill the requirements as structure.

6.2 Suggestions for future work

The following suggestions are given for the further investigation of vibration reduction potential using PeCCF composite structures.

- Stiffness limitations of the PeCCF composite structure in a valid range of optimization

Although the models are optimized successfully, the results for beam and wingbox models are not satisfactory due to their low stiffnesses. Therefore, the stiffness should be set up in a valid range when the best combinations of fibre orientations are sought in future research. The standard structural stiffness of already existing airplane wings should be used as a boundary conditions for the optimization procedure. With this limitation, the optimized structure can not only reduce vibrations but also satisfy the basic stiffness requirements for mechanical structures in aircraft.

- Considering the viscoelastic material laws influences on the damping effects

In this work, elastic materials are demonstrated, whilst in reality, materials are viscoelastic. Moreover, the viscoelastic effect of the material is a key factor for the structural damping effect. In a further studies, this property should be taken into account. Hence, the results of the simulation are more plausible and closer to reality. After considering the viscoelastic property the optimized

structure can be used to reduce the vibration when the resonant frequencies of noise are difficult to avoid.

- Considering the variational modulus of the polymer coating

As structure batterie, the carbon fibres generate heat when they transfer electric energy Furthermore, during the flight, the altitude of the aircraft varies greatly. Both factors lead to a significant temperature change. At the same time, Young's modulus of the polymer electrolyte coating varies considerably with temperature [33]. When the load and the carbon fibre orientation are aligned, this temperature change may have almost no effect on the structures vibration reduction effect as the longitudinal modulus of the fibre is much greater than that of the coating, although it does change a lot. However, if the force is perpendicular to the carbon fibres, which means that only the transverse modulus of the carbon fibre and composite matrix (2 GPa) works against the load. The transverse modulus of the fibre is 8 GPa while the modulus of the coating varies between 0.5 GPa and 2.0 GPa. In this situation, the variational modulus of the coating due to temperature must be considered.

References

[1] “www.scitechnol.com,” [Online]. Available: https://www.scitechnol.com/scholarly/multifunctional-materials-journals-articles-ppts -list.php#:~:text=Multifunctional%20Material%20is%20defined%20to ,magnetic%2C%20thermal%20etc.... [Accessed 22 July 2021].

[2] C. Multiphysics, “Micromechanics and Stress Analysis of a Composite Cylinder”.

[3] M. Schutzeichel, “Experimental characterization of multifunctional polymer electrolyte coated carbon fibres,” *Funct. Compos. Struct.,* 2019.

[4] M. Schutzeichel, “Fundamental characterization of multifunctional polymer electrolyte coated carbon fibres and evaluation of airframe integration potential,” *Master's thesis at Hamburg University of Applied Sciences,* 2017.

[5] A. Bismarck, “Development of novel composites through fibre and interface/interphase modification,” *IOP Conference Series: Material Science and Engineering,* 2016.

[6] P. Bhatt, Maximum Marks, Maximum Knowledge in Physics, Allied Publishers, 2009.

[7] “Newport,” [Online]. Available: https://www.newport.com/t/fundamentals-of-vibration#:~:text=The%20natural%20frequency%2C%20as%20the,which%20acts%20as%20a%20spring.. [Accessed 29 June 2021].

[8] S. P. TIMOSHENKO, History of Strength of Materials, New York: Dover Publications. Inc, 1953.

[9] J. W. STRUTT, Theory of Sound, London: Macmillan Publications Co., Inc, 1877.

[10] B. A. H. A. a. J. THOMAS, “The second frequency spectrum of Timoshenko beams,” *Journal of Sound and Vibration,* pp. 123-137, 1977.

[11] S. P. TIMOSHENKO, “On the correction for shear of the differential equation for transverse vibrations of bars of uniform cross-section,” *Philosophical Magazine,* p. 744, 1921.

[12] S. P. TIMOSHENKO, “On the transverse vibrations of bars of uniform cross-section,” *Philosophical Magazine,* p. 125, 1922.

[13] A. S. d. C. Azevêdo and S. d. S. Hoefel, “MODAL ANALYSIS FOR FREE VIBRATION OF FOUR BEAM THEORIES,” p. 1st, 6 December 2015.

[14] R. M. DAVIES, “The frequency of transverse vibration of a loaded "xed-free bar III. The e!ect of rotatory inertia of the bar,” *Philosophical Magazine,* p. 563, 1937.

[15] B. S. Gan, An Isogeometric Approach to Beam Structures, Koriyama, Fukushima, Japan: Springer, 2018.

[16] “Energy GOV,” [Online]. Available: https://www.energy.gov/eere/articles/ how-does-lithium-ion-battery-work #:~:text=The%20anode%20and%20 cathode%20store,at%20the%20 positive%20current%20collector.. [Accessed 20 July 2021].

[17] Samsung. [Online]. Available: https://www.samsungsdi.com/ column/technology/detail/55272.html ?listType=gallery. [Accessed 28 June 2021].

[18] E. Jacques, “Lithium intercalated carbon fibres, PhD thesis,” KTH School of Engineering, 2014.

[19] T. T. E. GmbH, “Delivery programme and characteristics for tenax,” Toho Tenax Europe GmbH, 2017.

[20] M. H. Kjell, “Pan-based carbon fibre negative electrodes or structural lithiumion,” *Journal of the Electrochemical Society,* 2011.

[21] M. Schutzeichel, “Effective stiffness and thermal expansion of three-phase multifunctional polymer electrolyte coated carbon fibre composite materials,” 2021.

[22] L. A. a. E. S. Greenhalgh, “Structural power composites,” *Composites Science and Technology,* pp. 41-61, 2014.

[23] S. Leijonmarck, “Solid polymer electrolyte-coated carbon fibres for structural,” *Composites Science and Technology,* 2013.

[24] COMSOL. [Online]. Available: https://doc.comsol.com/5.6/ doc/com.comsol.help.compmat/ compmat_ug_modeling.3.18.html. [Accessed 15 August 2021].

[25] D. Li, “Layerwise Theories of Laminated Composite Structures and Their Applications: A Review,” *Archives of Computational Methods in Engineering,* January 2020.

[26] J. H. Dolmans, “Application of Active Noise Control to Reduce Cabin Noise in Single Engine General Aviation Aircraft,” Embry-Riddle Aeronautical University, Daytona Beach, Florida, 1997.

[27] A. E. J. E. S. Eiben, “Introduction to evolutionary computing. Vol. 53.,” Heidelberg, springer, 2003.

[28] COMSOL, “Structural Mechanics Module User’s Guide,” 2019.

[29] M. P. a. R. H. Stepan Ozana, “Using MATLAB and COMSOL Multiphysics for Optimization of the Model of Underground Thermal Processes at Old Mining Dumps,” *Trans Tech Publications,* 2014.

[30] O. S. Rasmus E. Christiansen, “Compact 200 line MATLAB code for inverse design in photonics by topology optimization: tutorial,” *Journal of the Optical Society of America B,* February 2021.

[31] R. V. a. C. N. Juan S. Muñoz, “COMSOL and MATLAB® Integration to Optimize Heat Exchangers Using Genetic Algorithms Technique,” *Excerpt from the Proceedings of the COMSOL Conference,* 2008.

[32] M. Linke, Aufgaben zur Festigkeitslehre für den Leichtbau, Hamburg: Springer Vieweg, 2018.

[33] H. Maples, “Composites with Controllable Stiffness,” Philosophy of Imperial College London, London.

[34] T. E. Toolbox. [Online]. Available: https://www.engineeringtoolbox.com/ young-modulus-d_417.html. [Accessed 22 July 2021].

[35] Ingenieurkurse.de, [Online]. Available: https://www.ingenieurkurse.de/maschinenelemente-1/verbindungen-und-verbindungselemente/ kraftschluessige-verbindungen/klemmverbindungen.html. [Accessed 19 July 2019].

[36] “Johannes Strommer,” [Online]. Available: https://www.johannes-strommer.com/ rechner/flaechentraegheitsmoment- widerstandsmoment-querschnittsflaeche/. [Accessed 21 July 2021].

Appendix A – Matlab code for Timoshenko beam

Main Script

```
clear
clc

disp('please wait!!!!!!-The job is under run')

% Discretizing the Beam

nel=15;                 % number of elements
nnel=2;                 % number of nodes per element
ndof=2;                 % number of dofs per node
nnode=(nnel-1)*nel+1;   % total number of nodes in system
sdof=nnode*ndof;        % total system dofs

% Material properties
E1=7.0*10^10;            % Youngs modulus

% changed Youngs modulus
E2=6.898*10^11;


BB=0.03;                % Width
HH=0.15;               % Height
I=BB*HH^3/12;           % moment of inertia of cross-section
mass = 2700.0;            % mass density of the beam

Ae=BB*HH;
nu=0.33;                      % poission ratio
Kse=10*(1+nu)/(12+11*nu);     %Shear factor of rectangle
```

```
Ge1=E1/2/(1+nu);                %G modulus in N/m^2
Ge2=E2/2/(1+nu);                %G modulus in N/m^2

tleng = 1.4;                % total length of the beam
leng = tleng/nel;          % uniform mesh (equal size of
elements)

lengthvector = 0:leng:tleng ;

% Boundary Conditions
bc = 'c-f' ;                % clamped-free
%bc = 'c-c' ;               % clamped-clamped
%bc = 'c-s' ;               % clamped-supported
%bc = 's-s' ;               % supported-supported

kk=zeros(sdof,sdof);     % initialization of system
stiffness matrix

kk1=kk;
kk2=kk;

kkg=zeros(sdof,sdof);    % initialization of system geomtric
stiffness matrix

kkg1=kkg;
kkg2=kkg;

mm=zeros(sdof,sdof);     % initialization of system mass
matrix

mm1=mm;
mm2=mm;
```

```
index=zeros(nel*ndof,1);  % initialization of index vector

for iel=1:nel           % loop for the total number of
elements

index=elementdof(iel,nnel,ndof);  % extract system dofs
associated with element

[k1,kg1,m1]=beamT(E1,I,leng,mass,Kse,Ge1,Ae); % compute
element stiffness,geometric

[k2,kg2,m2]=beamT(E2,I,leng,mass,Kse,Ge2,Ae); % compute
element stiffness,geometric

kk1=assembel(kk1,k1,index); % assemble element stiffness
matrices into system matrix

kkg1=assembel(kkg1,kg1,index); % assemble geometric
stiffness matrices into system matrix

mm1=assembel(mm1,m1,index); % assemble element mass
matrices into system matrix

kk2=assembel(kk2,k2,index); % assemble element stiffness
matrices into system matrix

kkg2=assembel(kkg2,kg2,index); % assemble geometric
stiffness matrices into system matrix

mm2=assembel(mm2,m2,index); % assemble element mass
matrices into system matrix
end
```

```
%
% Applying the Boundary conditions
[nbcd,bcdof] = BoundaryConditions(sdof,bc); % Reducing the
matrix size

[kk1,mm1] = constraints(kk1,mm1,bcdof) ;
[kk1,kkg1] = constraints(kk1,kkg1,bcdof) ;
%
% Natural frequencies and Buckling load
[vecfreq1 freq1]=eig(kk1,mm1);   % solve the eigenvalue
problem for Natural Frequencies

freq1 = diag(freq1) ;
freq1=sqrt(freq1);   % UNITS :rad per sec
freqHz1 = freq1/(2*pi)  % UNITS : Hertz

[kk2,mm2] = constraints(kk2,mm2,bcdof) ;
[kk2,kkg2] = constraints(kk2,kkg2,bcdof) ;
%
% Natural frequencies and Buckling load
[vecfreq2 freq2]=eig(kk2,mm2);   % solve the eigenvalue
problem for Natural Frequencies

freq2 = diag(freq2) ;
freq2=sqrt(freq2);   % UNITS :rad per sec
freqHz2 = freq2/(2*pi)  % UNITS : Hertz

nmax = 10000;
nf = [0:1:nmax-1];
df = 1;
FF = df*nf;
Om = 2.0*pi*FF;
```

```
for i=1:nmax
    Cmat21 = kk1 - Om(i)^2*mm1;
    Nmat21 = inv(Cmat21);

    Hb111(i) = Nmat21(17,21);
    Hb221(i) = Nmat21(19,21);
    Hb331(i) = Nmat21(21,21);

    Kimat1=j*Om(i)*Nmat21;
    Vb111(i) = Kimat1(17,21);
    Vb221(i) = Kimat1(19,21);
    Vb331(i) = Kimat1(21,21);

    Cmat22 = kk2 - Om(i)^2*mm2;
    Nmat22 = inv(Cmat22);

    Hb112(i) = Nmat22(17,21);
    Hb222(i) = Nmat22(19,21);
    Hb332(i) = Nmat22(21,21);

    Kimat2=j*Om(i)*Nmat22;
    Vb112(i) = Kimat2(17,21);
    Vb222(i) = Kimat2(19,21);
    Vb332(i) = Kimat2(21,21);
end
%
% Magnitude
COMSOL=load('Displacement-Velocity-Frequenzgang-
10Elements.txt');

figure(1);
set(gca,'FontSize',17);
```

```
semilogx(FF,20*log10(abs(Hb331)),'-.k+','linewidth',1);hold
on;...
semilogx(FF,20*log10(abs(Hb332)),'k-','linewidth',2);hold
on;...
semilogx(COMSOL(:,1),20*log10(abs(COMSOL(:,2))),'b-
','linewidth',2);hold off;
grid on;

xlabel('frequency [Hz]','FontSize',20,'FontWeight','bold');
ylabel('Transversal displacement
20*log10(abs(v))[dB]','FontSize',20,'FontWeight','bold');
title('Frequenzgang des 2. und 3. sowie 4.
Knoten','Fontsize',30,'FontWeight','bold')
legend({'Matlab','10.Knoten-smaller Youngs
Modulus','COMSOL-
FrequencyDomain'},'Location','northwest','Fontsize',18,'Fon
tWeight','bold');

figure(2);
set(gca,'FontSize',17);
semilogx(FF,20*log10(abs(Vb331)),'-.k+','linewidth',1);hold
on;...
semilogx(FF,20*log10(abs(Vb332)),'k-','linewidth',2);hold
on;...
semilogx(COMSOL(:,1),20*log10(abs(COMSOL(:,3))),'b-
','linewidth',2);hold off;
grid on;
xlabel('frequency [Hz]','FontSize',20);
ylabel('velocity 20*log10(abs(v))
[dB]','FontSize',20,'FontWeight','bold');
```

```
title('Frequenzgang des 2. und 3. sowie 4.
Knoten','Fontsize',30,'FontWeight','bold','FontWeight','bol
d')
legend({'Matlab','10.Knoten-smaller Youngs
Modulus','COMSOL-
FrequencyDomain'},'Location','northwest','Fontsize',18,'Fon
tWeight','bold');
%
% Plot Mode Shapes

h = figure ;
set(h,'name','Mode Shapes of Beam in
Hz','numbertitle','off')
PlotModeShapes(vecfreq1,freqHz1,lengthvector,nbcd)

h = figure ;
set(h,'name','Mode Shapes of Beam in
Hz','numbertitle','off')
PlotModeShapes(vecfreq2,freqHz2,lengthvector,nbcd)
```

- Functions

Function assembel

```
function [kk]=assembel(kk,k,index)
%-------------------------------------------------------------
%  Purpose:
%     Assembly of element matrices into the system matrix
%
%  Synopsis:
%     [kk]=assembel(kk,k,index)
%
%  Variable Description:
```

```
%     kk - system matrix
%     k  - element matrix
%     index - d.o.f. vector associated with an element
%-------------------------------------------------------
-


 edof = length(index);
 for i=1:edof
   ii=index(i);
     for j=1:edof
       jj=index(j);
         kk(ii,jj)=kk(ii,jj)+k(i,j);
     end
 end
```

Function beamT (stiffness and mass matrix)

```
function [k,kg,m]=beamT(E,I,leng,mass,Kse,Ge,Ae)

%-------------------------------------------------------
---------
%  Purpose:
%     Stiffness, Goemetric stiffness and mass matrices for
Hermitian beam element
%   ><
%
%  Synopsis:
%     [k,m]=beam(E,I,leng,mass)
%
%  Variable Description:
%     k - element stiffness matrix (size of 4x4)
%     m - element mass matrix (size of 4x4)
```

```
%     E - elastic modulus
%     I - second moment of inertia of cross-section
%     leng - element length
%     mass - mass density (mass per unit volume)
%==========================================================
phi=12*E*I/Kse/Ge/Ae/leng^2;

Mmat1=Ae*mass*leng/((1+phi)^2)/210*[ [70*phi^2+147*phi+78
(35*phi^2+77*phi+44)*leng/4    35*phi^2+63*phi+27
-(35*phi^2+63*phi+26)*leng/4];...

[(35*phi^2+77*phi+44)*leng/4   (7*phi^2+14*phi+8)*leng^2/4
(35*phi^2+63*phi+26)*leng/4    -
(7*phi^2+14*phi+6)*leng^2/4];...
                                  [35*phi^2+63*phi+27
(35*phi^2+63*phi+26)*leng/4    70*phi^2+147*phi+78
-(35*phi^2+77*phi+44)*leng/4];...
                                  [-
(35*phi^2+63*phi+26)*leng/4  -(7*phi^2+14*phi+6)*leng^2/4
-(35*phi^2+77*phi+44)*leng/4
(7*phi^2+14*phi+8)*leng^2/4]];

Mmat3=mass*I/30/((1+phi)^2)/leng*[[36                -
(15*phi-3)*leng          -36              -(15*phi-
3)*leng];...
                           [-(15*phi-3)*leng
(10*phi^2+5*phi+4)*leng^2   (15*phi-3)*leng     (5*phi^2-
5*phi-1)*leng^2];...
                           [-36              (15*phi-
3)*leng            36              (15*phi-3)*leng];...
```

```
                                [-(15*phi-3)*leng  (5*phi^2-
5*phi-1)*leng^2    (15*phi-3)*leng
(10*phi^2+5*phi+4)*leng^2]];

% Calculate Element Stiffness Matrix
%=============================================================
Kmat=E*I/leng^3/(1+phi)*[[12       6*leng           -12
6*leng];...
                         [6*leng   (4+phi)*leng^2   -6*leng
(2-phi)*leng^2];...
                         [-12      -6*leng          12
-6*leng];...
                         [6*leng   (2-phi)*leng^2   -6*leng
(4+phi)*leng^2]];


%Element mass matrices
kg = Mmat3;

m = Mmat1+Mmat3;

%Element stiffness matrices
k = Kmat;
```

Function Boundary conditions

```
function [nbcd,bcdof] = BoundaryConditions(sdof,bc)

%-------------------------------------------------------------
---------------
% Purpose :
%         To get the arrested degree's of freedom for the
beam depending on
```

```
% type of the boundary conditions
%
% Synopsis :
%          [nbcd,bcdof] = BoundaryConditions(sdof,bc)
%
% Variable Description:
% INPUT parameters:
%           sdof : system degrees of freedom
%           bc : boundary condition type
%
% OUTPUT PARAMETERS :
%           bcdof : boundary degrees of freedom
%           nbcd : number of boundary conditions
%-----------------------------------------------------------

 if bc == 'c-c'     % clamped-clamped beam
    bcdof = [1 2 sdof-1 sdof] ;
    nbcd = length(bcdof) ;

 elseif bc == 'c-f' % clamped-free beam
      bcdof = [1 2] ;
%     bcdof = [1 2 3] ;
    nbcd = length(bcdof) ;

 elseif bc == 'c-s'     % clamped-supported beam
     bcdof = [1 2 sdof-1] ;
     nbcd = length(bcdof) ;

 elseif bc == 's-s'     % supported-supported beam
     bcdof = [ 1 sdof-1] ;
     nbcd = length(bcdof) ;
```

```
 end
```

Function constraints

```
function [kk,mm]=constraints(kk,mm,bcdof)

%-------------------------------------------------------------
------------
%  Purpose:
%     Apply constraints to eigenvalue matrix equation
%     [kk]{x}=lamda[mm]{x}
%
%  Synopsis:
%     [kk,mm]=feaplycs(kk,mm,bcdof)
%
%  Variable Description:
%     kk - system stiffness matrix before applying
constraints
%     mm - system mass matrix before applying constraints
%     bcdof - a vector containging constrained d.o.f
%-------------------------------------------------------------

 n=length(bcdof);
 sdof=size(kk);

 for i=1:n
    c=bcdof(i);
    for j=1:sdof
       kk(c,j)=0;
       kk(j,c)=0;
       mm(c,j)=0;
       mm(j,c)=0;
    end
    kk(c,c)=1;
```

```
    mm(c,c)=1;
 end
```

Function element DOF

```
function [index]=eldof(iel,nnel,ndof)
%-------------------------------------------------------------
%  Purpose:
%     Compute system dofs associated with each element in
one-
%     dimensional problem
%
%  Synopsis:
%     [index]=eldof(iel,nnel,ndof)
%
%  Variable Description:
%     index - system dof vector associated with element
"iel"
%     iel - element number whose system dofs are to be
determined
%     nnel - number of nodes per element
%     ndof - number of dofs per node

%-------------------------------------------------------------

 edof = nnel*ndof;
 start = (iel-1)*(nnel-1)*ndof;

   for i=1:edof
      index(i)=start+i;
   end
```

Function Mode Shape Plot

```
function PlotModeShapes(vec,fsol,beam,nbc)

%-------------------------------------------------------------
% Purpose :
%         To Plot the Mode Shapes
% Synopsis :
%          PlotModeShapes(vec,fsol,beam,nbc)
% Variable Description:
% INPUT parameters:
%           vec : Eigenvector
%           fsol : Eigenvalues
%           beam : length vector of the beam (length
discretization)
%           nbc : Number of boundary conditions
%-------------------------------------------------------------
v = vec(1:2:end,:) ;
V = zeros(size(v)) ;
for i = 1:size(v,2)
    V(:,i) = v(:,i)./(max(abs(v(:,i)))) ;
end


L = max(beam) ;          % Length of the beam
n = 1 ;

% Plot First Mode shape
subplot(1,10,1)
plot(V(:,nbc+1),beam,'-ob','linewidth',n) ;
h = fsol(nbc+1) ;
title(num2str(h),'FontSize',15)
axis([-1 ,+1,0,L])
```

```
axis off

% Plot Second Mode shape
subplot(1,10,2)
plot(V(:,nbc+2),beam,'-ob','linewidth',n) ;
h = fsol(nbc+2) ;
title(num2str(h),'FontSize',15)
axis([-1 ,+1,0,L])
axis off

% Plot Third Mode shape
subplot(1,10,3)
plot(V(:,nbc+3),beam,'-ob','linewidth',n) ;
h = fsol(nbc+3) ;
title(num2str(h),'FontSize',15)
axis([-1 ,+1,0,L])
axis off

% Plot Fourth Mode shape
subplot(1,10,4)
plot(V(:,nbc+4),beam,'-ob','linewidth',n) ;
h = fsol(nbc+4) ;
title(num2str(h),'FontSize',15)
axis([-1 ,+1,0,L])
axis off

% Plot fifth Mode shape
subplot(1,10,5)
plot(V(:,nbc+5),beam,'-ob','linewidth',n) ;
h = fsol(nbc+5) ;
title(num2str(h),'FontSize',15)
axis([-1 ,+1,0,L])
```

```
axis off

% Plot sixth Mode shape
subplot(1,10,6)
plot(V(:,nbc+6),beam,'-ob','linewidth',n) ;
h = fsol(nbc+6) ;
title(num2str(h),'FontSize',15)
axis([-1 ,+1,0,L])
axis off

% Plot seventh Mode shape
subplot(1,10,7)
plot(V(:,nbc+7),beam,'-ob','linewidth',n) ;
h = fsol(nbc+7) ;
title(num2str(h),'FontSize',15)
axis([-1 ,+1,0,L])
axis off

% Plot eighth Mode shape
subplot(1,10,8)
plot(V(:,nbc+8),beam,'-ob','linewidth',n) ;
h = fsol(nbc+8) ;
title(num2str(h),'FontSize',15)
axis([-1 ,+1,0,L])
axis off

% Plot ninth Mode shape
subplot(1,10,9)
plot(V(:,nbc+9),beam,'-ob','linewidth',n) ;
h = fsol(nbc+9) ;
title(num2str(h),'FontSize',15)
axis([-1 ,+1,0,L])
```

```
axis off

% Plot tenth Mode shape
subplot(1,10,10)
plot(V(:,nbc+10),beam,'-ob','linewidth',n) ;
h = fsol(nbc+10) ;
title(num2str(h),'FontSize',15)
axis([-1 ,+1,0,L])
axis off
```

Appendix B – COMSOL Tutorial for Timoshenko beam

After opening the COMSOL 5.5 the Model Wizard is selected via clicking

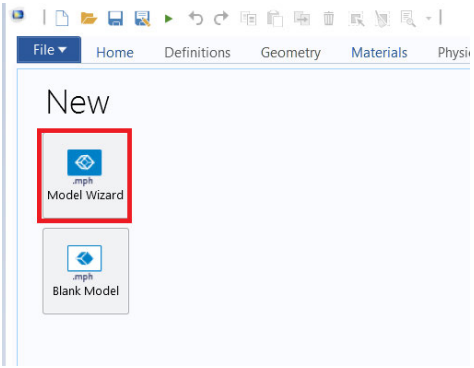

Then the 2D space dimesion is selected because of 2D simulation in Matlab.

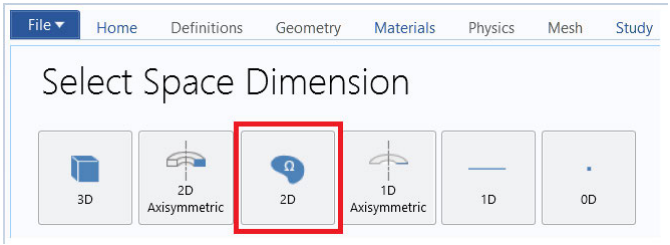

Later the structure type, *beam*, is under *Structural Mechanics* selected. The choosing is confirmed by clicking *Add*

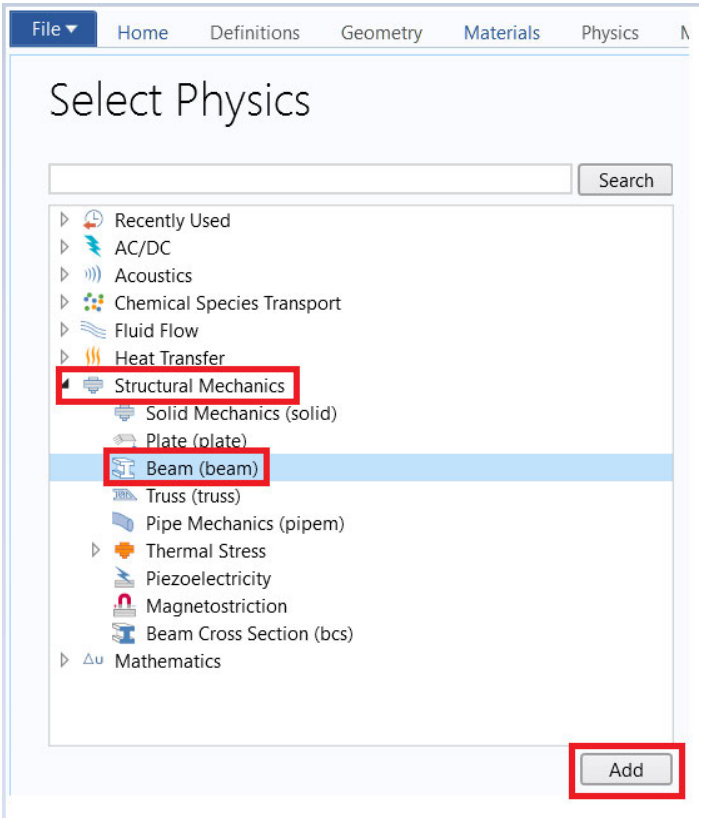

Clicking Study to get to study selection

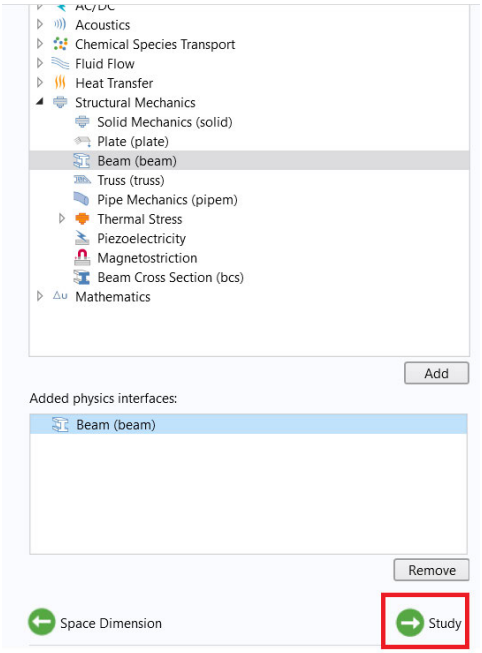

Here the *Eigenfrequency* is selected and confirmed by clcking *Done*.

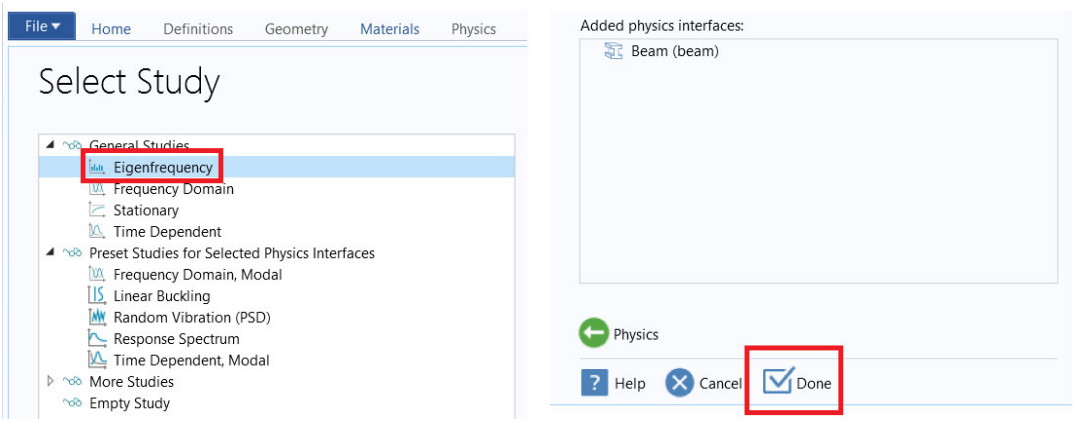

Now a 2D beam is built. By right clicking *Geometry* the *Line Segment* is selected.

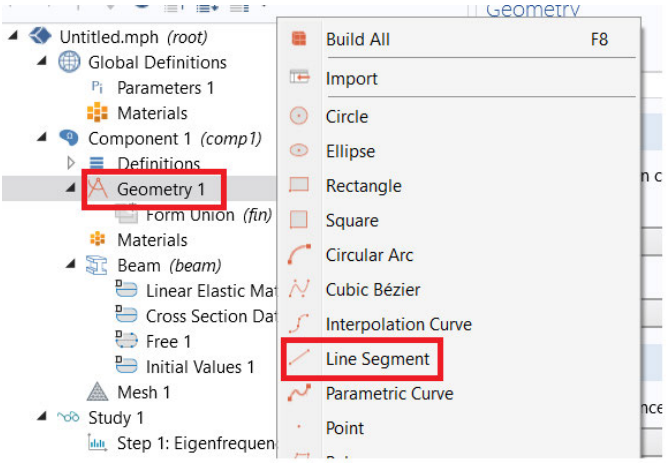

The beam is 1.4 meters long, so Line Segement is set as follows. After adding the coordinates of start and end point, the beam is built by clicking *Build Selected* above.

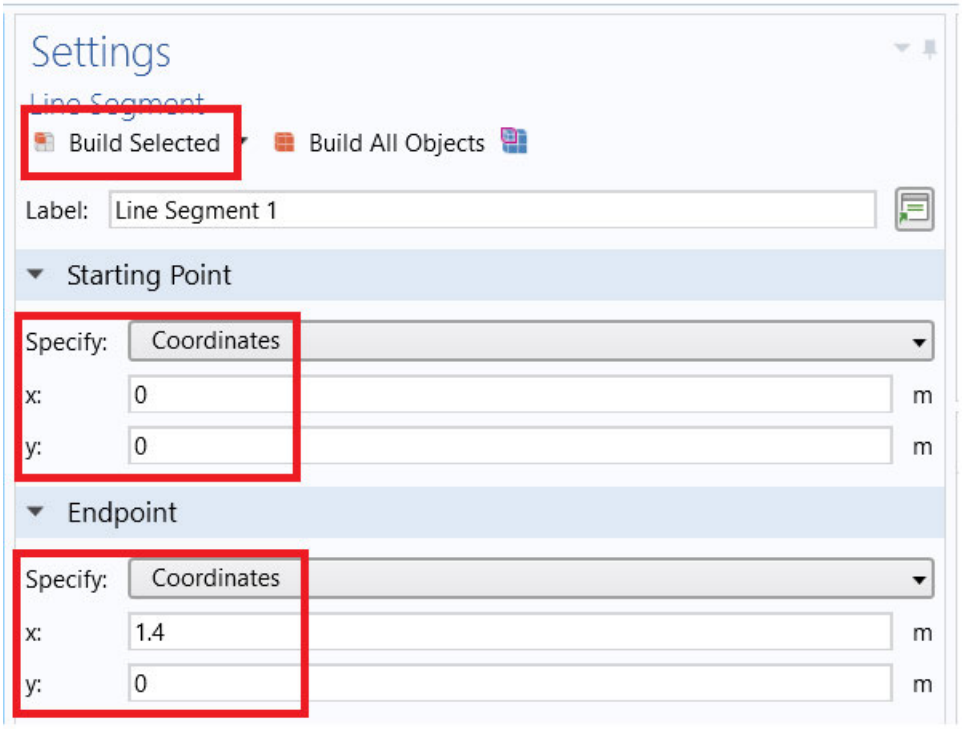

Afterwards the material of the beam is selected. Under *Home* by clcking the *Add Material* a new window will pop up on the right. Under *Built-in* a material can be selected by double clicking.

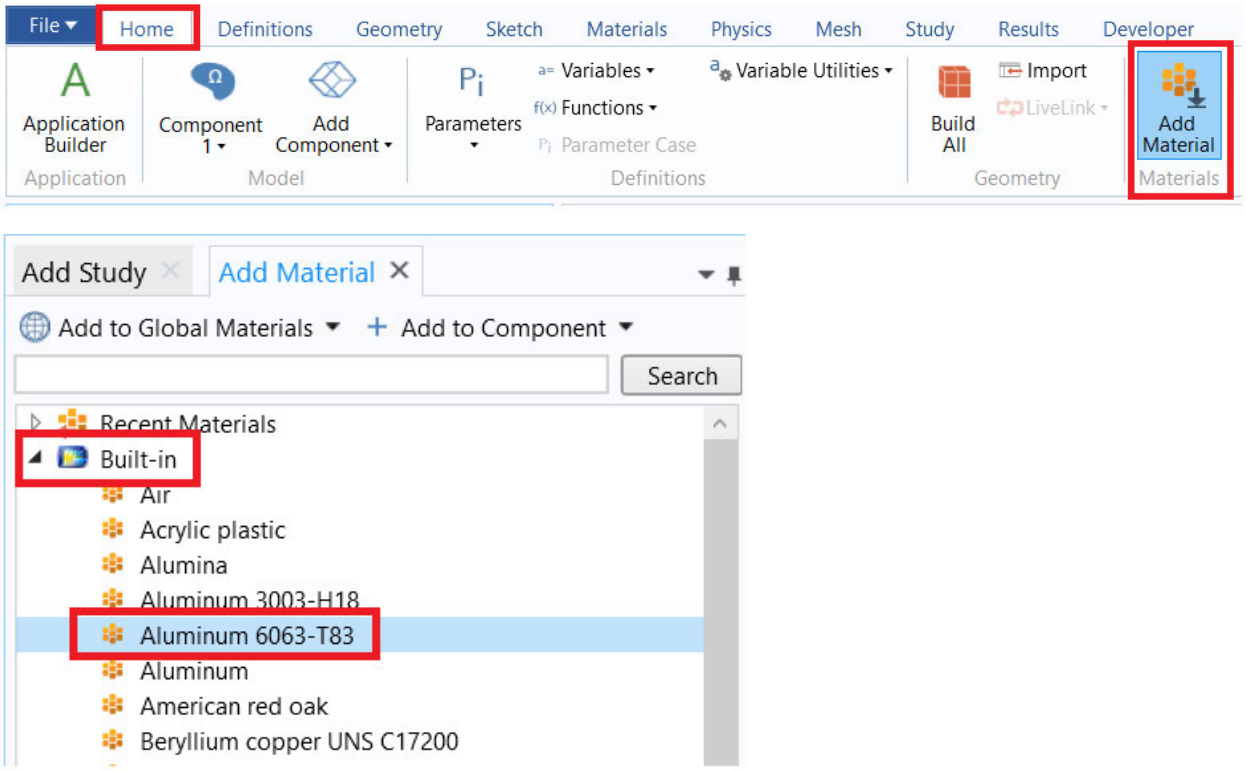

In material setting window the density, Young's modulus and Poission's ratio are input as follows:

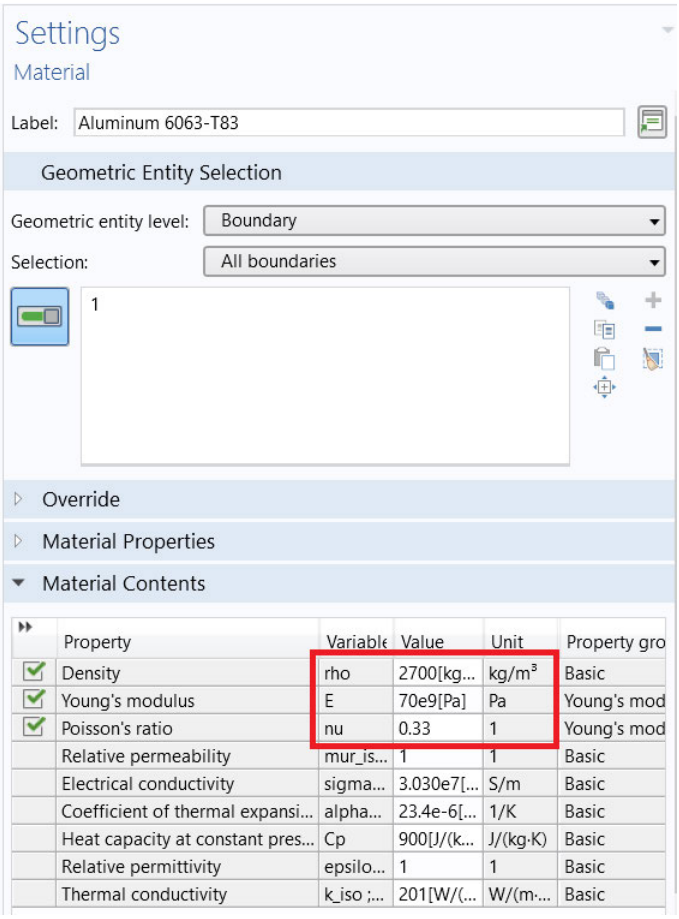

Then *Timoshenko* is under beam setting window selected.

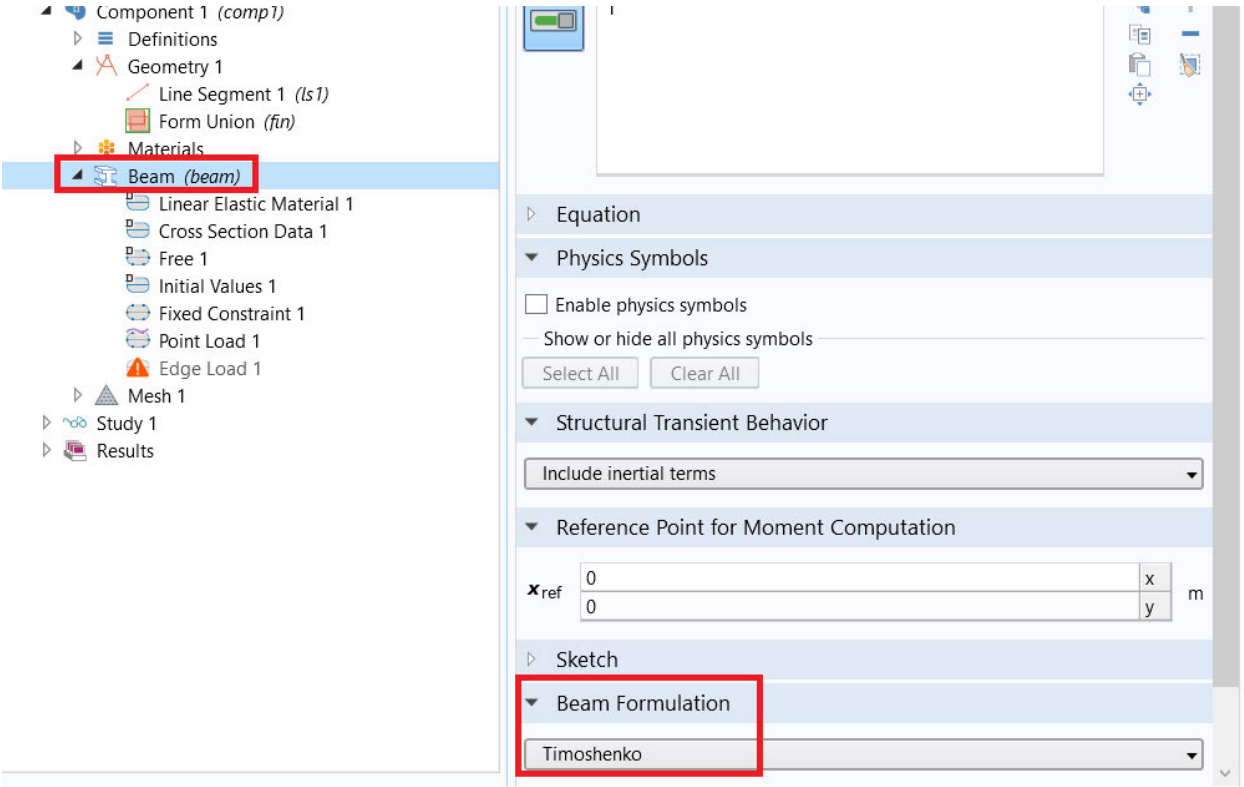

Besides, the cross section and the moment of inertia of the beam is set to the same values as in Matlab model under *Cross Section Data.* So that the natural frequencies in Matlab can be verified.

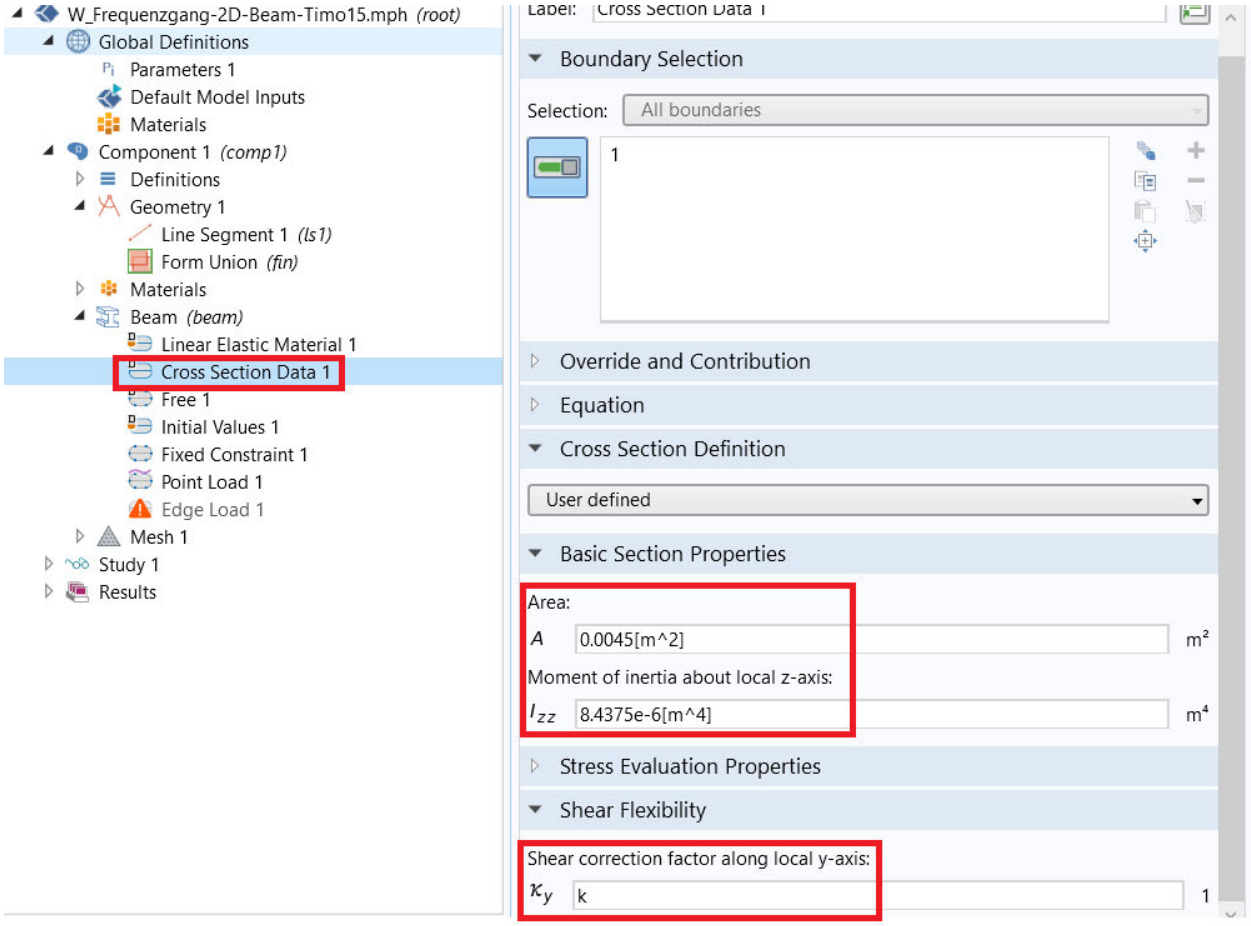

For rectangular cross section the *shear correction factor* k is set under parameters. *a* represents Poission's ratio here.

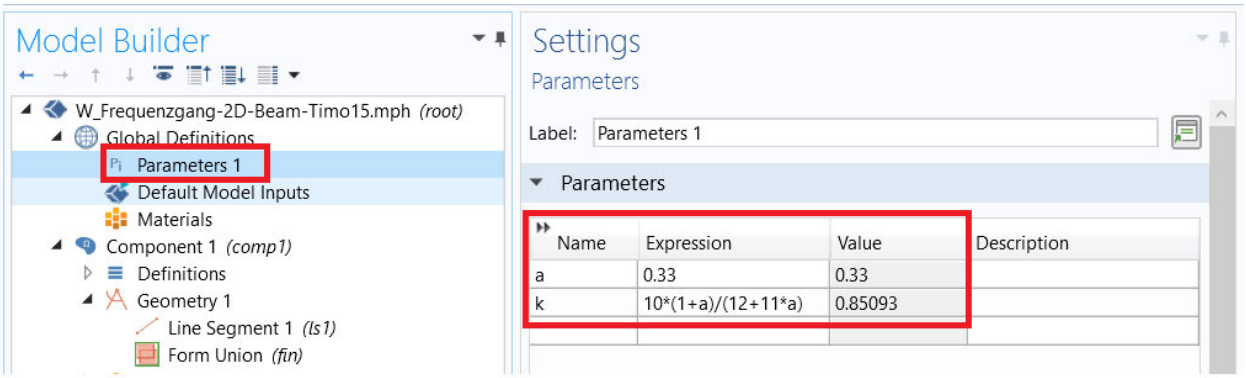

The beam is one end clamped, so that the *Fixed Constraint* is selected by right clicking *Beam*. In setting window the position of clamped constraint is input.

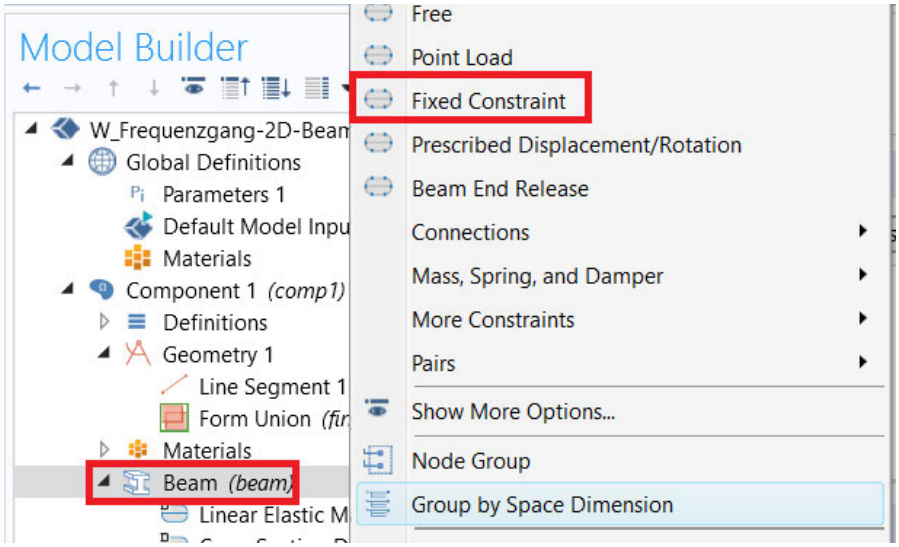

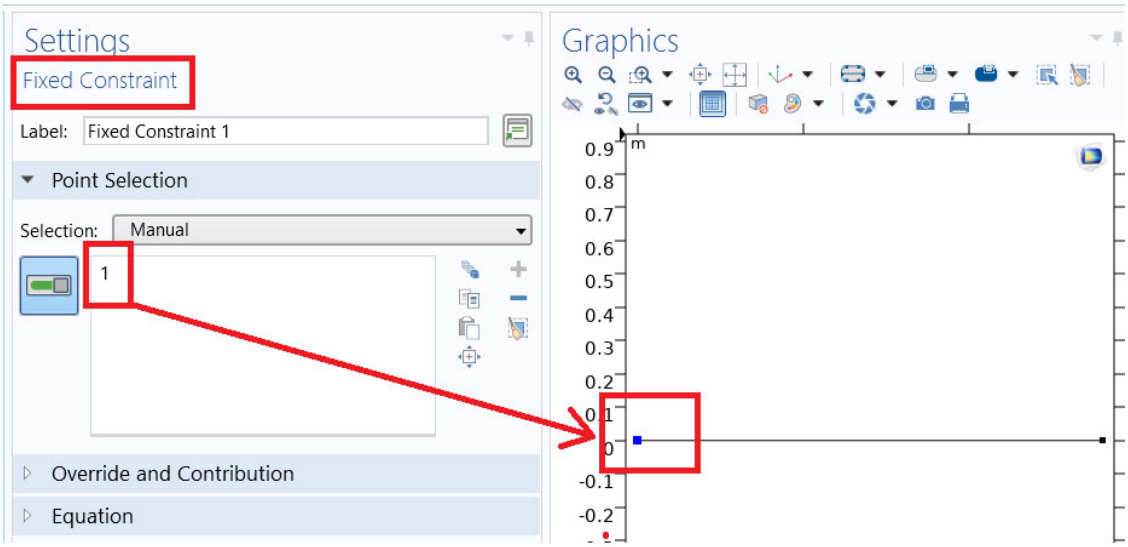

Then the model is meshed by clicking *Build All*. The settings are shown below:

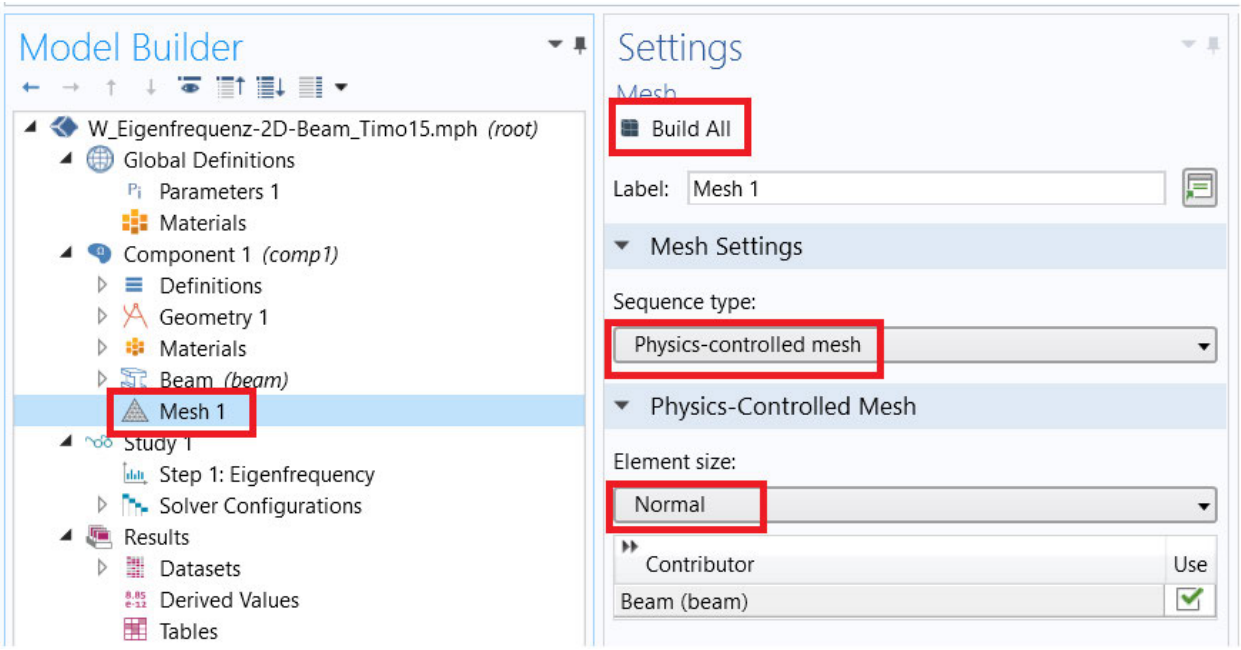

In the end the number of desired natural frequencies is input in the setting window. The number of natural frequencies can not exceed the number of DOF of all model elements. After clicking *Compute* above, the model is calculated.

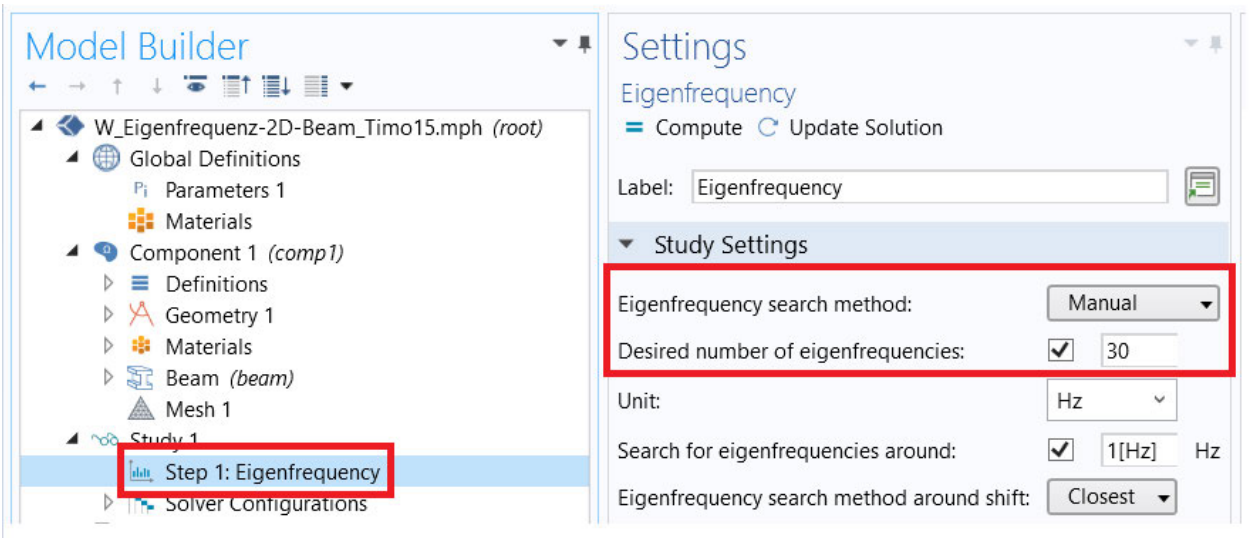

After calculating the natural frequencies and their mode shape are shown under *Results—Mode Shape*. By clicking *Plot* or arrows the different mode shape of different natural frequencies are shown.

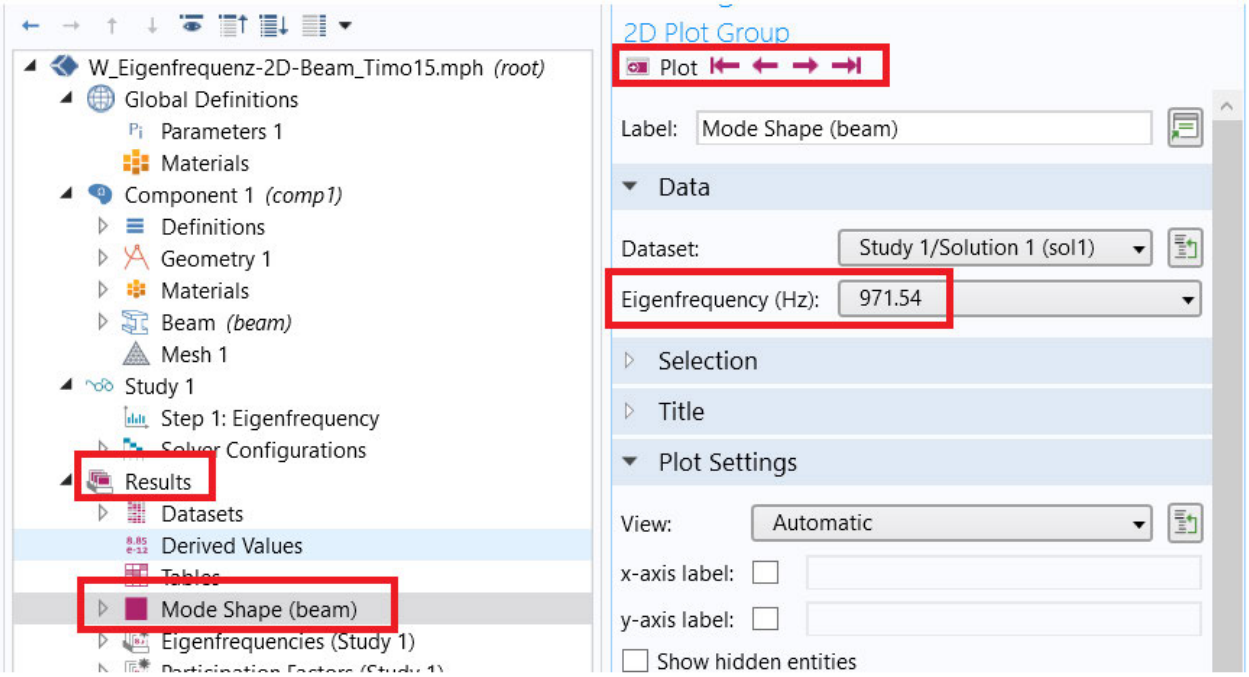

Appendix C – Matlab code for comparing total kinetic energy of beam with different Young's modulus

```
% For Function
close all
clc
clear all
model = mphopen('D:\Comsol\Masterarbeit\W_Frequenzgang-2D-
Beam-Timo10-E7-90Hz.mph');
E1=7e9:1e8:1e11;
aa=length(E1);
AA=zeros(aa,2)
for i =1:aa
model.param.set('E1',E1(i));
model.study('std1').run;
Ek=mphglobal(model,'beam.Wk_tot','dataset','dset1','solnum'
,1,'outersolnum',1);
AA(i,1)=Ek;
AA(i,2)=E1(i);
end

[Ekmin,Emodul]=min(AA(:,1))
AA

figure(1)
x=AA(:,2);
y=AA(:,1);
plot(x,y)
```

```
xlabel('Youngs Modules [Pa]','FontSize',25);
ylabel('Ekin Totol Kinetic Energy [J]','FontSize',25);
title('kinetic Energy Vs E-Modul at 60 Hz','FontSize',30);
```

Appendix D – Matlab code for comparing velocity along the beam with different parameters

```
COMSOL1=load('Ec_2_velocity_Frequenz-04590-90Hz.txt');
COMSOL2=load('Ec_05_velocity_Frequenz-04590-90Hz.txt');
COMSOL3=load('Ec_2_velocity_Frequenz-04590-90Hz-Vf08.txt');
COMSOL4=load('Ec_2_velocity_Frequenz-04590-90Hz-Vf02.txt');
COMSOL5=load('Ec_2_velocity_Frequenz-90450-90Hz.txt');
COMSOL6=load('Ec_2_velocity_Frequenz-301080-90Hz.txt');
COMSOL7=load('Ec_05_velocity_Frequenz-45-45-90Hz.txt');
COMSOL8=load('Ec_2_velocity_Frequenz-45-45-90Hz.txt');

x=0.1:0.1:1.4;

figure(1);
set(gca,'FontSize',18);
plot(x,20*log10(COMSOL1(1,2:15)./5e-8),'y-
','linewidth',6);hold on;

plot(x,20*log10(COMSOL2(1,2:15)./5e-8),'k-
','linewidth',2);hold on;

plot(x,20*log10(COMSOL3(1,2:15)./5e-8),'m-
','linewidth',3);hold on;

plot(x,20*log10(COMSOL4(1,2:15)./5e-8),'b-
','linewidth',3);hold on;
```

```
plot(x,20*log10(COMSOL5(1,2:15)./5e-8),'r-
','linewidth',3);hold on;

plot(x,20*log10(COMSOL6(1,2:15)./5e-8),'c-
','linewidth',3);hold on;

plot(x,20*log10(COMSOL7(1,2:15)./5e-8),'g-
','linewidth',6);hold on;

plot(x,20*log10(COMSOL8(1,2:15)./5e-8),'--
k','linewidth',2);hold off;

grid on;

xlabel('x coordinate of beam
[m]','FontSize',24,'FontWeight','bold');

ylabel('Level of velocity [dB] rel. 5e-8
m/s','FontSize',24,'FontWeight','bold');

title('Velocity along the beam at
f=90Hz','Fontsize',30,'FontWeight','bold');

legend({'[0/45/90]s-Vf-0.5-Ec-2','[0/45/90]s-Vf-0.5-Ec-
0.5','[0/45/90]s-Vf-0.8-Ec-2','[0/45/90]s-Vf-0.2-Ec-
2','[90/45/0]s-Vf-0.5-Ec-2','[30/10/80]s-Vf-0.5-Ec-2','[-
45/45/-45]s-Vf-0.5-Ec-0.5','[-45/10/-45]s-Vf-0.5-Ec-
2'},'Location','northwest','Fontsize',18);
```

Appendix E – Matlab code for orientation optimisation

Fitness function

```
function f = Funktion_Orientation_neu(x)

global model
global wink1,global wink2,
global m;
import com.COMSOL.model.*;
import com.COMSOL.model.util.*;
m=m+1;

wink1=x(1);
wink2=x(2);

model.param.set('wink1',wink1);
model.param.set('wink2',wink2);
model.study('std2').run;
Ek=mphglobal(model,'lshell.Wk_tot','dataset','dset6','solnu
m',1,'outersolnum',1);

AAA(m,1)=Ek
AAA(m,2)=wink1
AAA(m,3)=wink2

f=Ek
```

Genetic Algorithm

```
import com.COMSOL.model.*
import com.COMSOL.model.util.*

model =
mphload('Z:\19_April_2021\Unit_cell_stiffness_with_Beam_Fre
qDomain_Ec2_klein_fRange_2schicht_Kasten.mph');

global model
global wink1,
global wink2,
global m;

m=0;
fitFon=@Funktion_Orientation_neu;

nvars=2;
lb=[0 0];
ub=[90 90];
IntCon=[1 2];
opts = optimoptions('ga','PlotFcn', @gaplotbestf);
opts.PopulationSize = 10;
[x,fval,existflag,output, population,scores] =
ga(fitFon,nvars,[],[],[],[],lb,ub,[],IntCon,opts);

[x,fval] = ga(fitFon,nvars,[],[],[],[],lb,ub);
x
fval
```

Hochschule für Angewandte Wissenschaften Hamburg
Hamburg University of Applied Sciences

Erklärung zur selbstständigen Bearbeitung einer Abschlussarbeit

Gemäß der Allgemeinen Prüfungs- und Studienordnung ist zusammen mit der Abschlussarbeit eine schriftliche Erklärung abzugeben, in der der Studierende bestätigt, dass die Abschlussarbeit „– bei einer Gruppenarbeit die entsprechend gekennzeichneten Teile der Arbeit [(§ 18 Abs. 1 APSO-TI-BM bzw. § 21 Abs. 1 APSO-INGI)] – ohne fremde Hilfe selbständig verfasst und nur die angegebenen Quellen und Hilfsmittel benutzt wurden. Wörtlich oder dem Sinn nach aus anderen Werken entnommene Stellen sind unter Angabe der Quellen kenntlich zu machen."

Quelle: § 16 Abs. 5 APSO-TI-BM bzw. § 15 Abs. 6 APSO-INGI

Dieses Blatt, mit der folgenden Erklärung, ist nach Fertigstellung der Abschlussarbeit durch den Studierenden auszufüllen und jeweils mit Originalunterschrift als letztes Blatt in das Prüfungsexemplar der Abschlussarbeit einzubinden.
Eine unrichtig abgegebene Erklärung kann -auch nachträglich- zur Ungültigkeit des Studienabschlusses führen.

Erklärung zur selbstständigen Bearbeitung der Arbeit

Hiermit versichere ich,

Name: Wang

Vorname: Yi

dass ich die vorliegende Masterarbeit bzw. bei einer Gruppenarbeit die entsprechend gekennzeichneten Teile der Arbeit – mit dem Thema:

Development of a simulation framework for dynamically loaded multifunctional composite structures and evaluation of vibration control performance

ohne fremde Hilfe selbständig verfasst und nur die angegebenen Quellen und Hilfsmittel benutzt habe. Wörtlich oder dem Sinn nach aus anderen Werken entnommene Stellen sind unter Angabe der Quellen kenntlich gemacht.

- die folgende Aussage ist bei Gruppenarbeiten auszufüllen und entfällt bei Einzelarbeiten -

Die Kennzeichnung der von mir erstellten und verantworteten Teile der -bitte auswählen- ist erfolgt durch:

Hamburg	30.08.2021	[redacted]
Ort	Datum	Unterschrift im Original